Novel Supercritical Carbon Dioxide Power Cycle Utilizing Pressurized Oxy-combustion in Conjunction with Cryogenic Compression

FINAL REPORT

DOE Project DE-FE0009395
SwRI® Project No. 17899

Principal Investigator

Klaus Brun, Ph.D.
Southwest Research Institute
Klaus.Brun@swri.org
210-522-5449

Prepared by

Aaron McClung, Ph.D.
Southwest Research Institute
Aaron.McClung@swri.org
210-522-2677

John Davis
Thar Energy
John.Davis@tharenergyllc.com
412-963-7500

Prepared for
U.S. Department of Energy
NETL, Morgantown, WV

Period of Performance
October 1, 2012 through March 31, 2014

Submitted on
April 9, 2014

SOUTHWEST RESEARCH INSTITUTE®
6220 Culebra Road
San Antonio, Texas 78238

DUNS Number: 00-793-6842

SOUTHWEST RESEARCH INSTITUTE®

SOUTHWEST RESEARCH INSTITUTE®
6220 Culebra Road
San Antonio, Texas 78238

Novel Supercritical Carbon Dioxide Power Cycle Utilizing Pressurized Oxy-combustion in Conjunction with Cryogenic Compression

FINAL REPORT

DOE Project DE-FE0009395
SwRI® Project No. 17899

Principal Investigator

Klaus Brun, Ph.D.
Southwest Research Institute
Klaus.Brun@swri.org
210-522-5449

Prepared by

Aaron McClung, Ph.D.
Southwest Research Institute
Aaron.McClung@swri.org
210-522-2677

John Davis
Thar Energy
John.Davis@tharenergyllc.com
412-963-7500

Prepared for
U.S. Department of Energy
NETL, Morgantown, WV

Submitted on
April 9, 2014

Approved:

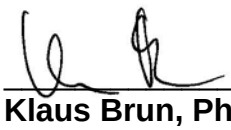

Klaus Brun, Ph.D.
Program Director
Machinery Program

SOUTHWEST RESEARCH INSTITUTE®

DISCLAIMER

This report was prepared as an account of work sponsored by an agency of the United States Government. Neither the United States Government nor any agency thereof, nor any of their employees, makes any warranty, express or implied, or assumes any legal liability or responsibility for the accuracy, completeness, or usefulness of any information, apparatus, product, or process disclosed, or represents that its use would not infringe privately owned rights. Reference herein to any specific commercial product, process, or service by trade name, trademark, manufacturer, or otherwise does not necessarily constitute or imply its endorsement, recommendation, or favoring by the United States Government or any agency thereof. The views and opinions of authors expressed herein do not necessarily state or reflect those of the United States Government or any agency thereof.

ABSTRACT

The team of Southwest Research Institute® (SwRI) and Thar Energy LLC (Thar) applied technology engineering and economic analysis to evaluate two advanced oxy-combustion power cycles, the Cryogenic Pressurized Oxy-combustion Cycle (CPOC), and the Supercritical Oxy-combustion Cycle. This assessment evaluated the performance and economic cost of the two proposed cycles with carbon capture, and included a technology gap analysis of the proposed technologies to determine the technology readiness level of the cycle and the cycle components. The results of the engineering and economic analysis and the technology gap analysis were used to identify the next steps along the technology development roadmap for the selected cycle.

The project objectives, as outlined in the FOA, were 90% CO_2 removal at no more than a 35% increase in cost of electricity (COE) as compared to a Supercritical Pulverized Coal Plant without CO_2 capture. The supercritical oxy-combustion power cycle with 99% carbon capture achieves a COE of $121/MWe. This revised COE represents a 21% reduction in cost as compared to supercritical steam with 90% carbon capture ($137/MWe). However, this represents a 49% increase in the COE over supercritical steam without carbon capture ($80.95/MWe), exceeding the 35% target.

The supercritical oxy-combustion cycle with 99% carbon capture achieved a 37.9% HHV plant efficiency (39.3% LHV plant efficiency), when coupling a supercritical oxy-combustion thermal loop to an indirect supercritical CO_2 (sCO_2) power block. In this configuration, the power block achieved 48% thermal efficiency for turbine inlet conditions of 650°C and 290 atm. Power block efficiencies near 60% are feasible with higher turbine inlet temperatures, however a design tradeoff to limit firing temperature to 650°C was made in order to use austenitic stainless steels for the high temperature pressure vessels and piping and to minimize the need for advanced turbomachinery features such as blade cooling.

The overall technical readiness of the supercritical oxy-combustion cycle is TRL 2, Technology Concept, due to the maturity level of the supercritical oxy-combustor for solid fuels, and several critical supporting components, as identified in the Technical Gap Analysis. The supercritical oxy-combustor for solid fuels operating at pressures near 100 atm is a unique component of the supercritical oxy-combustion cycle. In addition to the low TRL supercritical oxy-combustor, secondary systems were identified that would require adaptation for use with the supercritical oxy-combustion cycle. These secondary systems include the high pressure pulverized coal feed, high temperature cyclone, removal of post-combustion particulates from the high pressure cyclone underflow stream, and micro-channel heat exchangers tolerant of particulate loading.

Bench scale testing was utilized to measure coal combustion properties at elevated pressures in a CO_2 environment. This testing included coal slurry preparation, visualization of coal injection into a high pressure fluid, and modification of existing test equipment to facilitate the combustion properties testing. Additional bench scale testing evaluated the effectiveness of a rotary atomizer for injecting a coal-water slurry into a fluid with similar densities, as opposed to the typical application where the high density fluid is injected into a low density fluid.

The swirl type supercritical oxy-combustor was developed from initial concept to an advanced design stage through numerical simulation using FLUENT and Chemkin to model the flow through the combustor and provide initial assessment of the coal combustion reactions in the flow path. This effort enabled the initial combustor mechanical layout, initial pressure vessel design, and the conceptual layout of a pilot scale test loop.

A pilot scale demonstration of the supercritical oxy-combustion cycle is proposed as the next step in the technology development. This demonstration would advance the supercritical oxy-combustion cycle and the supercritical oxy-combustor from a current TRL of 2, *Technology Concept*, to TRL 6, *Pilot Scale System Demonstrated in a Relevant Environment*, and enable the evaluation and continued refinement of the supercritical oxy-combustor and critical secondary systems.

TABLE OF CONTENTS

List of Figures

List of Tables

1. EXECUTIVE SUMMARY

The team of Southwest Research Institute® (SwRI) and Thar Energy LLC (Thar) applied technology engineering and economic analysis to evaluate two advanced oxy-combustion power cycles, the Cryogenic Pressurized Oxy-combustion Cycle (CPOC), and the Supercritical Oxy-combustion Cycle. This assessment evaluated the performance and economic cost of the two proposed cycles with carbon capture, and included a technology gap analysis of the proposed technologies to determine the technology readiness level of the cycle and the cycle components. The results of the engineering and economic analysis and the technology gap analysis were used to identify the next steps along the technology development roadmap for the selected cycle.

The project objectives, as outlined in the FOA, were 90% CO_2 removal at no more than a 35% increase in cost of electricity (COE) as compared to a Supercritical Pulverized Coal Plant without CO_2 capture. The supercritical oxy-combustion power cycle with 99% carbon capture achieves a COE of $121/MWe. This revised COE represents a 21% reduction in cost as compared to supercritical steam with 90% carbon capture ($137/MWe). However, this represents a 49% increase in the COE over supercritical steam without carbon capture ($80.95/MWe), exceeding the 35% target. The revised $121/MWe COE reflects the removal of installation labor costs included in the Total Overnight Cost (TOC) and increasing coal cost per QGESS fuel guidelines based on feedback provided by DOE for the Phase II application, and updates to the fuel consumption rates to match the cycle efficiencies predicted by the cycle models. These revisions reflect a significant decrease from the initial $162/MWe COE estimate provided in the *Technology Engineering Design and Ecconomic Analysis* report submitted with the Phase II proposal. The project effort included four top level tasks; (1) *Project Management and Planning* to ensure the timely and responsible completion of the project objectives; (2) *Technology Engineering Design and Economic Analysis* which included cycle modeling to refine the proposed cycles and predict cycle performance, bench scale testing provide combustion properties at pressure to support the cycle and oxy-combustor design, and economic analysis of the cycle refined cycle to benchmark against current technologies; (3) *Technology Gap Analysis* to assess the TRL of cycle components and related systems in order to outline a technology development roadmap required for the commercial development of the selected oxy-combustion cycle; and (4) submission of the Phase II application for the demonstration of critical components or the integrated system at the bench or pilot scale. The executive summary presents a general overview of the technology and the execution of the top level tasks in the following sections.

1.1 OVERVIEW OF THE TECHNOLOGY

Two concepts for supercritical oxy-combustion cycles were examined, the Cryogenic Pressurized Oxy-Combustion Cycle (CPOC) and the Advanced Supercritical Oxy-Combustion Cycle. Both cycle concepts seek to maximize net plant efficiencies by maximizing the efficiency of the power block, minimizing power loss due to accessory systems, and increasing combustion efficiencies. These cycles leverage recent advances in supercritical CO_2 (sCO_2) power cycles and current development efforts for CO_2 turbo-machinery[1] by utilizing sCO_2 as the working fluid for the power block. Direct fired and indirect fired configurations were considered for each cycle configuration.

[1] DE-EE0005804, "Development of a high efficiency hot gas turbo-expander and low-cost heat exchangers for optimized CSP supercritical CO_2 operation," Southwest Research Institute, General Electric Global Research, and Thar Energy

The CPOC cycle is a trans-critical power cycle that leverages recent advances in iso-thermal compression to minimize recompression costs, while the advanced supercritical oxy-combustion cycle maintains supercritical pressures. Thermodynamic analysis of the power blocks for the two cycle configurations concluded that the recompression-closed Brayton cycle provides greater thermal efficiencies than the transcritical CPOC cycle.

Analysis of the supercritical oxy-combustion cycle indicated that the dual loop configuration, shown in Figure 1-1, was advantageous over the direct fired configuration due to the decoupling of the combustor pressure from the turbine inlet pressure. The indirect configuration allows the combustor to operate near 100 atm, or just above the critical point in order to take advantage of reduced cost of compression for the captured CO2 stream, while allowing the power block to operate with a turbine inlet pressure of 290 atm, a favorable operating pressure significantly greater than the combustion loop. The injection of solid fuel into the supercritical oxy-combustor was the limiting factor in determining the combustion loop operating pressure.

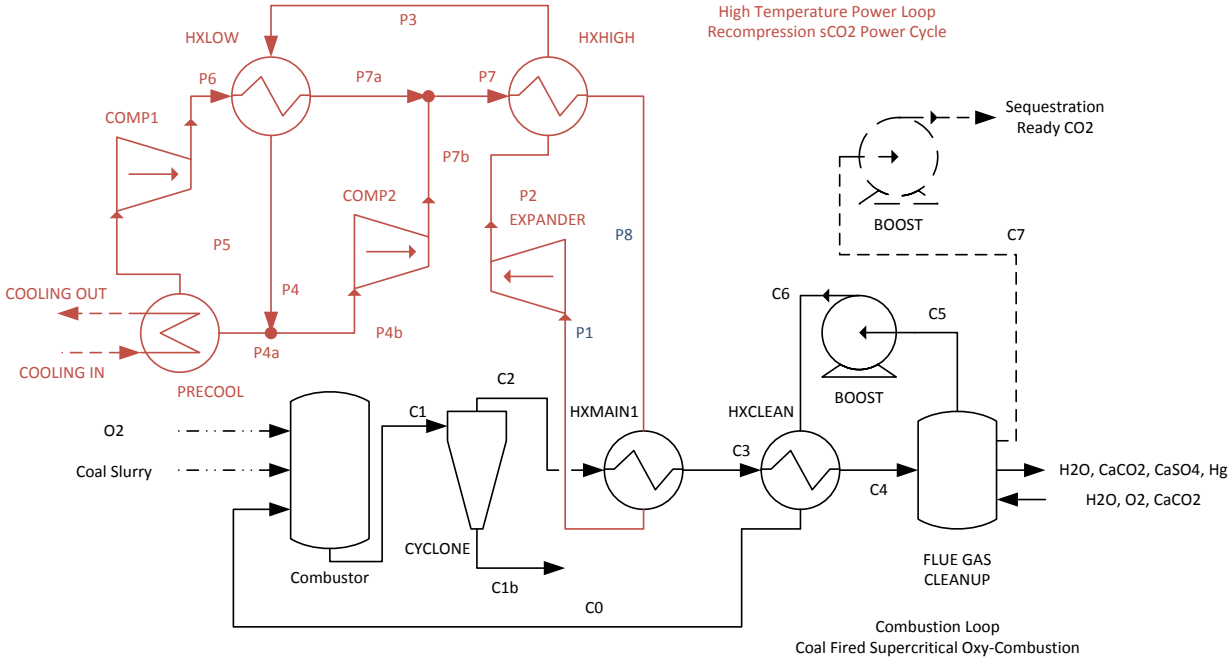

Figure 1-1. Indirect supercritical oxy-combustion cycle layout with a recompression sCO_2 power block

The Technical Gap Analysis identified the supercritical oxy-combustor as a low TRL component that is unique to the supercritical oxy-combustion concept. In addition to the supercritical oxy-combustor, it was identified that the handling of particulates for both injection into and removal from the supercritical process streams are not fully addressed by commercially available components. The indirect supercritical oxy-combustion loop coupled with a recompression closed Brayton cycle power block makes extensive use of heat exchangers and recouperators. This extensive use of heat exchangers emphasizes the need for low cost, compact heat exchangers in order to take advantage of the compact sCO_2 turbomachinery and ensure a minimal increase in the cost of electricity. In addition to cost and efficiency, there is additional uncertainty associated with the impact of particulate loading in the compact microchannel heat exchangers on performance, and the effectiveness of cleaning methods at removing the particulate buildup.

1.2 TASK 1.0 – PROJECT MANAGEMENT AND PLANNING

Execution of the Engineering and Economic Analysis, the Technology Gap Assessment, and the Phase II Proposal required regular communication between all project participants. This regular communication ensured that progress in each task was reflected in the other tasks, such that advances in the cycle analysis were reflected in the components examined for the technology gap assessment, and the state of the components was incorporated into the cycle concept and analysis.

1.3 TASK 2.0 – TECHNOLOGY ENGINEERING DESIGN AND ECONOMIC ANALYSIS

1.3.1 CYCLE ANALYSIS

Process models for the CPOC and the Supercritical Oxy-Combustion Concept were developed in Aspen Plus in accordance with QGESS: Process Modeling Design Parameters. These models provided the basis for examining various cycle layouts and component configurations.

The final configuration selected for further development in the proposed Phase II effort is the indirect supercritical oxy-combustion cycle, shown in Figure 1-1. This cycle configuration is able to achieve 37.9% HHV plant efficiency (39.3% LHV plant efficiency) with 99% carbon capture for a COE of $121/MWe. This represents a 21% reduction in cost as compared to supercritical steam with 90% carbon capture ($137/MWe). However, this represents a 49% increase in the COE over supercritical steam without carbon capture ($80.95/MWe). The selection of 650 as the firing temperature represents a design tradeoff to limit firing temperature in order to use austenitic stainless steels for the high temperature pressure vessels and piping, and to minimize the need for advanced turbomachinery features such as blade cooling.

1.3.2 IDENTIFICATION OF CRITICAL TECHNOLOGIES FOR BENCH SCALE TESTING

The initial assessment of the CPOC and supercritical oxy-combustion cycles identified the limited availability of combustion properties above 30 atm as a significant risk to the supercritical oxy-combustor design and cycle analysis. In addition to the combustion properties, the preparation and injection of coal water slurry into a high pressure combustor was deemed a significant technology risk to warrant bench scale examination.

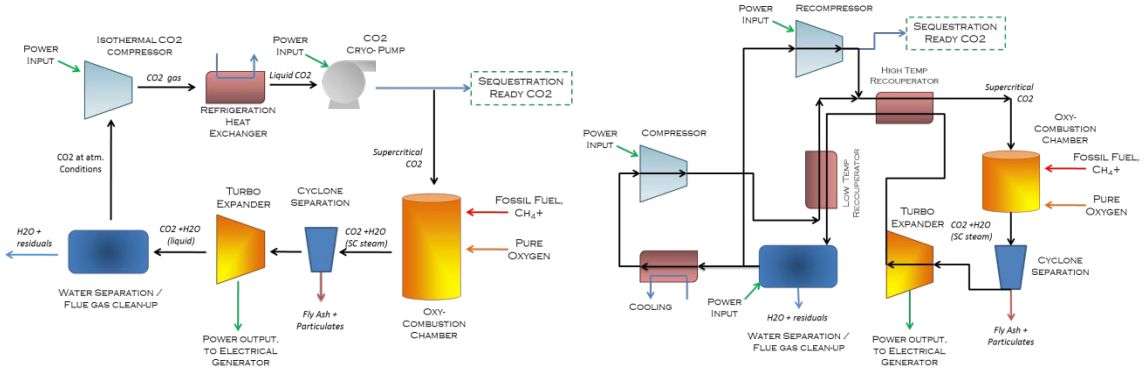

Figure 1-2. Single loop, direct-fired supercritical oxy-combustion cycles, Cryogenic Pressurized Oxy-combustion Cycle, left, and the Advanced Supercritical Oxy-combustion Cycle, right.

1.3.3 BENCH SCALE TESTING

Bench scale testing was utilized to measure coal combustion properties at elevated pressures in a CO_2 environment. An Ignition Quality Tester (IQT) was utilized to estimate coal slurry autoignition delay. As part of the test preparation, coal slurries of various concentrations and compositions were prepared and evaluated to maintain suspension of the coal in the slurry, and to identify slurry compositions compatible with the IQT. An additional element of the test preparation was visualization of slurry injection techniques, as shown in Figure 1-3.

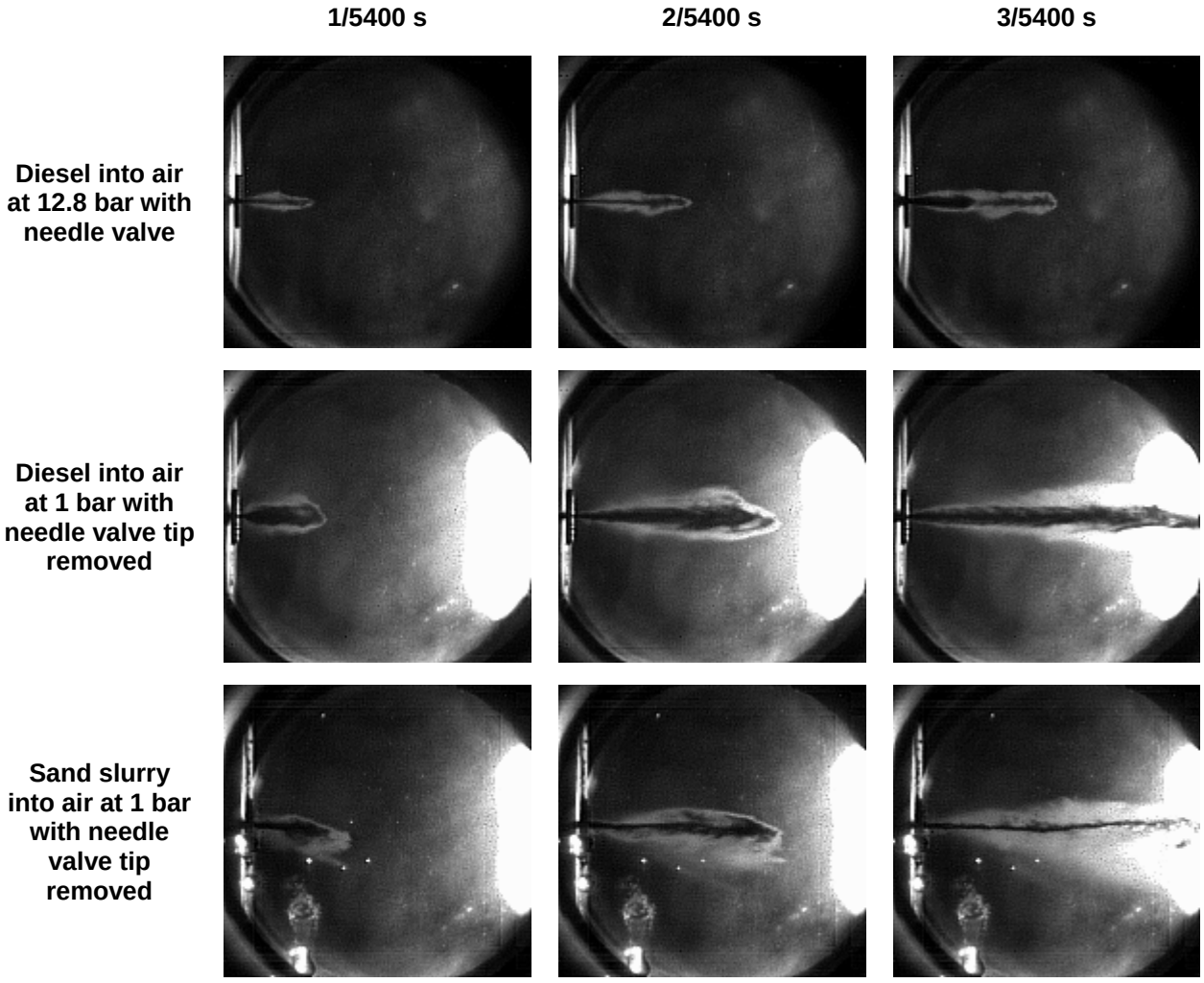

Figure 1-3. Comparison of Slurry versus Liquid Diesel Injected with Same Differential Pressure

Additional bench scale testing evaluated the effectiveness of a rotary atomizer for injecting coal-water slurry into a fluid with similar densities, as opposed to the typical application where the high density fluid is injected into a low density fluid.

Figure 1-4. Droplets produced with impeller turning at 1100 RPM and 1.75 gpm water flow rate through chamber

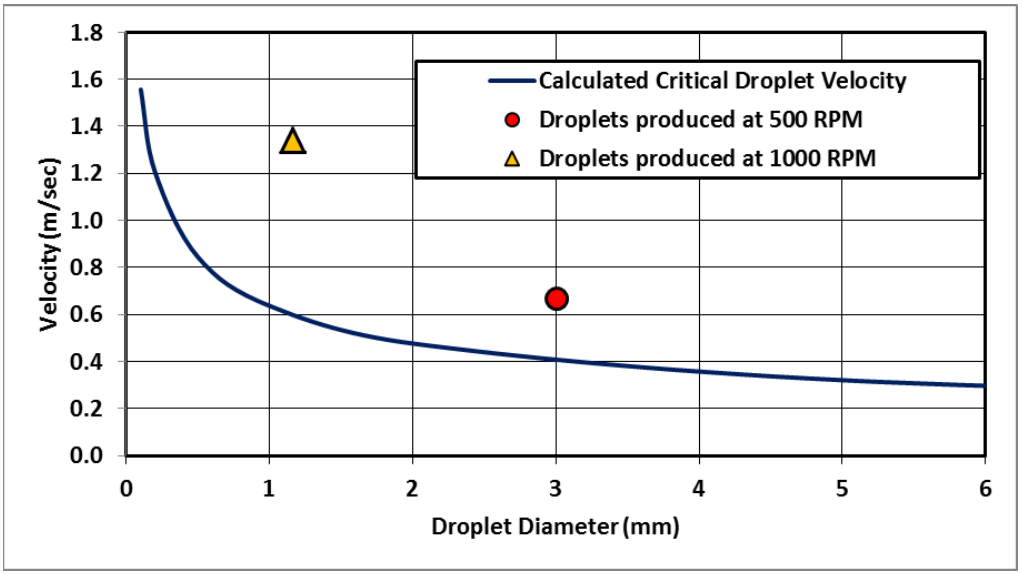

Figure 1-5. Comparison of calculated variation of critical velocity of slurry droplets with diameter to observed droplet sizes produced by different impeller tip speeds

1.3.4 INITIAL ECONOMIC MODEL IMPLEMENTATION

Economic cost analysis was performed using the *NETL Power Systems Financial Model (PSFM)* in accordance with *QGESS: Cost Estimation Methodology for NETL Assessments of Power Plant Performance*. The PSFM was used to evaluate costs for two indirect supercritical oxy-combustion cycle configurations which were selected during the technical evalustion of the power cycles based on their thermodynamic performance. The economic cost analysis utilized data collected for the Technical Gap analysis for equipment size, availability and cost. In some cases – such as cyclones for particulate removal – the technology is well commercialized and cost quotations were obtained for the size of equipment needed for the model 550-MW power plant. For many other process components, the TRL is too low and commercial example are unavailable. In such cases, the knowledge gained through literature searching and subsequent analysis was used to formulate cost estimates.

According to the revised PSFM model, the estimated Cost of Electricity (COE) using the single power-block flowscheme is $121/MWe. This is 49% greater than the benchmark COE of $80.95/MWe for Case 11 of the latest NETL cost assessment for pulverized coal plants without sequestration. This exceeds the stated program objectives of 35% increase in COE; however, the supercritical oxy-combustor represents a 21% reduction in COE when compared to current

power generation technologies with 90% CO_2 capture, while capturing and sequestering 99% of the generated CO_2.

The revised $121/MWe COE reflects the removal of installation labor costs included in the Total Overnight Cost (TOC) and increasing coal cost per QGESS fuel guidelines based on feedback provided by DOE for the Phase II application, and updates to the fuel consumption rates to match the cycle efficiencies predicted by the cycle models. These revisions reflect a significant decrease from the initial $162/MWe COE estimate provided in the *Technology Engineering Design and Ecconomic Analysis* report submitted with the Phase II proposal.

1.4 TASK 3.0 – TECHNOLOGY GAP ANALYSIS

A Technical Gap Analysis of the supercritical oxy-combustion power cycle identified one critical component with a low Technology Readiness Level (TRL). The supercritical oxy-combustor operating at pressures near 100 atm is a unique component to the supercritical oxy-combustion cycle. In addition to the low TRL supercritical oxy-combustor, several secondary systems were identified that are commercially available, but would require adaptation for use with the supercritical oxy-combustion cycle. These secondary systems include the high pressure pulverized coal feed, the high temperature cyclone, the removal of post-combustion particulates from the high pressure cyclone underflow stream, and micro-channel heat exchangers tolerant of particulate loading.

Key findings of the technical gap analysis include:

- Air separation is a major cost item, exaggerated by the need to pressurize the O2 stream to nearly 100 bar. While the technology and manufacturing capability to provide oxygen in the quantity required of a 550 MW oxy-combustion power plant, the state-of-the-art for pumping/compression components is not yet up to commercial readiness.
- Particulate removal technology is available, but with the following caveats: Process engineering is required to develop a system for de-pressurization and recovery of solids. Cyclones should be outfitted with replaceable inner jackets, so as to manage abrasion and wear. The particulates that escape from cyclone separation will likely be in a size range of 1-5 microns; the downstream heat exchangers must be capable of handling these particles.
- Cyclones, heat exchangers, air separation units, and flue gas desulfurization systems should be specified as multiple smaller units in parallel. This is advantages for economy of scale and sparing.
- Compact, low cost heat exchangers are a key technology impacting footprint and cost of the supercritical oxy-combustion cycle. Microchannel heat exchangers are currently at a low TRL, but are actively being developed for multiple applications including supercritical CO_2 power cycles. Because it is expected that 1-5 micron may pass through the cyclone separator, heat exchanger sparing and cleaning are important considerations.
- Metals removal, particularly mercury, can occur in the same equipment as used for flue gas desulfurization.
- Desulfurization using limestone slurry with recovery of gypsum byproduct is the preferred flue gas desulfurization method at elevated pressured.
- For slurry handling, conventional progressive-cavity pumps can be used for conveying slurry at low pressure differential into holding tanks. There, the pressurized stream of recycle CO_2 can be used to bring the slurry to pressure. Direct feed of dry pulverized

coal would be preferred to maximize plant efficiencies, however direct feed systems at high pressures are at a low TRL.

1.5 TASK 4.0 – PHASE II APPLICATION

The early identification of the supercritical oxy-combustor as a critical low TRL component facilitated an initial combustor design based on a pressurized swirl combustor concept. Design efforts included numerical simulation using FLUENT and Chemkin to handle the coal combustion reactions, combustor mechanical layout, initial pressure vessel design, and the conceptual layout of a pilot scale test loop.

A Phase II effort is proposed to demonstrate the supercritical oxy-combustion cycle at the pilot scale. This demonstration would advance the supercritical oxy-combustion cycle and the supercritical oxy-combustor from a current TRL of 2, *Technology Concept*, to TRL 6, *Pilot Scale System Demonstrated in a Relevant Environment*, and enable the evaluation and refinement of the high TRL secondary systems.

2. REPORT

The team of Southwest Research Institute® (SwRI) and Thar Energy LLC (Thar) applied technology engineering and economic analysis to evaluate two advanced oxy-combustion power cycles, the Cryogenic Pressurized Oxy-combustion Cycle (CPOC), and the Supercritical Oxy-combustion Cycle. This assessment evaluated the performance and economic cost of the two proposed cycles with carbon capture, and included a technology gap analysis of the proposed technologies to determine the technology readiness level of the cycle and the cycle components. The results of the engineering and economic analysis and the technology gap analysis were used to identify the next steps along the technology development roadmap for the selected cycle.

The project objectives, as outlined in the FOA, were 90% CO2 removal at no more than a 35% increase in cost of electricity (COE) as compared to a Supercritical Pulverized Coal Plant without CO2 capture. The supercritical oxy-combustion power cycle with 99% carbon capture achieves a COE of $121/MWe. This represents a 21% reduction in cost as compared to supercritical steam with 90% carbon capture ($137/MWe). However, this represents a 49% increase in the COE over supercritical steam without carbon capture ($80.95/MWe), exceeding the 35% target.

The supercritical oxy-combustion cycle with 99% carbon capture achieved a 37.9% HHV plant efficiency (39.3% LHV plant efficiency), when coupling a supercritical oxy-combustion thermal loop to an indirect supercritical CO2 (sCO2) power block. In this configuration, the power block achieved 48% thermal efficiency for turbine inlet conditions of 650 °C and 290 atm. Power block efficiencies near 60% are feasible with higher turbine inlet temperatures, however, a design tradeoff to limit firing temperature to 650 °C was made in order to use austenitic stainless steels for the high temperature pressure vessels and piping and to minimize the need for advanced turbomachinery features such as blade cooling.

The overall technical readiness of the supercritical oxy-combustion cycle is TRL 2, Technology Concept, due to the maturity level of the supercritical oxy-combustor for solid fuels, and several critical supporting components, as identified in the Technical Gap Analysis. The supercritical oxy-combustor for solid fuels operating at pressures near 100 atm is a unique component of the supercritical oxy-combustion cycle. In addition to the low TRL supercritical oxy-combustor, secondary systems were identified that would require adaptation for use with the supercritical oxy-combustion cycle. These secondary systems include the high pressure pulverized coal feed, high temperature cyclone, removal of post-combustion particulates from the high pressure cyclone underflow stream, and micro-channel heat exchangers tolerant of particulate loading.

Bench scale testing was utilized to measure coal combustion properties at elevated pressures in a CO2 environment. This testing included coal slurry preparation, visualization of coal injection into a high pressure fluid, and modification of IQT injectors to facilitate the combustion properties testing. Additional bench scale testing evaluated the effectiveness of a rotary atomizer for injecting coal-water slurry into a fluid with similar densities, as opposed to the typical application where the high density fluid is injected into a low density fluid.

The swirl type supercritical oxy-combustor was developed from initial concept to an advanced design stage through numerical simulation using FLUENT and Chemkin to model the flow through the combustor and provide initial assessment of the coal combustion reactions in the flow path. This effort enabled the initial combustor mechanical layout, initial pressure vessel design, and the conceptual layout of a pilot scale test loop.

A pilot scale demonstration of the supercritical oxy-combustion cycle was proposed as a follow on effort. This demonstration would advance the supercritical oxy-combustion cycle and the

supercritical oxy-combustor from a current TRL of 2, Technology Concept, to TRL 6, Pilot Scale System Demonstrated in a Relevant Environment, and enable the evaluation and continued refinement of the supercritical oxy-combustor and critical secondary systems.

2.1 GOALS AND OBJECTIVES FOR THE PROJECT

The objective of this project was to demonstrate the feasibility of achieving 90% CO_2 removal for less than a 35% increase in the cost of electricity (COE) with the proposed Cryogenic Pressurized Oxy-Combustion Cycle and the supercritical oxy-combustion cycles. The cycle performance and COE was demonstrated through system process and economic modeling to evaluate overall plant performance and economic cost. This demonstration was accompanied by a technology assessment of critical components to document the research and development path required to achieve the proposed cycle.

2.2 OVERVIEW OF THE TECHNOLOGY

Two concepts for supercritical oxy-combustion cycles were proposed that seek to address the cost of electricity through an increase in cycle efficiency. These concepts are the Cryogenic Pressurized Oxy-Combustion Cycle (CPOC) and the Advanced Supercritical Oxy-Combustion Cycle. Both cycle concepts seek to maximize net plant efficiencies by maximizing the efficiency of the power block, minimizing power loss due to accessory systems, and increasing combustion efficiencies. Both cycle concepts leverage recent advances in supercritical CO_2 (sCO_2) power cycles and current development efforts[2] for CO_2 turbo-machinery by utilizing sCO_2 as the working fluid for the power block. In the direct-fired configurations, the sCO_2 working fluid is the flue gas and includes products of combustion. In the indirect cycle configurations, the flue gas and products of combustion are contained within the combustion loop, and high quality CO_2 is used as the working fluid in the power block.

The CPOC cycle is a trans-critical power cycle that leverages recent advances in iso-thermal compression to minimize recompression costs, while the advanced supercritical oxy-combustion cycle maintains supercritical pressures throughout the cycle. The cycle layouts are shown as initially proposed in Figure 2-1. Thermodynamic analysis of the power blocks for the two cycle configurations concluded that the recompression closed Brayton cycle provides greater thermal efficiencies than the transcritical CPOC cycle.

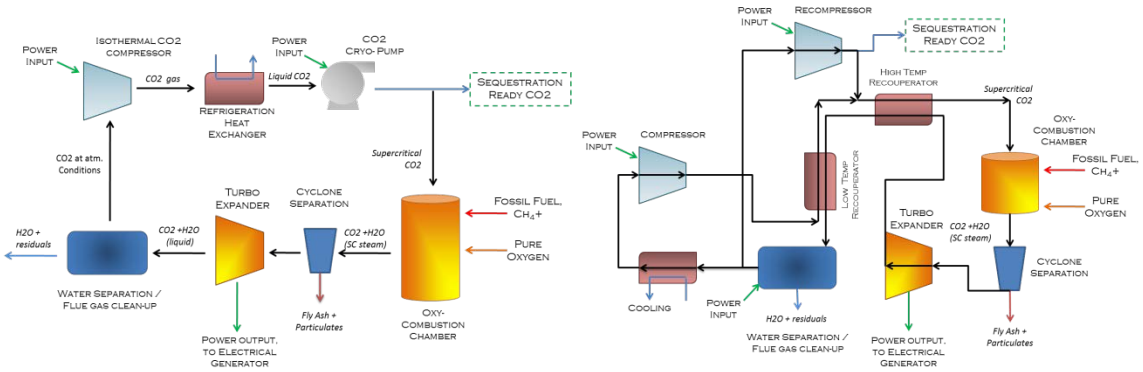

Figure 2-1. Single loop, direct-fired supercritical oxy-combustion cycles, Cryogenic Pressurized Oxy-combustion Cycle, left, and the Advanced Supercritical Oxy-combustion Cycle, right.

[2] DE-EE0005804, "Development of a high efficiency hot gas turbo-expander and low-cost heat exchangers for optimized CSP supercritical CO_2 operation," Southwest Research Institute, General Electric Global Research, and Thar Energy

For the supercritical oxy-combustion cycle, the dual loop configuration is advantageous because it decouples the combustor pressure from the turbine inlet pressure, as shown in the revised cycle configuration in Figure 2-2. The indirect configuration allows the combustor to operate near 100 atm, or just above the critical point in order to take advantage of reduced cost of compression for the captured CO_2 stream, while allowing the power block to operate with a turbine inlet pressure of 290 atm, a favorable operating pressure significantly greater than the combustion loop. The indirect supercritical oxy-combustion loop coupled with a recompression closed Brayton cycle power block makes extensive use of heat exchangers and recuperators. This extensive use of heat exchangers emphasizes the need for low cost, compact heat exchangers in order to take advantage of the compact sCO2 turbomachinery and ensure a minimal increase in the cost of electricity.

The Technical Gap Analysis identified the supercritical oxy-combustor as a low TRL component that is unique to the supercritical oxy-combustion concept. In addition to the supercritical oxy-combustor, it was identified that the handling of particulates for both injection into and removal from the supercritical process streams are not fully addressed by commercially available components. Additionally, there is uncertainty associated with the impact of particulate loading in the compact microchannel heat exchangers on performance, and the effectiveness of cleaning methods at removing the particulate buildup.

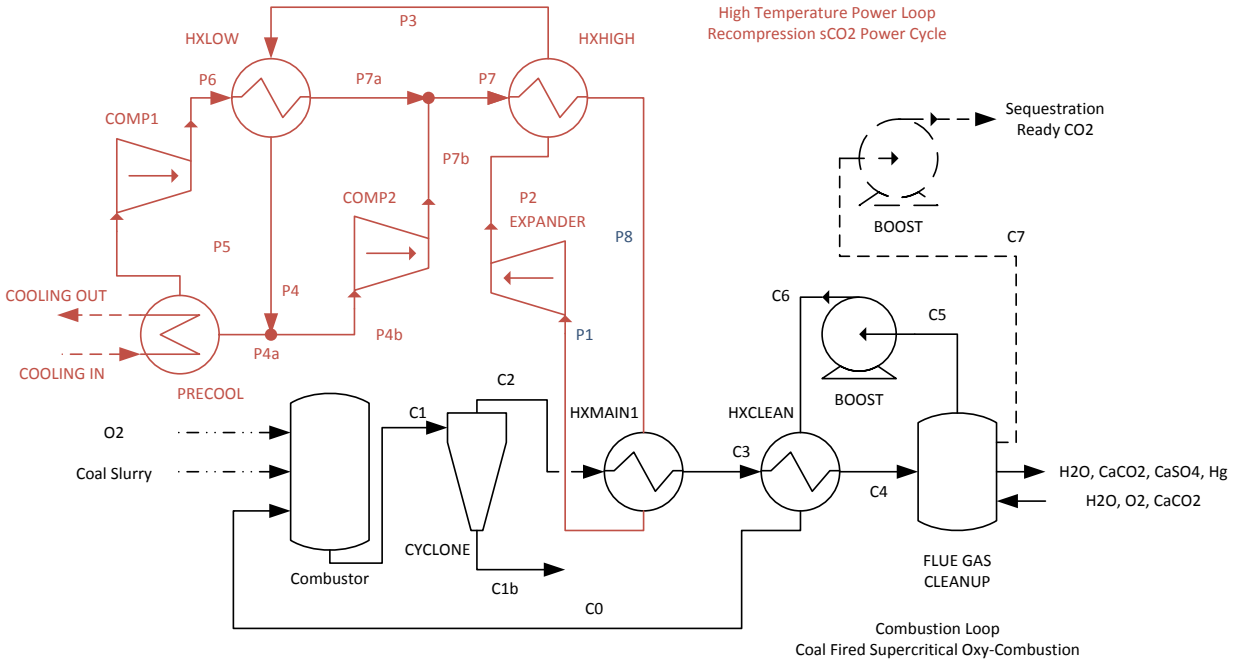

Figure 2-2. Indirect supercritical oxy-combustion cycle layout with a recompression sCO_2 power block

2.3 TASK 1.0 – PROJECT MANAGEMENT AND PLANNING

Execution of the Engineering and Economic Analysis, the Technology Gap Assessment, and the Phase II Proposal required regular communication between all project participants. This regular communication ensured that progress in each task was reflected in the other tasks, such that advances in the cycle analysis were reflected in the components examined for the technology gap assessment, and the state of the components was incorporated into the cycle concept and analysis.

2.3.1 SUBTASK 1.1 – REVISE PROJECT MANAGEMENT PLAN

The Project Management Plan was revised in the first quarter of the project to reflect the outcome of the final contract negotiations, including expanded bench scale testing.

2.3.2 SUBTASK 1.2 – REVISE RISK MANAGEMENT PLAN

The risk management plan was revised during the first quarter of the project to reflect the inclusion of additional bench scale testing in the project scope.

2.3.3 SUBTASK 1.3 – COORDINATION OF PARTICIPANTS

Bi-weekly meetings were used to communicate progress of the Engineering Design Analysis and the Technology Gap Analysis between participants at SwRI and Thar. Additional, task specific communication ensured that updates to the Technology Gap Analysis were incorporated into the Engineering Design analysis, and that changes to the cycle layout were reflected in the Technology Gap Analysis.

2.4 TASK 2.0 – TECHNOLOGY ENGINEERING DESIGN AND ECONOMIC ANALYSIS

The technology engineering and economic analysis demonstrated that the supercritical oxy-combustion cycle achieves a COE of $121/MWe. This represents a 21% reduction in cost as compared to supercritical steam with 90% carbon capture ($137/MWe). However, this represents a 49% increase in the COE over supercritical steam without carbon capture ($80.95/MWe), exceeding the 35% target[3].

The thermodynamic evaluation of the cycle performance utilized Aspen Plus to model the supercritical coal combustion and the supercritical CO2 power cycles. The economic evaluation utilized information gathered during the Technology Gap Analysis evaluation of the indirect supercritical oxy-combustion cycle, and performance predictions of the Engineering Design analysis. This data was utilized in the *NETL Power Systems Financial Model* to predict economic costs associated with the cycle.

2.4.1 SUBTASK 2.1 – DEFINITION OF CYCLE MODEL

Process models for the CPOC and the Supercritical Oxy-combustion Concept were developed in Aspen Plus in accordance with *QGESS: Process Modeling Design Parameters*. Per the project guidelines, the plant is sited in accordance with the Midwest ISO location, as described in Table 2-1. Per Attachment A of the FOA, Illinois #6 Bituminous, Rosebud PRB, and Texas Lignite were the fuel types available for this study. After considering heating value, sulfur content, ash content, and current cost, Rosebud PRB was selected as the fuel choice for this study.

[3] DOE/NETL-341/082312 Updated Costs (June 2011 Basis) for Selected Bituminous Baseline Cases

Table 2-1 Site Conditions

Site Conditions	Midwest (ISO)
Elevation, m (ft)	0 (0)
Barometric Pressure, MPa (psia)	0.101 (14.7)
Design Ambient Dry Bulb Temperature, °C (°F)	15 (59)
Design Ambient Wet Bulb Temperature, °C (°F)	10.8 (51.5)
Design Ambient Relative Humidity, %	60
Cooling Water Temperature, °C (°F)	15.6 (60)
Air composition mass %	
H_2O	0.616
AR	1.280
CO_2	0.050
O_2	22.999
N_2	75.055
Total	**100.00**

Table 2-2. Selected Feedstock

Rank	Low-Sodium Lignite		Sub-Bituminous		HV Bituminous	
Seam	Wilcox Group		Montana Rosebud PRB, Area D		Illinois #6 (Herrin)	
Sample Location	TX		Montana		Franklin Co., IL	
Proximate Analysis (Weight %)						
	AR	Dry	AR	Dry	AR	Dry
Moisture	32	0	25.77	0	11.12	0
Ash	15	22.06	8.19	11.04	9.7	10.91
Volatile Matter	28	41.18	30.34	40.87	34.99	39.37
Fixed Carbon (BD)	25	36.76	35.7	48.09	44.19	49.72
HHV, kJ/kg	15,243	22,417	19,920	26,787	27,113	30,506
HHV, Btu/lb	6,554	9,638	8,564	11,516	11,666	13,126
LHV, kJ/kg	14,601	21,472	19,195	25,810	26,151	29,444
LHV, Btu/lb	6,277	9,231	8,252	11,096	11,252	12,712
Ultimate Analysis (Weight %)						
	AR	Dry	AR	Dry	AR	Dry
Moisture	32	0	25.77	0	11.12	0
Carbon	37.7	55.44	50.07	67.45	63.75	71.72
Hydrogen	3	4.41	3.38	4.56	4.5	5.06
Nitrogen	0.7	1.03	0.71	0.96	1.25	1.41
Chlorine	0.02	0.03	0.01	0.01	0.29	0.33
Sulfur	0.9	1.32	0.73	0.98	2.51	2.82
Ash	15	22.06	8.19	11.03	9.7	10.91
Oxygen (BD)	10.68	15.71	11.14	15.01	6.88	7.75
Sulfur Analysis (Weight %)						
	AR	Dry	AR	Dry	AR	Dry
Pyritic	-	0.43	-	0.63	-	1.14
Sulfate	-	0.04	-	0.01	-	0.22
Organic	-	0.85	-	0.34	-	1.46
Trace Components (ppmd)						
Mercury	-	0.206	-	0.081	-	0.15

2.4.2 SUBTASK 2.2 – IDENTIFICATION OF CRITICAL TECHNOLOGIES FOR BENCH SCALE TESTING

An initial assessment of the CPOC and supercritical oxy-combustion cycles identified the limited availability of combustion properties above 30 atm as a significant risk to the supercritical oxy-combustor design and cycle analysis. In addition to the combustion properties, the preparation and injection of coal water slurry into a high pressure combustor was deemed a significant technology risk to warrant bench scale examination.

2.4.3 SUBTASK 2.3 – BENCH SCALE TESTING

Bench scale testing was used to evaluate coal injection using a rotary atomizer and orifice type injectors, and fill in gaps in coal combustion properties at supercritical pressures.

2.4.3.1 COAL SLURRY PREPARATION

An Ignition Quality Tester (IQT) was utilized to estimate coal slurry autoignition delay in supercritical CO2. However, in order to measure combustion properties in the existing instrument, the slurry was required to pass through a needle valve having an orifice opening of approximately 50 microns. Due to this limitation, the pulverized coal received from CPS Energy in San Antonio required additional refining prior to experimental testing. Preparation of suitable coal slurry was performed using a ball milling technique by SwRI's Chemistry and Chemical Engineering Division, as shown in Figure 2-3. In addition to the milling, gravity filtering was employed to reach a final average particle size of 15 microns.

A selection of slurry fluids and surfactants was assessed to identify a slurry composition suitable for testing in the IQT. A line-up of these prepared samples is shown in Figure 2-4. It was found that agglomeration of the coal particles is a significant concern for the slurry, as demonstrated by Figure 2-5. Based on results, it was decided 50% coal by weight was the maximum particulate concentration that could be used while keeping the mixture both "flowable" and homogeneous for this particle size distribution.

Figure 2-3. Ball mill used to refine the pulverized coal

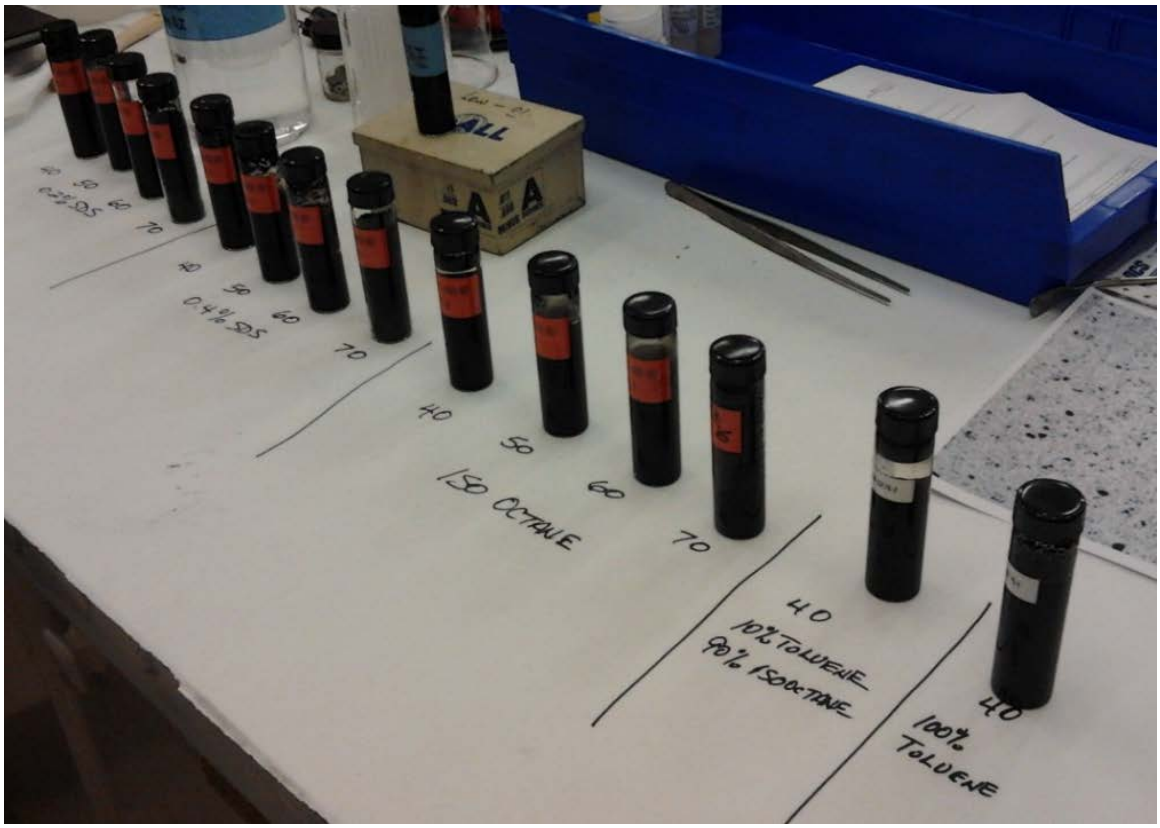

Figure 2-4. Coal slurry samples prepared for testing

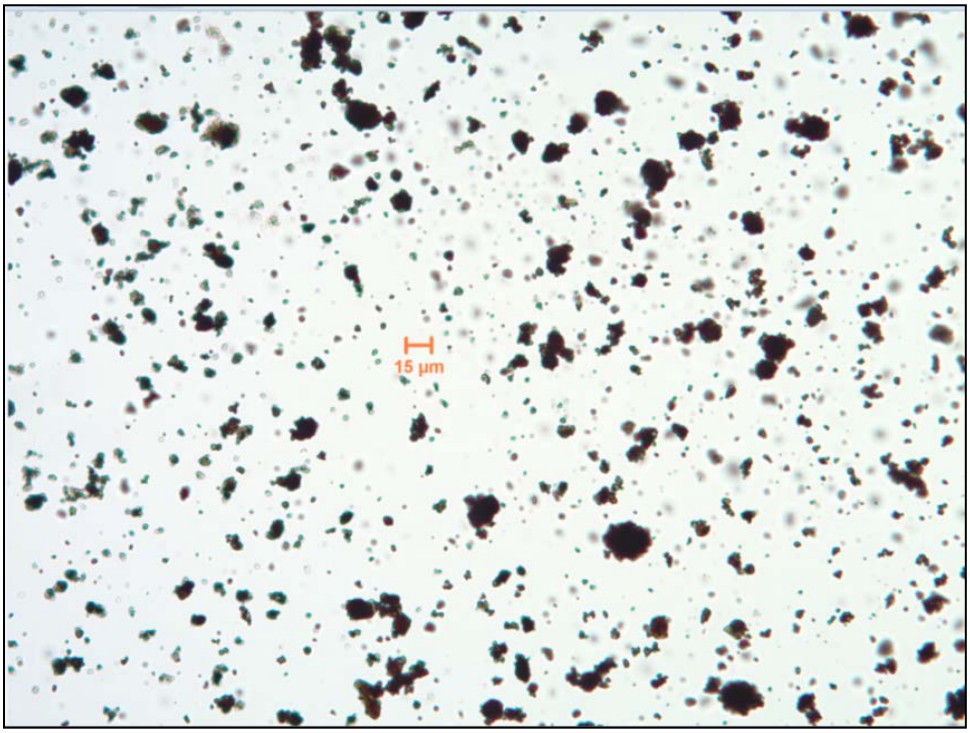

Figure 2-5. Particulate distribution and agglomeration in a 20% coal and iso-octane slurry

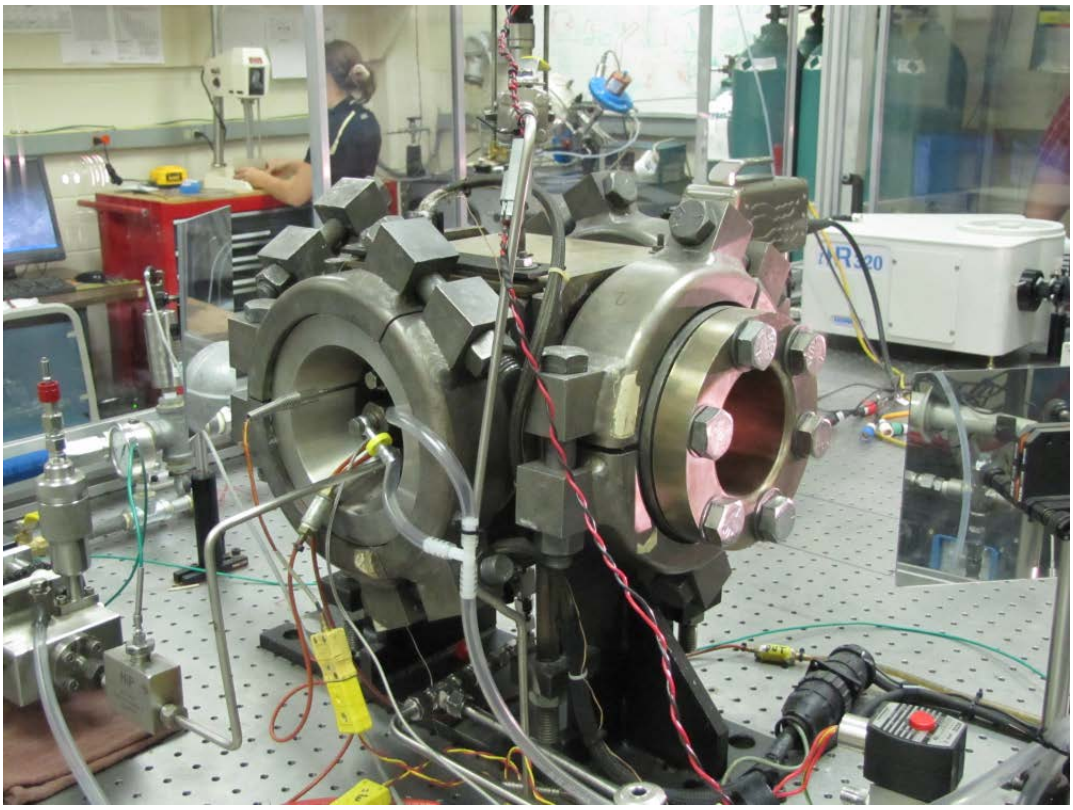

Figure 2-6. Optical bomb used for injector visualization

2.4.3.2 INJECTOR VISUALIZATION

An optical bomb operated by the Engines, Emissions and Vehicle Research Division, shown in Figure 2-6, was employed to assess the ability of the IQT injector to handle the coal slurry using high-speed photography. Initial testing revealed that the injector became clogged using a slurry of only 20% particulates by weight. Recall that the particulates milled for this testing had an average particle size of 15 microns. Modifications to the injector were required, which initially involved removing the needle from the injector entirely, leaving only the approximately 50 micron orifice opening. This resolved the clogging difficulty, but created problems controlling the slurry flow. It was then decided to remove only the end from the injector tip, past the sealing surface. This worked well, allowing control of the injected flow while providing a sufficiently large opening to prevent nozzle clogging.

Preliminary visualization results showed that the slurry injection is carried with greater momentum compared to more typical diesel injection. An example of this is shown in Figure 2-7 which provides a comparison of diesel penetration versus that of the slurry. Note that in addition to hitting the opposite wall, part of the slurry jet rebounded off the wall to travel in the reverse direction. The optimal differential injection pressure for the slurry was empirically determined from experiments. After modification of the injection system to achieve a proper penetration length, the IQT testing commenced.

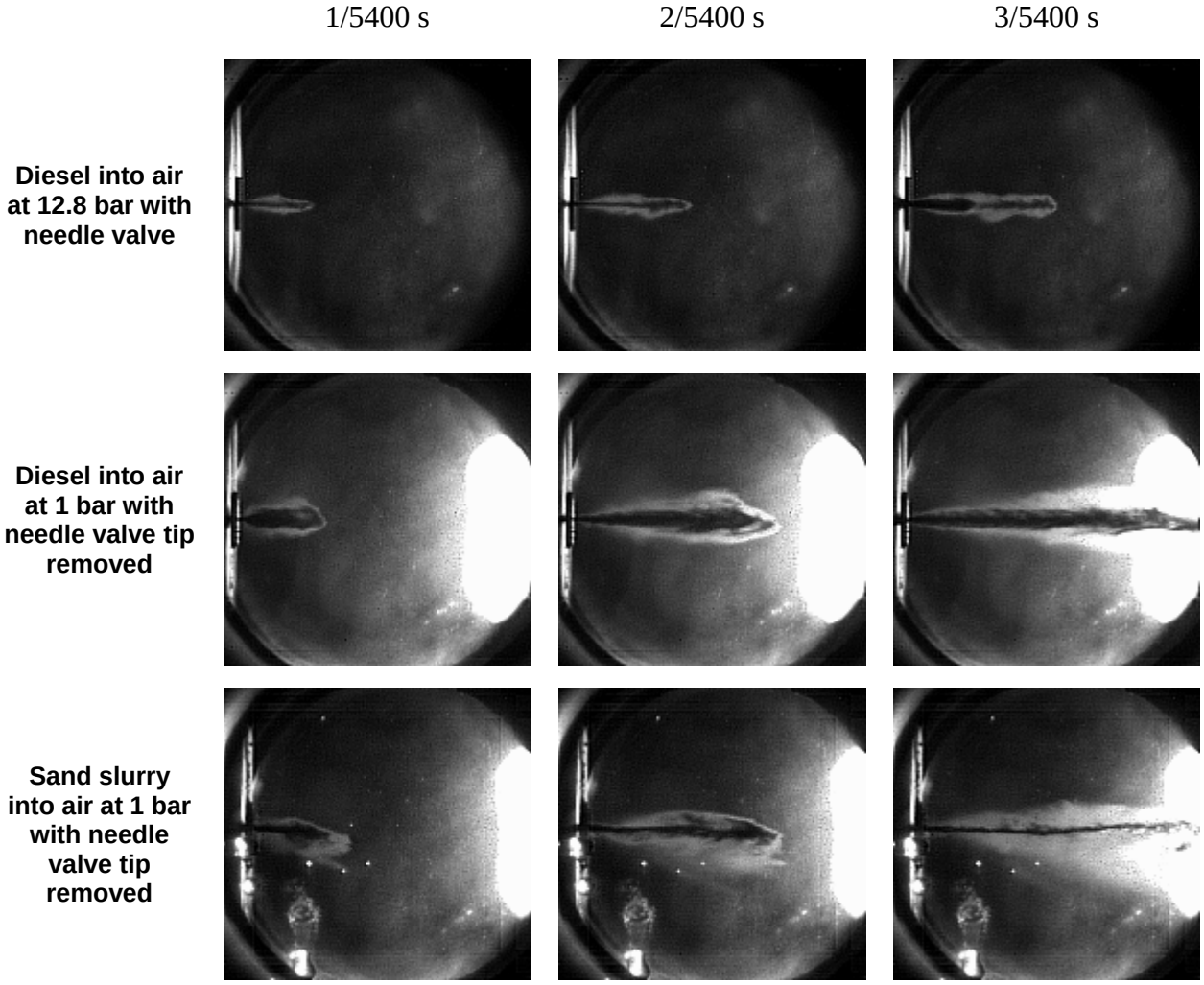

Figure 2-7. Comparison of Slurry versus Liquid Diesel Injected with Same Differential Pressure

Combustion Testing

The Ignition Quality Test Apparatus (IQT™), Figure 2-8, is a bench top constant-volume combustion chamber that can be used to quickly quantify the reactivity, i.e. ignition delay, of fuel and lubricants. Prior to combustion, the heated combustion chamber is filled with compressed gas at elevated pressure. Using a pump-line-nozzle injector, the test fluid is injected and the ignition delay is then measured as shown in Figure 2-9. For the current testing, the stock fuel pump was replaced with a variable displacement pump. Recall that initial work in the optical vessel indicated that the stock injector would not allow the slurry to be injected due to the small opening area. The tip of the needle, which normally develops the spray pattern, needed to be removed to allow the slurry to flow through the injector, shown in Figure 2-10. Modifications made to the IQT were outside the normal parameters of the control program. Therefore, it was necessary to run the test stand in diagnostics mode and acquire the needle lift and combustion trace on an oscilloscope. The test conditions are given in Table 2-3.

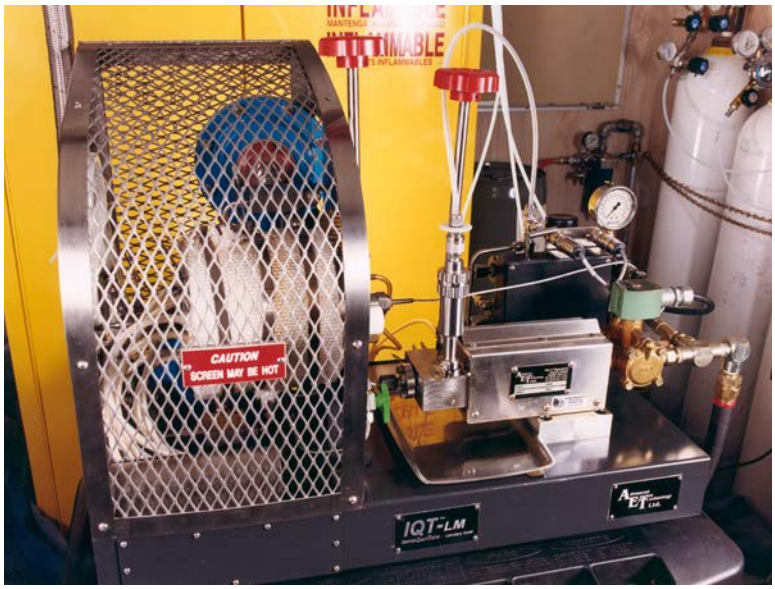

Figure 2-8. Ignition Quality Test Apparatus

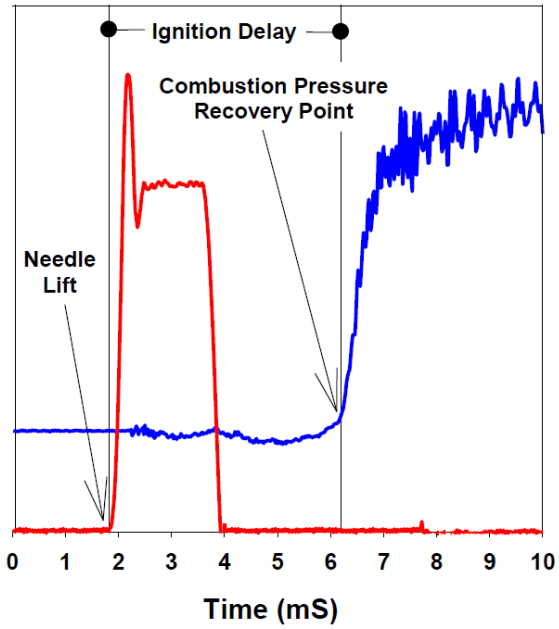

Figure 2-9. IQT measurement of ignition delay

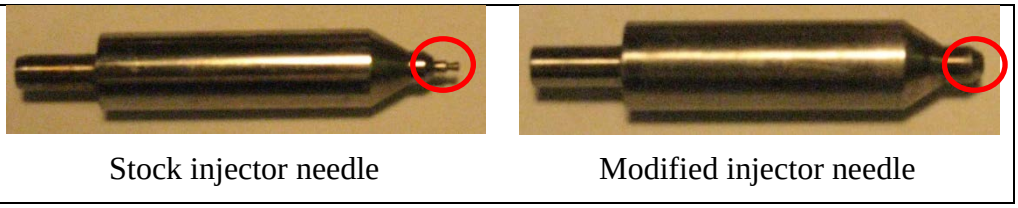

Figure 2-10. Injector needle modification

Table 2-3. Test Conditions

Combustion vessel temperature (°C)	568
Combustion vessel pressure (psi)	310
Fuel reservoir pressure (psi)	50
Fuel pump pressure (psi)	176
Gas concentrations: CO_2/O_2 (%)	70/30

Testing has been successfully performed to confirm that slurry composed of pulverized coal and isooctane combusts in the IQT. After isooctane was tested as a baseline, the 40% coal mixture with a 15 μm average particle size was tested. As can be seen in Figure 2-11, combustion did occur. However, the injector clogged after two injection events, requiring the injector to be removed and cleaned.

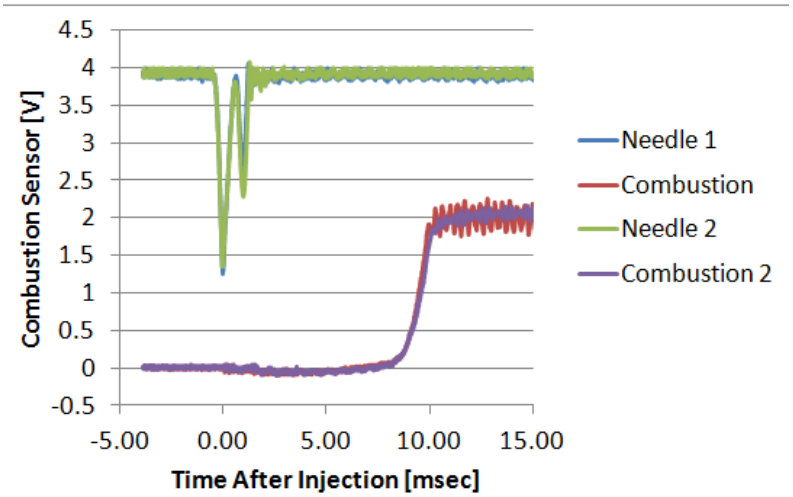

Figure 2-11. Initial testing with 40% coal fraction

The next fuel tested was the 20% coal slurry with average particle sizes of 7 μm, 7.5 μm, and 8 μm. Six injection events were performed before the injector tip clogged for the initial 7 μm case. Figure 2-12 through Figure 2-14 show the combustion trace and the injector needle movement for all the three particle size distributions. Looking at the needle movement of Figure 2-12, it is apparent that the injector was starting to clog during this run as the needle lift is not as high as previous runs and the opening duration is longer. It is interesting to note that the ignition delay was shorter for each consecutive run using the same particle size slurry. A working theory is that there are some hot coal particles that remain on the surface of the combustion vessel and may be mixing during injection. The impact of varying the coal particle size up to approximately 10% appears to be negligible, as the differences observed are within the bounds of repeatability.

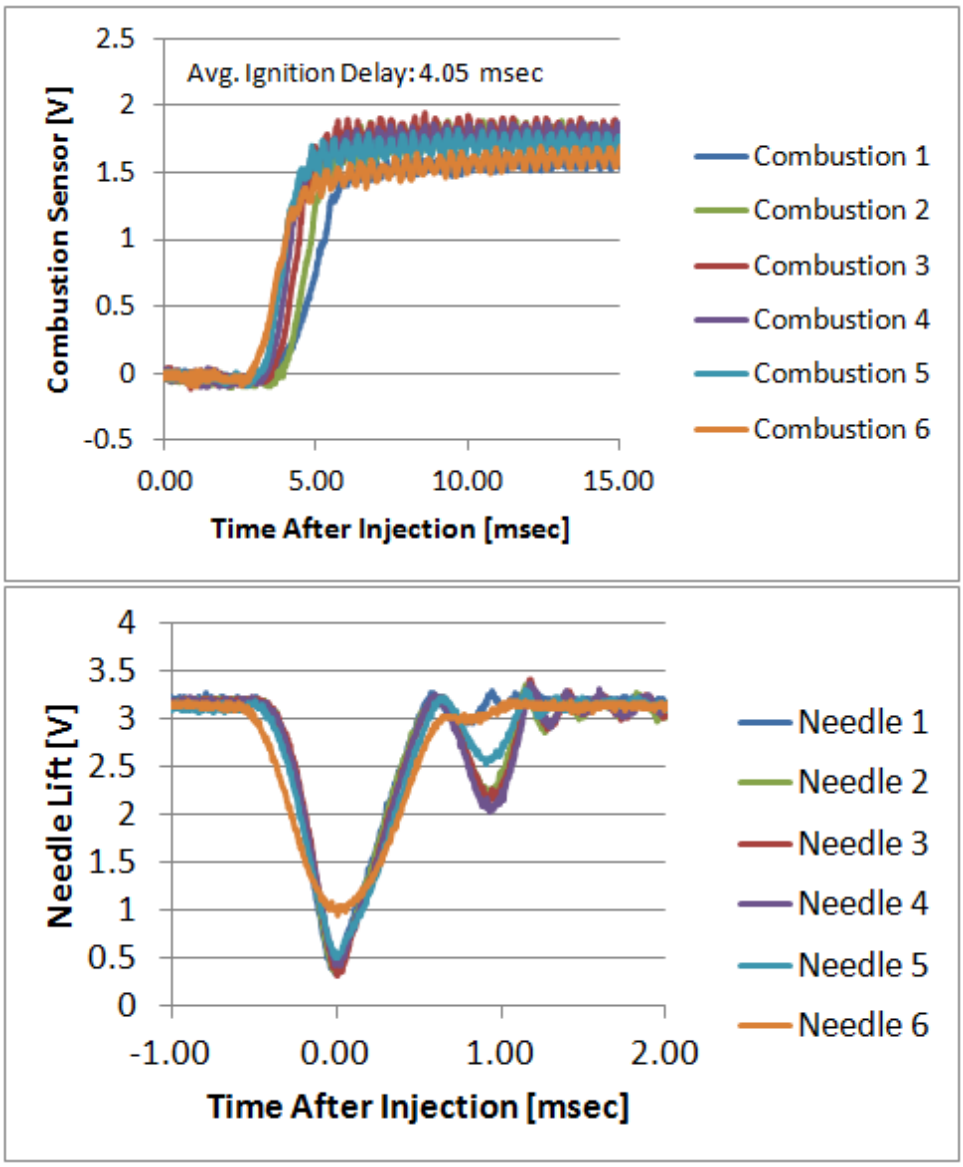

Figure 2-12. 20% coal fraction with 7 μm average particle size, (a) combustion trace and (b) injector needle movement

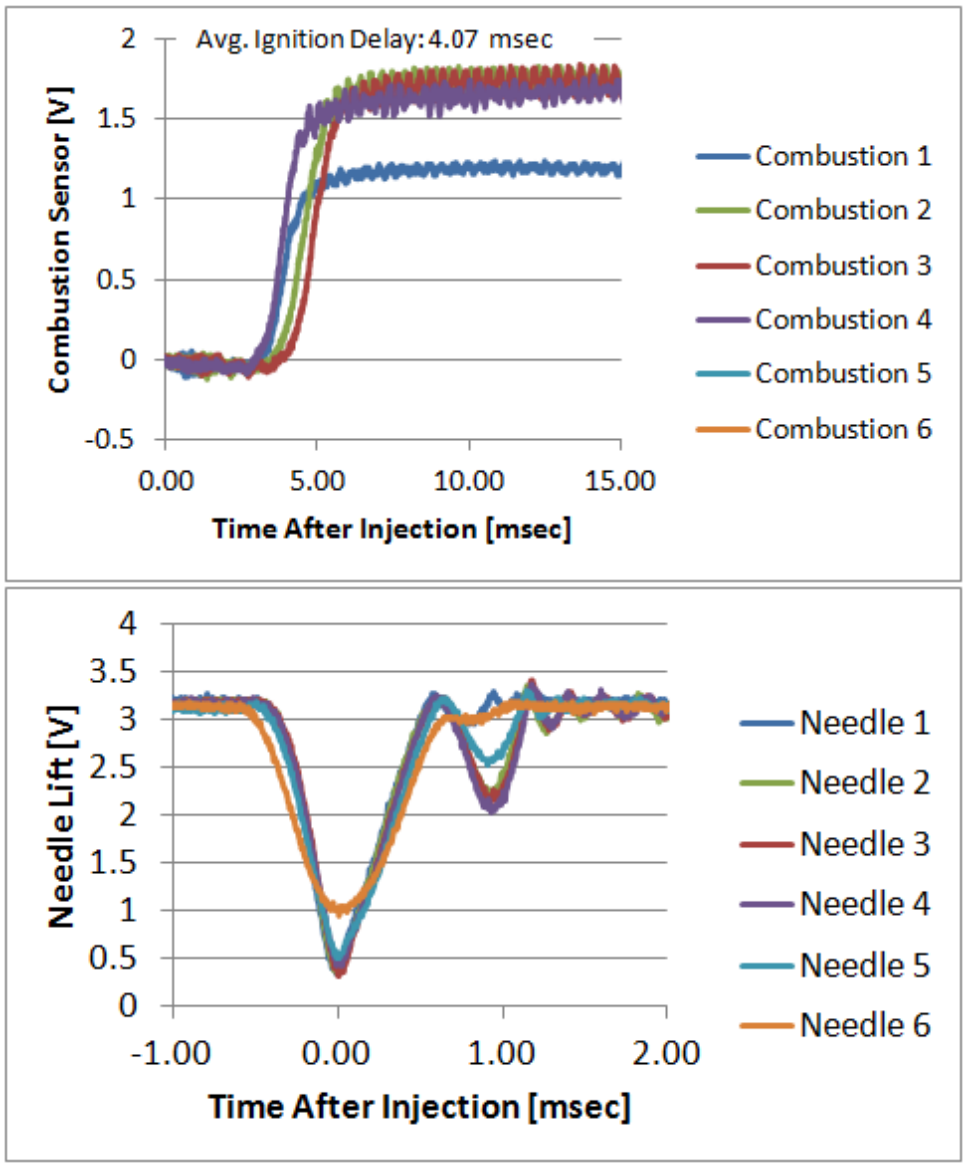

Figure 2-13. 20% coal fraction with 7.5 μm average particle size, (a) combustion trace and (b) injector needle movement

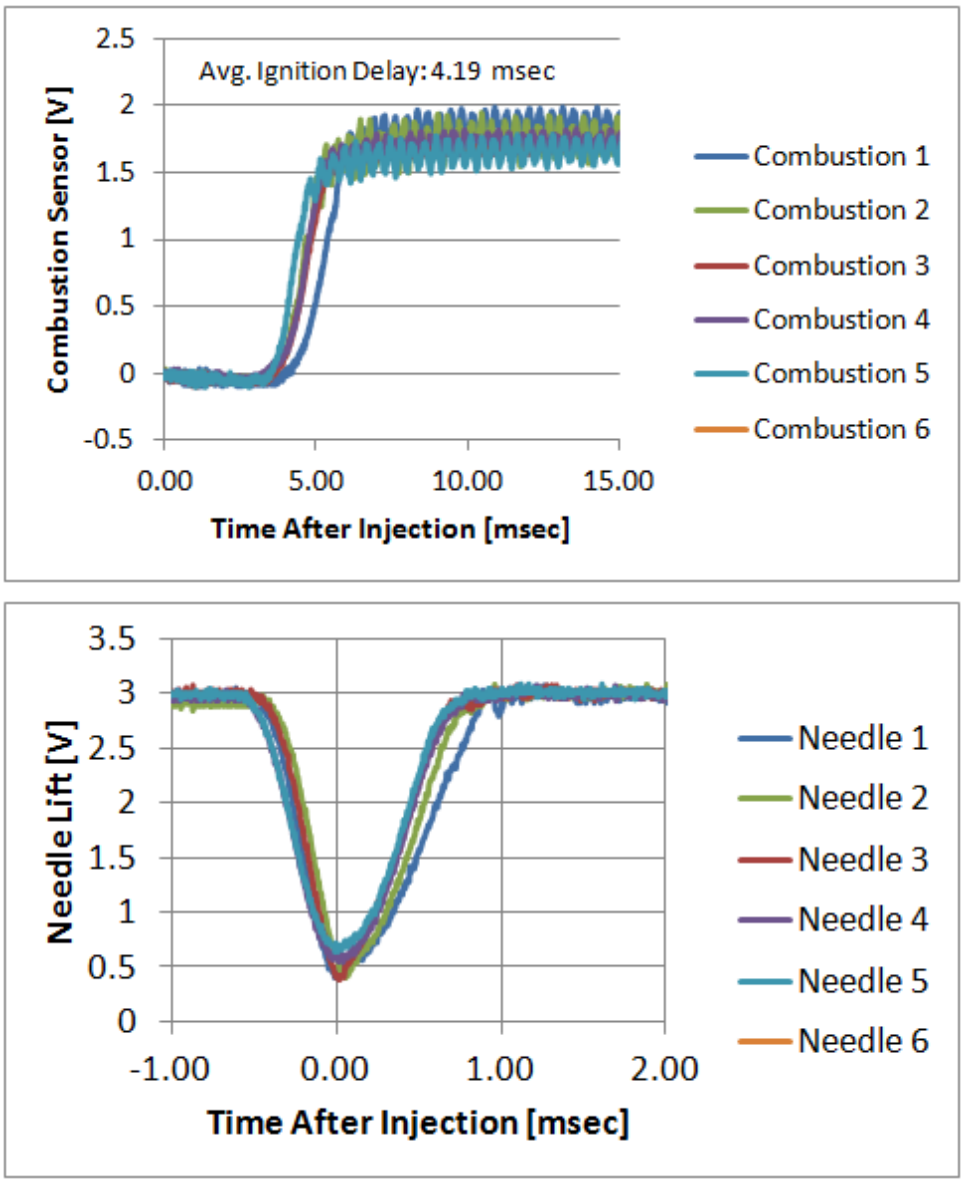

Figure 2-14. Coal fraction with 8 μm average particle size, (a) combustion trace and (b) injector needle movement

Comparing the fuel concentrations tested to date in Figure 2-15, it can be seen that concentration has a significant impact on the ignition delay. It was expected that the ignition delay would increase with increasing coal concentration in the slurry, but the trend is the opposite. The ignition delay was shortened from 10.25 msec with the isooctane baseline to about 4.1 msec with the 20% coal slurry concentration. The cause for this behavior has not been conclusively determined.

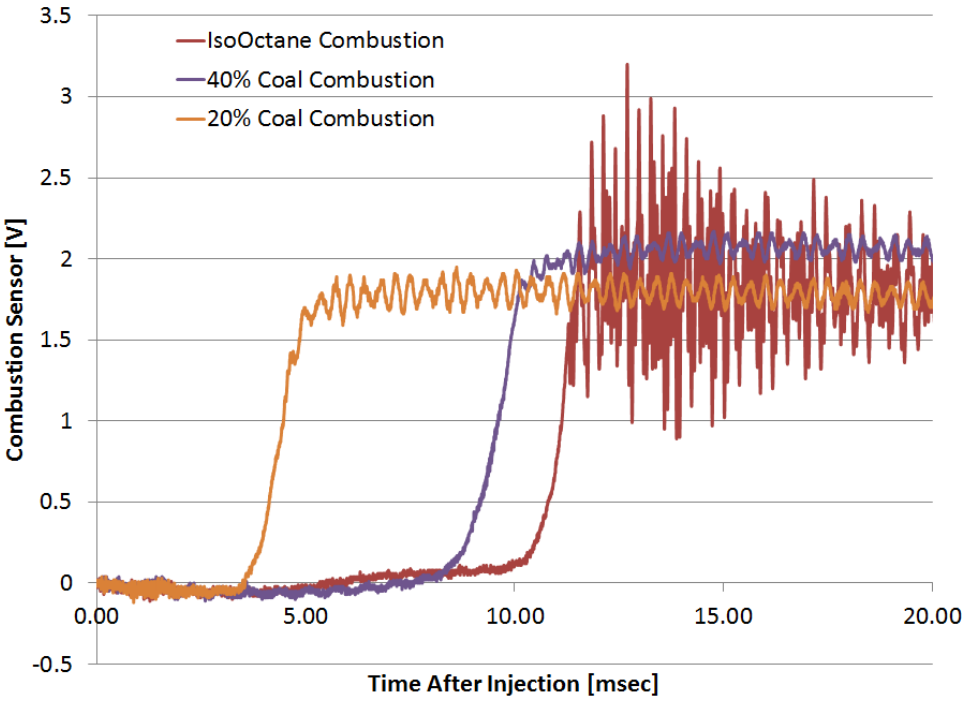

Figure 2-15. Comparison of fluids tested

The minimum temperature for ignition to occur was investigated by reducing the controlled skin temperature of the combustion vessel until stable combustion was no longer observed. Due to the high variance of this test, the results are approximate values only. The results of this test are detailed in Table 2-4. The minimum charge air temperature needed for stable combustion was approximately 400 °C for isooctane and 390 °C for the 20% concentration coal mixture with a 7.5μm average particle size. Cells highlighted in yellow are where partial burns or high variability in ignition delay was observed.

The final test was to attempt to combust a coal/water solution. Isooctane was decanted off the 20% concentration coal slurry and replaced with de-ionized water of a similar volume. This solution was unable to stay mixed for an acceptable period of time to load the injector, and therefore no injection events were possible.

Table 2-4. Details of minimum ignition temperature study

Fuel	Skin Temperature	Charge Air Temperature	Avg. Ignition Delay
	[°C]	[°C]	[msec]
Iso-Octane	568	538	9.7748
	500	475	12.4238
	450	420	27.321
	437.5	411	32.543
	431	406	38.695
	428	400	38.982
	426	399	40.705
	425	398	42.9845
	425.5	398	40.852
	400	376	no-combustion
20% Coal Concentration, 7.5μm Particle Size	423	395	20.052
	423	395	14.968
	420	394	21.167
	415	391	28.653
	400	376	27.879
	400	373	46.721
	400	373	27.209

Atomizer Testing

Achieving a consistent specified level of atomization of coal slurry is expected to be an important requirement for achieving successful oxy-combustion in a burner with large amounts of recirculated CO2. The use of an atomizer which employs a rotating element rather than a pressure to produce droplets of slurry of a size suitable for combustion is an attractive proposition for at least 2 reasons:

1. A rotary atomizer produces droplets by mechanical transfer of momentum to the slurry rather than through a sudden expansion through a fine orifice driven by imposed upstream fluid pressure. This allows the rotary atomizer to employ relatively large diameter passages that are less susceptible to clogging and erosion by slurry containing solid particles, some of which could be of larger than expected size.
2. In a rotary atomizer then energy imparted to the flow to be atomized is relatively, perhaps largely independent of flow rate, unlike the case of a nozzle where flow both flow rate and droplet size will depend strongly on imposed pressure. Droplet size can be controlled through variation of the speed of the rotating element, allowing the potential for successful operation with slurries with varying physical properties (i.e. ratio of coal solids to water, particle size).

As discussed in *Atomization and Sprays,*[4] rotary atomizers of various styles have been successfully employed in a variety of applications. A few examples of these applications include spraying of pesticides, application of paint, and for rapid drying of liquids into fine powders in processes such as the production of powdered milk. The rotary elements successfully employed in these applications have included a number of geometries. These include a variety of disks,

[4] A. H. Lefebvre, Atomization and Sprays, Hemisphere Publishing.

both smooth and with toothed edges, open cups and dishes, hollow wheels with holes in the outer edges, and vaned designs similar in shape to the impellers of centrifugal pumps and compressors. An impeller type rotary atomizer has been proposed by SwRI as the type most suitable for the oxy-combustion application.

One significant difference between most previous uses of rotary atomizers and the high pressure oxy-combustion application is in the density ratio between the liquid to be atomized and that of the surrounding fluid. Most of these previous applications involve dispersal of a liquid having a density similar to water into air or other gas at low pressure, in which the liquid is roughly three orders of magnitude more dense than the surrounding fluid. The dispersal of coal slurry into supercritical CO2 presents a markedly different situation in this respect in that the slurry and CO2 may well be of comparable densities. Of course the exact ratio will depend on the precise temperatures and pressures involved, but in some instances, the density ratio could be in the neighborhood of 1:1.

Since no complete self-consistent theoretical treatment of atomization exists, particularly one that is applicable to industrial machinery, the available predictive methods rely on empirical relationships the depend on correlation with experimental data collected for atomizers of specific styles and configurations. Moreover, while computational fluid dynamics (CFD) and combustion chemistry computations, and other numerically intensive physical computations will doubtless play a vital role in the engineering of a practical high pressure oxy-combustion burner, such computations will need to be supported by reliable and well calibrated empirical models for the initial atomization of the bulk coal slurry.

Lefebvre[5] contains an extensive treatment of models of atomization, including the various styles of rotary atomizers, and cites a number of references relating to them. Specific to vaned rotary atomizers, equations for predicting droplet sizes given by Friedman et al[6], Herring and Marshall[7], Fraser et al[8] and Scott et al[9] are described. However, these equations are based on experience with formation of liquid droplets in gases having much lower density than the liquid. Therefore, the accuracy with which these equations can predict atomization in high pressure oxy-combustion applications is not known. It would therefore appear to be useful to gain some experience with the atomization produced by impellers when working with two fluids having similar densities. Being able to predict atomization in such situations would provide useful insight for the engineering of an impeller type atomizer or oxy-combustion of coal slurry in high-pressure CO2.

2.4.3.2.1 EXPERIMENTAL APPROACH

Based upon the perceived need to gain some experience with atomizing a slurry in a fluid of a similar density, it was decided to undertake some exploratory experimental work during the current contract period with a fairly simple rotary atomizer apparatus. The approach taken was based on the supposition that relevant dynamics of atomization processes relevant to high-pressure oxy-combustion could be usefully studied in a “cold flow” apparatus using a simulated coal slurry and with the CO_2 represented by a liquid.

The intent was to provide some proof of concept experience for this technique. If preliminary tests were found to be promising, a more detailed and rigorous test program base on this

[5] A. H. Lefebvre, Atomization and Sprays, Hemisphere Publishing.
[6] S. G. F. a. M. W. Friedman, *Chem. Eng. Prog.*, vol. 48, no. 4, p. 181, 1952.
[7] W. a. M. W. Herring, *J. Am. Inst. Chem. Eng.*, vol. 1, no. 2, p. 200, 1955.
[8] R. E. P. a. D. N. Fraser, *Br. Chem Eng.*, vol. 2, no. 9, p. 196, 1957.
[9] M. R. M. P. J. a. L. R. Scott, *J. Pharm. Sci.*, vol. 53, no. 6, p. 670, 1964.

concept could be employed in follow-on work aimed at engineering a workable oxy-combustion burner.

As will be described below, flow visualization tests were run in a simulated combustor chamber using two immiscible liquids. One liquid was paraffin oil (kerosene) into which was mixed silicon carbide powder in order to make a slurry. Water which is immiscible with paraffin oil was used to simulate the high-pressure CO2 which would be circulated through the proposed oxy-combustion burner. A rotary atomizer, consisting of a radial-vaned impeller driven by a variable speed motor, was fed with bulk slurry through a manifold leading to the impeller inlet eye. The flow of droplets of slurry produced by the impeller was recorded with video which could be studied and from which still photos could be extracted.

2.4.3.2.2 EXPERIMENTAL APPARATUS

Figure 2-16 includes both a photograph of the test apparatus and an annotated diagram showing the major components. Principal physical dimensions of selected components are given in Table 2-5.

The outer boundaries of the simulated combustion chamber consist of a cylindrical tank with side walls and floor made of transparent acrylic. The tank is fitted with a removable lid in order to allow access to the components within. Two feed tubes are provided in the lid of the chamber to provide a flow of water that is used to simulate the CO2 flow that would be present in an actual combustion chamber. Likewise, a hole is provided at the bottom of the chamber to allow the water to exit. This drain hole is centered in the floor of the chamber. Water, which is used to represent the recirculated high-pressure CO2, is circulated through the chamber by means of a centrifugal pump.

Details of the slurry feed and water feed components are shown in Figure 2-17 and Figure 2-18. The slurry is introduced into the chamber through a rotary atomizer, which employs a centrifugal impeller with straight radial blades. The impeller is driven by a shaft connected to an electric motor with variable speed. Rotating speed is measured electronically via an optical pickup aimed at the drive shaft. The simulated fuel slurry is carried from outside through a feed tube which leads to a manifold that faces the eye of the impeller The impeller has a rotating shroud attached to its lower side. On its upper side it is unshrouded, but fits closely to the stationary wall of the fuel manifold. This serves to guide the flow of slurry in the impeller so that it exits from the impeller tips. In the photo comprising Figure 2-18 the impeller has been removed in order to show the inside of the slurry manifold and also the surfaces which face the unshrouded end of the impeller. The impeller is shown in Figure 2-19.

Two hemispherical shells were fitted near the upper and lower ends of the combustor simulation chamber. The purpose of these hemispheres is to serve as baffles that will divert the flow toward the outer walls of the chamber. The placement of the upper baffle is intended to create a re-circulation or “dead water” zone ahead of the impeller which in an actual combustor would increase the residence time of the burning slurry so that complete combustion is achieved before exiting the combustion chamber. The lower baffle forces the flow to pass to the outside of the chamber, rather than being drawn directly to the center exit hole. For the present trials the hemispherical baffles used were approximately about 5.7 inches in diameter. Baffles of this size have a cross-sectional area of about 52% of that of the cylindrical area of the chamber. This causes the water velocity to increase as it passes the baffles. Provision is made in the present configuration for adjusting the vertical position of both baffles. Movement of the upper baffle allows its position relative to the impeller to be altered, while movement of the lower baffle allows the effective overall length of the simulated combustor to be varied. In this manner, the position and extent of a recirculation zone can be varied.

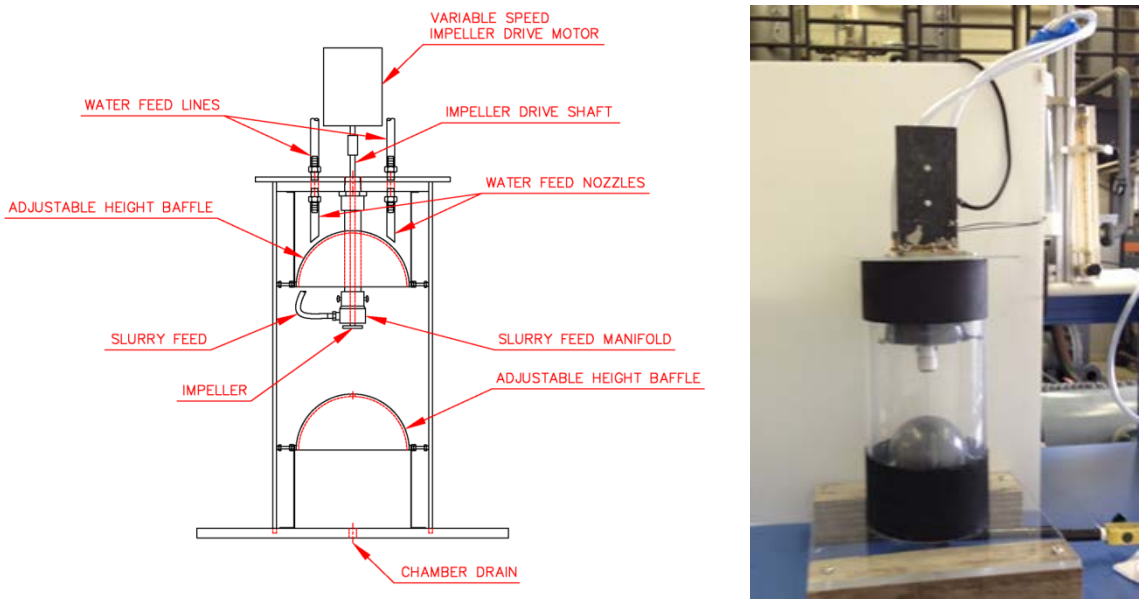

Figure 2-16. Experimental cold-flow combustor simulation apparatus. Left: Diagram at left shows major components. Right: Photo of apparatus configured for tests.

Table 2-5. Principal Dimensions of Test Apparatus

Chamber Inside Diameter (inches)	7.88
Useable Chamber Depth (inches)	16.81
Impeller Diameter (inches)	0.99
Impeller Exit Width (inches)	0.12
Number of Impeller Blades	6
Diameter of Hemispherical Baffles (inches)	5.69

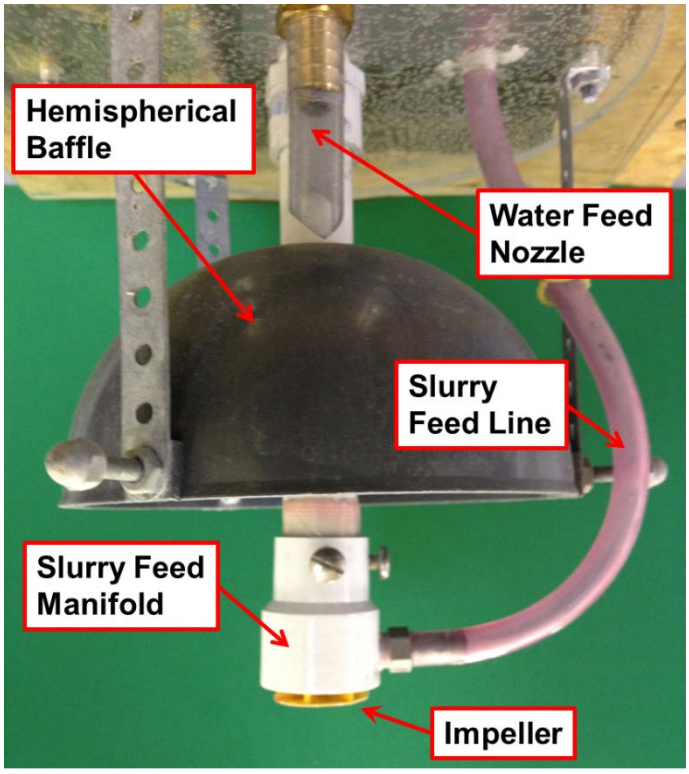

Figure 2-17. Components of slurry feed and impeller atomizer system

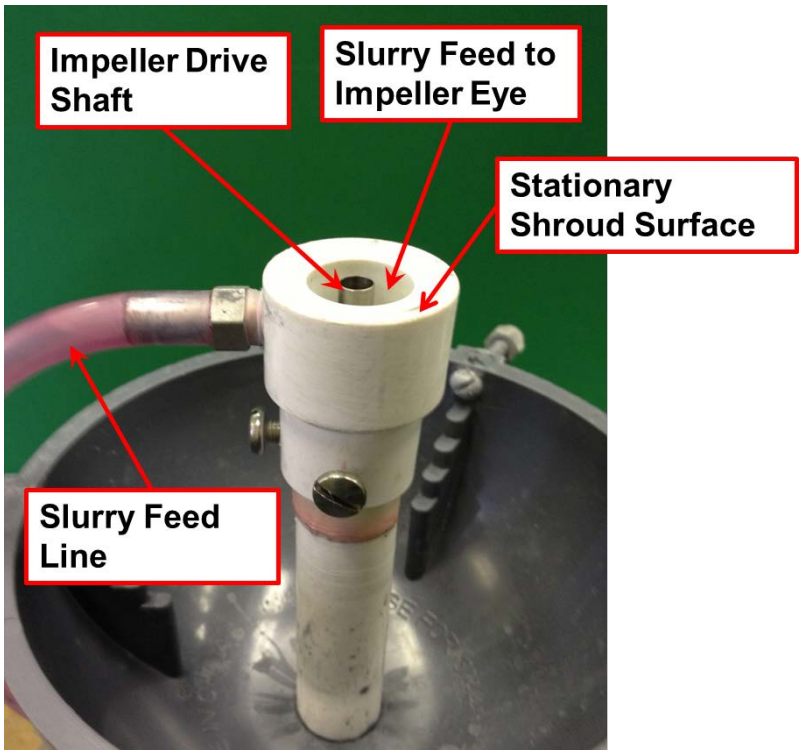

Figure 2-18. Impeller removed to show details of slurry feed system and impeller drive

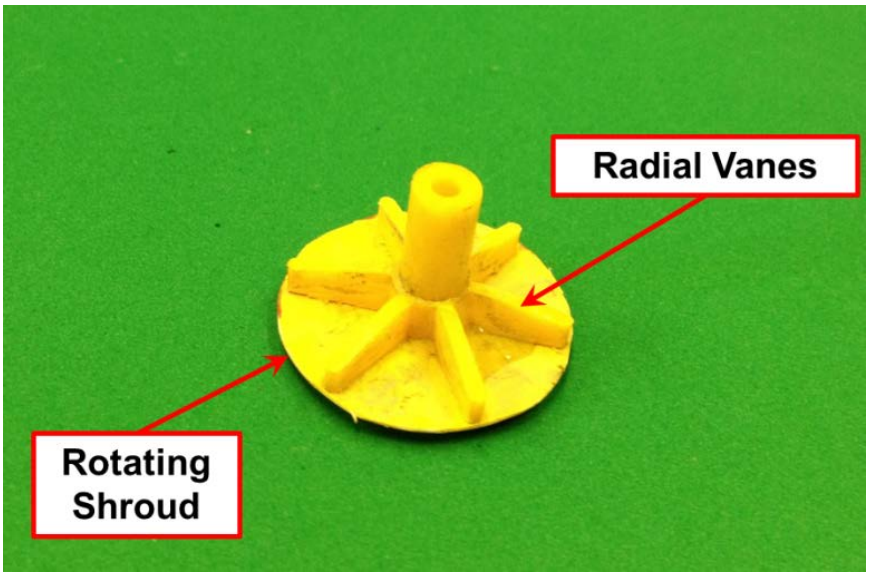

Figure 2-19. Details of slurry impeller

2.4.3.2.3 WATER CIRCULATION SYSTEM

Figure 2-20 is a schematic diagram showing the configuration of the circulation system for the water. A centrifugal pump is connected to the sump at the bottom of the test chamber, and provides suction to pull the water through the chamber. Following the pump, the flow passes through a flow meter of the rotameter type. Following the flow meter, the water enters a manifold. There is a single inlet to the manifold, but two exits, which serves to split the flow into two streams for being fed into the chamber. Orienting the manifold with the two feed lines pointing downward was found to be beneficial in separating any air the system, thereby helping to prevent air bubbles entering the chamber.

For the exploratory tests carried out during the present contract period, the closed loop configuration shown in the figure was deemed to be desirable. Since the source of water fed to the chamber through the feed tubes is that which is extracted from the chamber exit by the pump, the water level in the chamber remains very nearly constant. However, after a short period of running some of the slurry, particularly small droplets that are easily carried by the water, tended to cloud the fluid. For future tests, an open loop arrangement with provision for level control in the combustion chamber and/or an effective system to filter out slurry that exits from the chamber may be needed. This would be especially helpful if long running durations are desired in future tests.

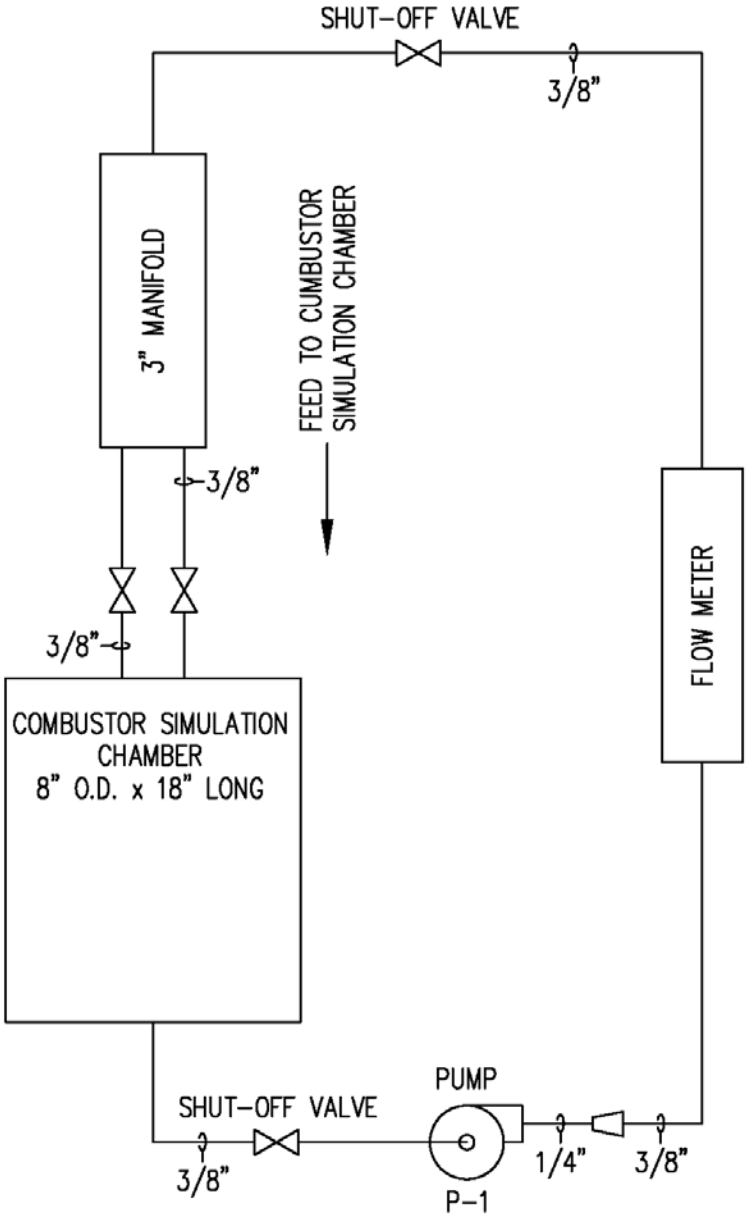

Figure 2-20. Schematic of water circulation system

2.4.3.2.4 MATERIALS USED TO SIMULATE HIGH-PRESSURE CO_2 AND COAL SLURRY

Several factors were considered in choosing the materials used to represent the high pressure CO_2 and coal slurry. They included:

- Immiscibility of the two fluids – Droplets representing the slurry should have minimal propensity to mix with the fluid representing the high-pressure CO_2.
- Transparency of the simulated CO_2 – Fluid should be clear or at least have sufficient transparency to permit easy visualization and photography.

- Appropriate density – Slurry and simulated CO_2 should have densities of the same order of magnitude, with slurry having the higher density of the two.
- Safety and environment – Fluid used in the quantities required to simulate the CO_2 should not be present a flammability or toxicity hazard. Fluids should be compatible with apparatus (not attack materials) and not present an environmental hazard.

After consideration of various options, it was chosen to use water for the simulation of the CO_2 component. The slurry used consisted of silicon carbide powder mixed with paraffin oil. The density of Paraffin oil is approximately 0.8 g/cm^3, about 20% less than that of water. Silicon carbide is considerably heavier than water with a density of about 3.2 g/cm^3. The result of this density difference is that the buoyancy of the slurry can be varied over a fairly large range of negative and positive values simply by varying the proportion of silicon carbide powder to paraffin oil.

The density of the slurry is plotted as a function of the weight percentage of silicon carbide powder used in Figure 2-21. The plot shows that the slurry becomes neutrally buoyant in water when the percentage of silicon carbide powder used is about 27% by weight. For the tests carried out in this phase, the slurry was composed of equal weights of silicon carbide and paraffin oil, yielding a density about 28% greater than that of water.

The slurry composed of silicon carbide powder and paraffin oil takes on the dark grey color of the powder and is opaque. This provides good contrast for photos and videos, particularly when a light colored surface is placed behind the chamber.

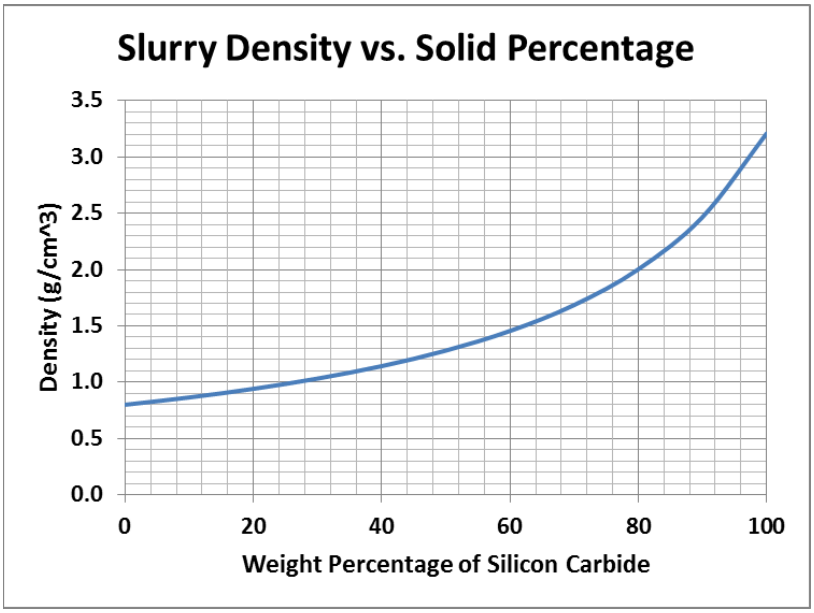

Figure 2-21. Variation of density of slurry made of paraffin oil and silicon carbide with proportion of solid constituent

2.4.3.2.5 TESTS AND RESULTS

During the present contract period, a short series of tests was run with the cold-flow chamber with impeller atomizer. The primary goal of these tests was to demonstrate the viability of the apparatus for studying slurry injection and droplet formation. In other words, the primary intent was to demonstrate proof of concept. These rather preliminary tests were sufficient to show that the concepts and apparatus produced a droplet spray that could be studied using flow visualization techniques. The results obtained show that such a cold flow apparatus, perhaps

after some further development and fine tuning of technique, is likely to provide useful guidance for the design of a coal slurry combustor using an impeller for fuel distribution.

2.4.3.2.6 TESTS CONDUCTED IN A STATIC CHAMBER

Initial tests were run without circulating water through the chamber (circulating pump was shut off). In these tests the slurry was injected through the impeller both with the impeller switched off, and with the impeller running at (approximately) 500 and 1000 RPM. The slurry was fed at a slow (but not measured) rate. This meant that there was very little flow through the impeller, compared to its design value as a pump impeller. This amounts to running the impeller essentially at what would be termed as “shutoff” conditions in a pump.

Figure 2-22 shows images of the droplets produced when the impeller is not turning. In this case, the slurry simply drips out of the impeller passages due to the action of gravity. A slurry droplet breaks off from the bulk of slurry inside the impeller when a droplet grows to a size sufficient for its weight to overcome the surface tension force. By reference to the geometry of the apparatus in the images, the size of the droplets are observed to be approximately 0.3 – 0.4 inches (~8-10 mm) in diameter.

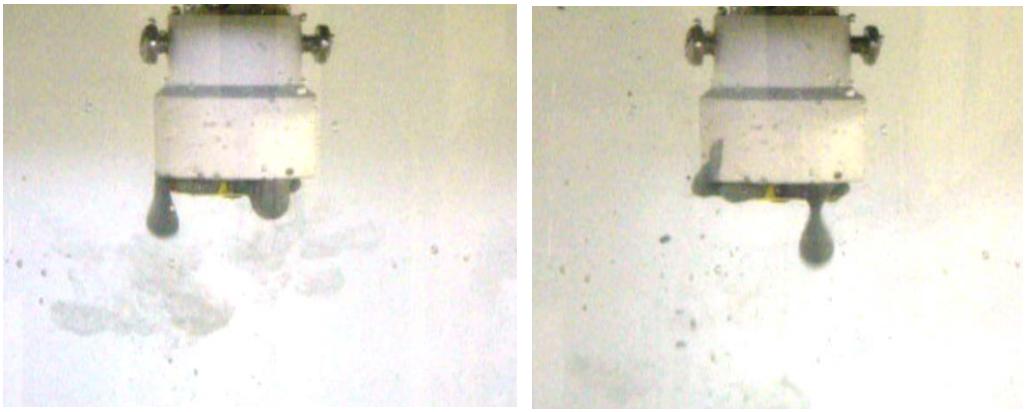

Figure 2-22. Droplets produced when impeller is static

Figure 2-23 shows two stills captured from video taken when the impeller was rotating at 500 RPM. With the impeller of the size fitted (0.99 inches diameter) the tangential speed at the tip is about 2.2 ft/sec. Unfortunately, the images captured for this case were of rather poor quality, but they are sufficient to show that the action of the impeller is producing smaller droplets from the slurry feed. It appears that the diameter of the majority of the droplets is comparable with the dimension of the impeller exit height (0.12 inches or about 3 mm). Review of the video shows that the large droplets travel radially only no more than about 1 impeller diameter in the time that they are within the field of view, and appear to have lost much of the momentum imparted by the impeller. No evidence is observed of breakup into smaller droplets after exit from the impeller.

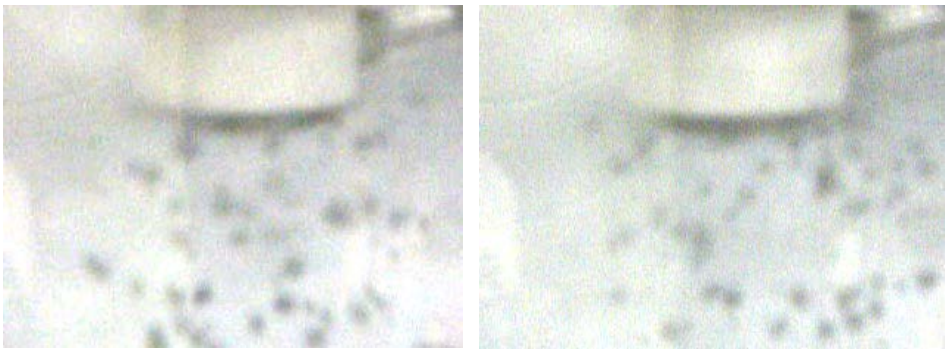

Figure 2-23. Droplets produced with impeller turning at 500 RPM

When the speed was increased to 1000 RPM, giving an impeller tip speed of about 4.4 ft./sec, the droplets exiting from the impeller became considerably smaller. See Figure 2-24. The higher momentum of the droplets also allowed them to travel further in the horizontal direction, with some appearing to strike the outer walls of the chamber. The diameters of the larger droplets seen in the photos appear to be approximately in the range of 1/3 to ½ of the 0.11 inch impeller tip width dimension. This range of sizes would range from slightly under 1 mm to perhaps about 1 1/2 mm. Owing to their smaller size, the droplets had a visibly slower falling velocity than did the larger droplets emitted in the previous cases.

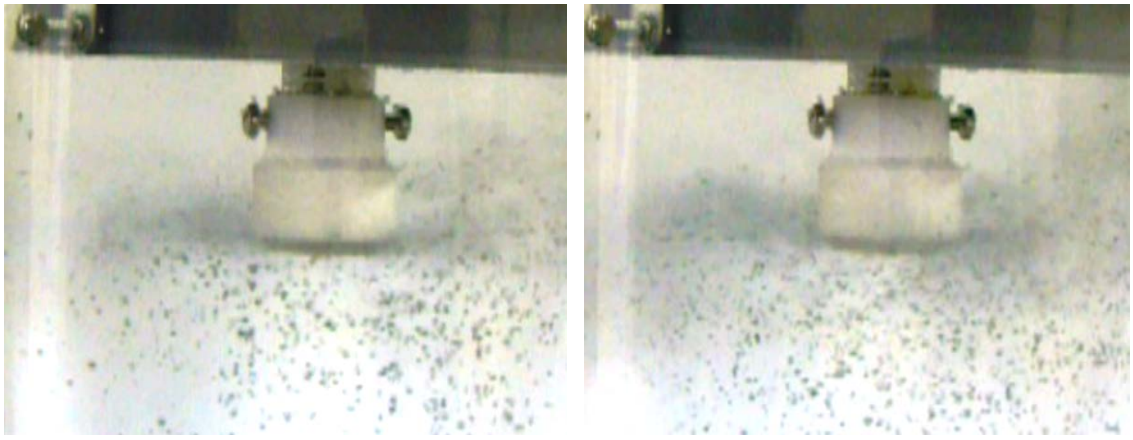

Figure 2-24. Droplets produced with impeller turning at 1000 RPM

With the increase of speed, one feature which emerged was a cloudy appearing region which formed around near the slurry manifold at a height slightly above the plane of the impeller. It appears that either these are very small droplets of slurry, or alternatively may be solid particles that have somehow become separated from the paraffin oil. This may have occurred due to the particles either settling out of the oil, or perhaps from shearing forces exerted by the impeller. In any case, these small particles appeared to be small enough to essentially follow the flow of the surrounding water.

Examination of the videos also shows a small fraction of the larger particles also being carried upward into the cloudy region. It therefore appears that there is at least a small region of flow with a strong upward component. It is hypothesized that this may occur because the flow exiting the impeller is at a higher pressure than in the surrounding tank, and that a portion of this higher pressure flow turns upward when it reaches the edge of the outer diameter of the slurry manifold.

There was little in the way of evidence for further breakup of large droplets occurring in the regions away from the impeller where the individual droplets could be seen clearly. It appears that by this stage, they had dropped below the velocity needed for further atomization.

2.4.3.2.7 TESTS WITH FLOWING WATER

Following the tests described above, observations of the slurry atomization were made with the circulating pump activated. With the current configuration and the chosen pump, flow rates in the chamber of only about 1.75 gallons/minute were achievable. This flow rate produced an average vertical velocity in the open region of the chamber (flow rate divided by net cross sectional area) of about 0.14 in/sec. In the region where the hemispherical baffles block part of the chamber cross section, the average velocity would be about 0.29 in/sec at the achieved flow rate. These velocities are quite modest compared to impeller tip speeds, but some effect was seen on flow patterns, particularly near the outer part of the chamber.

For this test, the impeller rotating speed was approximately 1100 RPM, slightly higher than that used previously. In addition for this test, higher fidelity photo equipment was used which permitted more detail to be observed. As might be expected, the droplet formation observed was quite similar to that which was observed when there was no water circulation through the chamber. However, near the chamber walls some effect of the through-flow could be seen; droplets approaching the walls could be seen to turn downward as they reached positions at or near the outer rim of the hemispherical baffles. It is expected that a larger pump producing higher chamber through-flow velocities would show this effect in a much more pronounced manner. In an actual combustor, such turning of the flow would keep burning slurry particles from imposing excessive temperatures on the combustor chamber walls. Figure 2-25 shows two still images of the droplet pattern produced in this test case. The improved photo quality shows the droplets and the cloudy produced by the small dispersed particles to good advantage. Some frame by frame review of video clips did not show instances of the larger diameter particles breaking up. The images do however show that the larger droplets present are fairly consistent in terms of their diameter.

Figure 2-25. Droplets produced with impeller turning at 1100 RPM and 1.75 gpm water flow rate through chamber.

2.4.3.2.8 ANALYSIS OF DROPLET SIZES

In this section, a comparison is made between the size of droplets observed above, and a theoretical minimum size of a spherical droplet moving at a particular speed. As described in Lefebvre [10], the breakup of fluid droplets moving in a stream of surrounding fluid is governed by the relationship of external aerodynamic forces on the droplet and surface tension forces

[10] A. H. Lefebvre, Atomization and Sprays, Hemisphere Publishing

exerted within the droplet. For droplets moving through a given fluid, breakup can only occur if the aerodynamic forces are sufficient to overcome the surface tension forces which tend to hold the droplet together. Since the aerodynamic forces increase with velocity, it follows that for a droplet of a given size there will be a "critical speed", U_{crit}, at which the aerodynamic forces are just equal to the surface tension forces

Below the critical speed, aerodynamic forces cannot overcome surface tension and no breakup of the droplet can occur. Above the critical speed, the aerodynamic forces exceed those exerted by surface tension, and the process of breakup may occur. Even when the critical speed is exceeded, droplet breakup is not necessarily guaranteed, particularly if the droplet decelerates below critical speed more quickly than it takes for the breakup process to occur.

Assuming for purposes of the calculation that the droplets are approximately spherical, the surface tension force holding a droplet of slurry together is given by;

$$F_{surf} = \pi \sigma_{slurry} D$$

where D is the diameter of the droplet, and σ_{slurry} is the surface tension of the slurry. The aerodynamic force on the spherical droplet when moving at the critical speed through water is the aerodynamic drag force given by;

$$F_{drag} = \frac{1}{2} \rho_{water} U_{crit}^2 C_D \pi \frac{D^2}{4}$$

where, ρ_{water} is the density of the water, and C_D is the drag coefficient of the droplet. For low-speed flows, the dimensionless drag coefficient is a function of the Reynolds number of the moving droplet. When the droplet is moving at the critical speed, and using the symbol μ_{water} to represent the viscosity of the water, the Reynolds number of the droplet is given by;

$$Re = \frac{\rho_{water} U_{crit} D}{\mu_{water}}$$

For a range of Reynolds number from about 0.2 to 2000, the drag coefficient of a sphere may be approximated by (See Reference II);

$$C_D = 0.25 + \frac{6.3}{\sqrt{Re}} + \frac{21.12}{Re}$$

These formulas were used to calculate the critical speed for a range of droplet sizes. For these calculations, the parameters shown in Table 2-6 were used. Since the surface tension of the slurry had not been measured, it was taken to have the same value as that of the paraffin oil carrier fluid.

Table 2-6. Parameters used in calculation of critical droplet velocities

Parameter	Value
ρ_{water}	1000 kg/m^3
μ_{water}	1.002×10^{-3} Pa-s
σ_{slurry}	0.027 N/m

The calculated critical speeds are plotted for a range of droplet diameters in Figure 2-26. Also included are the impeller tip speeds for the 500 and 1000 RPM tests, plotted against the average observed droplet diameters produced at these speed settings. What the plot indicates is that tip speeds somewhat higher than the calculated critical breakup velocity is required to produce droplets of a given diameter. However, while the required tip velocities are higher, they are still of the same order of magnitude as the calculated critical velocities. It is to be expected that the impeller mechanical speed would need to be somewhat higher because;

1. The slurry ejected from the impeller would not be expected to achieve the full mechanical speed of the impeller. This is because there is some fluid dynamic "slip" between the impeller and the fluid; the slip phenomenon is well known in the design of pumps and compressors.
2. Even if droplets enter the fluid with velocities above the critical value, the drag forces may cause the droplets to decelerate below the critical value before the process of breaking the surface tension has occurred.

It should be pointed out that the quantitative values of the increment of impeller speed required as reported here are of a somewhat preliminary nature. Experiments with more precise measurement of droplet size and more careful monitoring of impeller speed and control of slurry injection rates would help to quantify more precisely the velocities needed to produce droplets of a required size. An additional factor that also needs further study is the surface tension of slurries of various compositions. It was assumed in making the calculations that the slurry had the same surface tension as that of paraffin oil. Such a study of the effects of slurry composition on surface tension and perhaps other relevant fluid properties (such as viscosity perhaps) would also appear to be important for the coal-water slurries to be used in combustion experiments if these values have not been adequately quantified already.

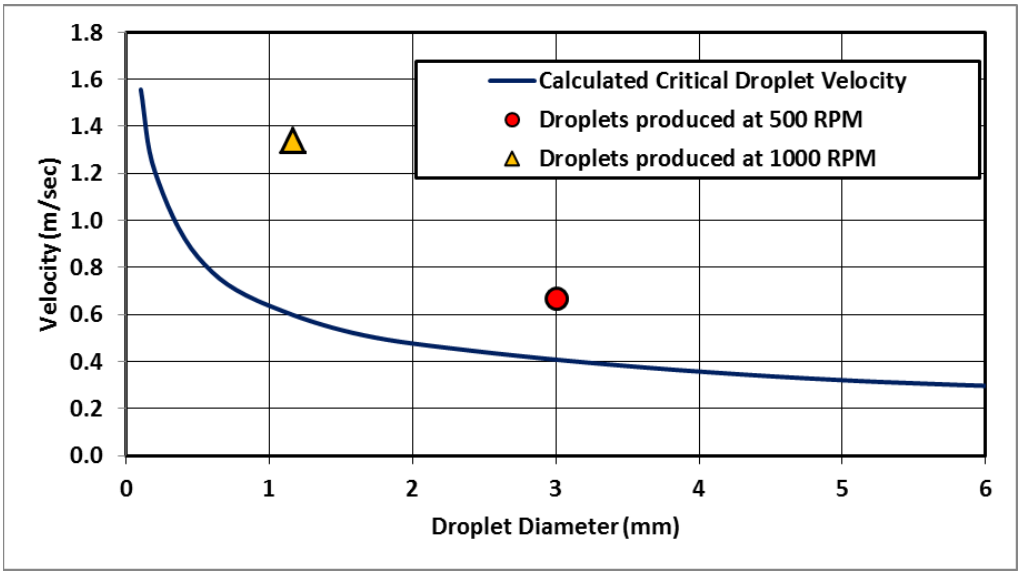

Figure 2-26. Comparison of calculated variation of critical velocity of slurry droplets with diameter to observed droplet sizes produced by different impeller tip speeds.

2.4.4 SUBTASK 2.4 – INITIAL SYSTEM LEVEL MODEL IMPLEMENTATION

Initial Aspen Plus models included generic coal combustion models and supercritical CO2 power blocks for use as verification cases to demonstrate and check assumptions inherent in the cycle models. Equations of state, including REFPROP, PENG-ROB, and RKASPEN were evaluated for the anticipated conditions and gas compositions. The three equations of state all provided reasonable agreement for the supercritical power block; however, RKASPEN was the only equation of state that could handle both the supercritical CO_2 and the non-conventional solids required to model the coal based combustion. Figure 2-27 shows a process flow sheet for a sCO_2 power cycle from literature.

Models were developed to evaluate the efficiencies of the power blocks for the respective cycle configurations using a generic thermal input device, along with a model of the supercritical combustor for eventual integration with the power blocks. The decoupling of the combustor and the power blocks enabled rapid optimization and evaluation of cycle configurations and conditions using relatively simple models, minimizing the time needed to modify and solve complex integrated models to evaluate certain parameters. An example parametric study of thermal to electric conversion efficiency for the cryogenic power block using a generic heating element is shown in Figure 2-28 and Figure 2-29.

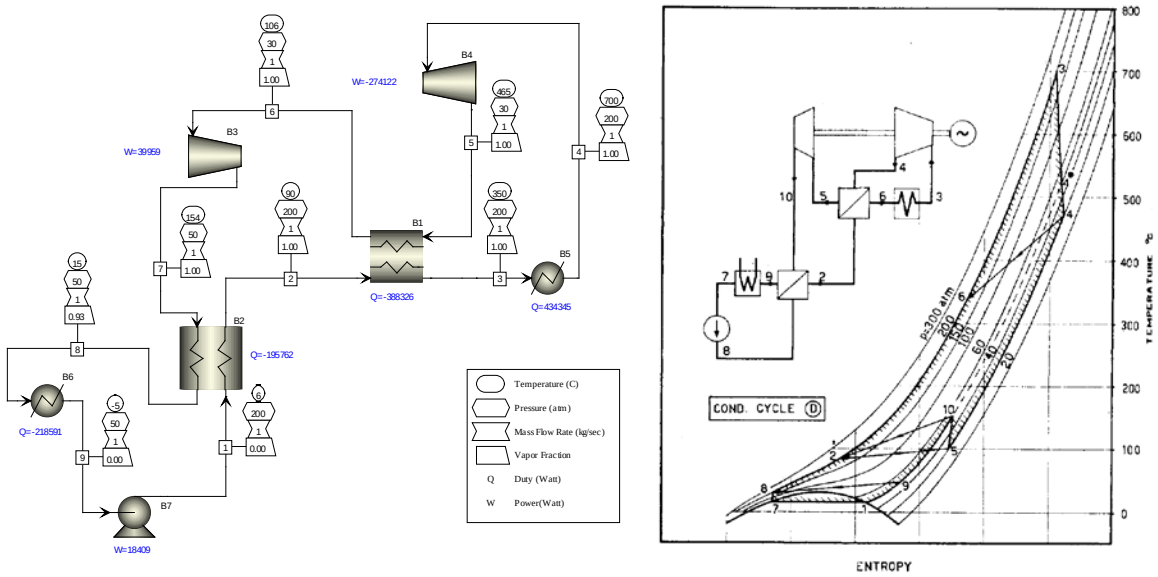

Figure 2-27. Supercritical CO_2 power cycle verification case from literature[11]

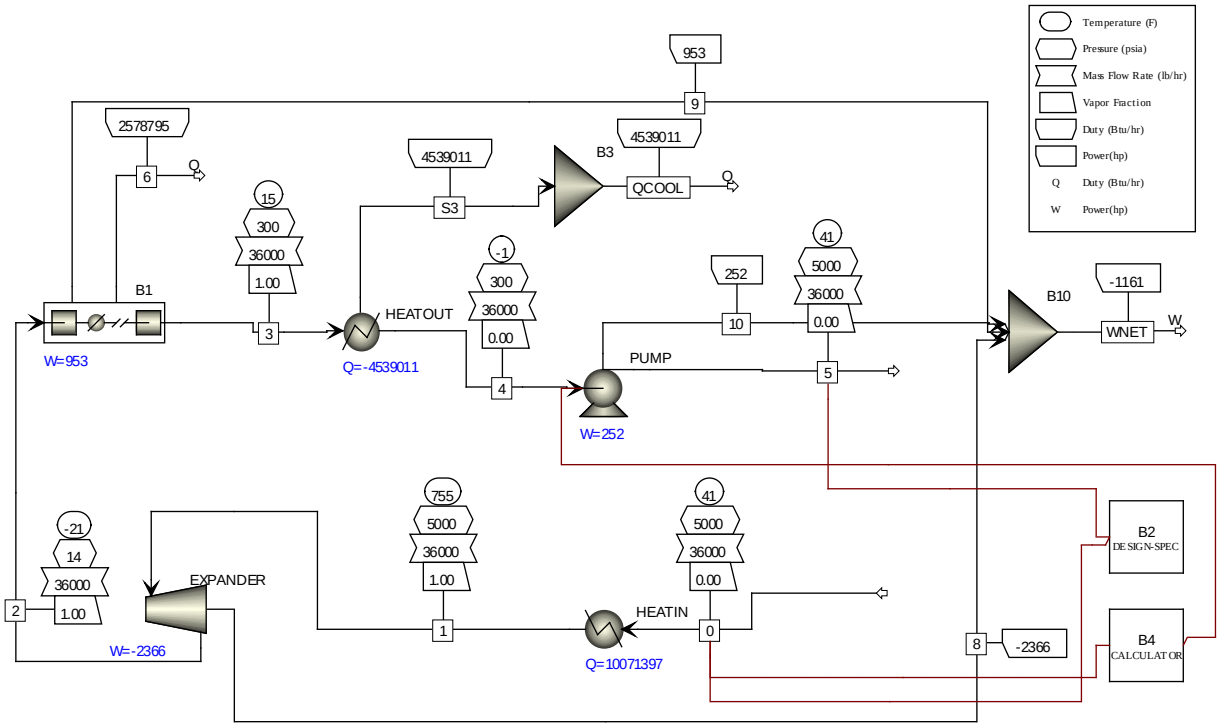

Figure 2-28. Aspen Plus layout of the cryogenic oxy-combustion power block using an idealized thermal source

[11] G. Angelino, "Carbon Dioxide Condensation Cycles for Power Production," *Journal of Enginering for Power.*

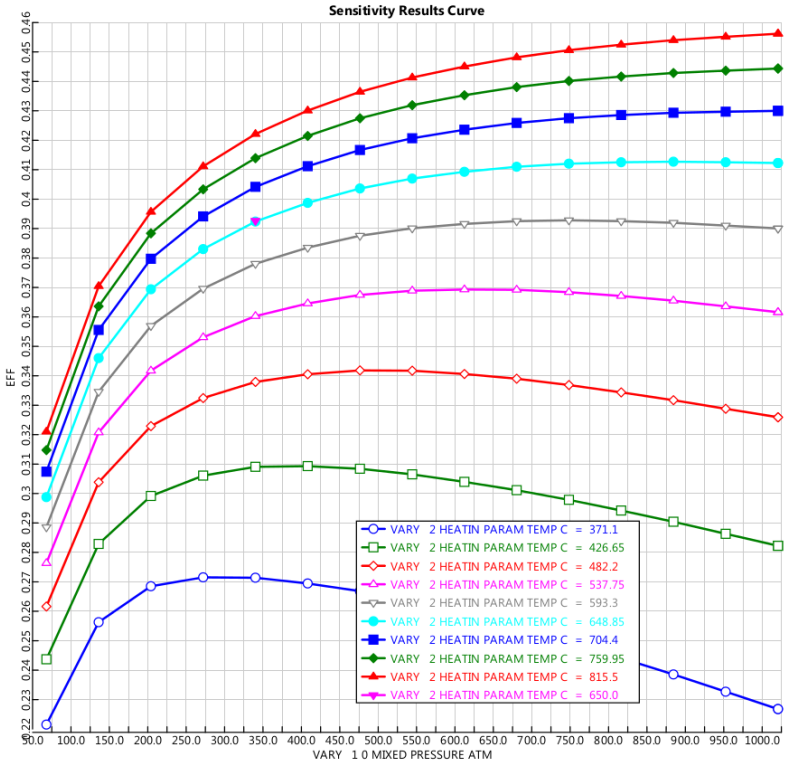

Figure 2-29. Cryogenic oxy-combustion power block efficiency as a function of pressure and temperature

2.4.5 SUBTASK 2.5 – INITIAL ECONOMIC MODEL IMPLEMENTATION

The economic cost analysis was performed using the *NETL Power Systems Financial Model (PSFM)* in accordance with *QGESS: Cost Estimation Methodology for NETL Assessments of Power Plant Performance*. The PSFM was used to evaluate costs for two indirect supercritical oxy-combustion cycle configurations which were selected during the technical evalustion of the power cycles based on their thermodynamic performance.

As part of the Technical Gap analysis undertaken for this project, data for equipment size, availability and cost were routinely collected and reported within the various chapters. In some cases – such as cyclones for particulate removal – the technology is well commercialized and cost quotations were obtained for the size of equipment needed for the model 550-MW power plant. For many other process components, however, the stage of technology development is too immature, and no commercial example exists. In such cases, the knowledge gained through literature searching and subsequent analysis was put to use to formulate our own cost estimates.

2.4.5.1 PRESSURIZED OXY-COMBUSTION - SINGLE POWER BLOCK

A summary of the estimated equipment costs is presented in Table 2-7 for the case of a single power block. The results for a dual power block are presented later in this chapter. The data in Table 2-7 are for the Bare Erected Costs (BECs) for the "Core" components of the oxy-combustion plant – including a power block that is the subject of another DOE investigation[12] –

[12] DOE Cooperative Agreement No. DE-EE0005804, "Development of a high efficiency hot gas turbo-expander and low-cost heat exchangers for optimized CSP supercritical CO2 operation."

as well as for “Ancillary” systems that were not part of the Tech Gap analysis of this study but would nonetheless be required for the model power plant. The cost data for these systems were drawn from Document DOE/NETL-341/082312, “Updated Costs (June 2011 Basis) for Selected Bituminous Baseline Cases,” adopting Case 12 (supercritical pulverized coal with sequestration) as the basis of comparison.

The core and ancillary categories of equipment correspond to the “process equipment” and “support facilities” categories as prescribed by NETL’s *Quality Guidelines for Energy System Studies* (QGESS).[13] To the sum of these capital costs, $1,428 million, a factor of 80% was applied to account for installation costs. This brings the total BEC for a 550-MW pressurized coal-burning oxy-combustion plant, including support facilities, to $2,481 million, as shown in Table 2-7. Finally, in preparation for applying this estimate to NETL’s *Power Systems Financial Model* (PSFM), a surcharge of 10% was tacked on to account for Engineering Project Costs (EPC), in accordance with QGESS. The new figure, $2,729 million, was input on the Plant Inputs page as EPC “Initial capital and financing costs.” The remaining rows of data shown in Table 2-8 are for cross-checking of the PSFM model. These rows make use of parameters that were entered into the PSFM model (as shown in the “Factor” column), but the ensuing lines for Total Project Costs (TPC), Total Overnight Cost (TOC) and Total As-Spent Capital (TASC) were made without recourse to the many PSFM tools for fine-tuning finance costs. The difference between this hand calculation and the more rigorous PSFM calculation is 5.5%, which is considered close enough for confirmation purposes.

[13] “Cost Estimation Methodology for NETL Assessments of Power Plant Performance,” DOE/NETL-2011/1455, April 2011.

Table 2-7. Estimated equipment costs, 550 MW pressurized oxy-combustion power plant, single power block

Process equipment	Base cost $ Million	Units operating	Spare cost $ Million	Spares on hand	Total $ Million
Core systems					
Cyclones, inc. linings, peripherals	$53	18			52.7
- Spare cyclones			2.9	2	5.9
FGD, inc. metals removal	$45	1			45.0
-- Spare scrubber		6	1.7	1	1.7
-- Spare hydrocyclone		12	0.1	2	0.2
Piping, combustion side	$30	1			29.9
ASU ex pumps	$160	4			160.0
-- Standby ASU spare			40.0	1	40.0
Pumps for liq. O2	$6	8			6.0
-- Spare pump			0.8	1	0.8
Coal slurry preparation	$2	1	2.0	1	4.4
SunShot power loop @ $1,200/kWe	$660	1	66.0	1	726.0
HXs, combustion side	$140	8			140.1
-- Spare HX			17.5	2	35.0
Combustor, No spare	$68	1	68.0	0	67.7
1st Subtotal (BEC), Core systems	$1,164				1,315.3
Support facilities*					
Coal receiving					24.4
Coal crushing					16.6
Ducting and stack					21.3
Ash handling					6.5
Accessory electric plant					32.2
Instrumentation & control					12.1
2nd Subtotal (BEC), Ancilliary systems					113.1
Total BEC, equipment					1,428.4

** Numbers drawn from NETL Bituminous Coal Utility study, 2012 update, Case 12 (PC with sequestration)*

Other parameters were input at appropriate points in the PSFM model to adhere to QGESS instructions. Tables 1-3 of the QGESS guidelines are incorporated in Table 2-8, “Factors” column. Parameters that account for such global economic assumptions as taxes, contracting terms, analysis time periods and cost escalation are dictated by Table 4 of the QGESS.

The last data set for the model accounts for operating and maintenance cost, presented in Table 2-9. Labor rates derive from the Design Basis document of this study, which was delivered in October, 2012. It prescribes the use of Bureau of Labor Statistics data for hourly wages, specifically for NAICS industrial category 221100, “Electric Power Generation, Transmission and Distribution, “ job category 51-0000, “Production Occupations.” Numbers for May 2013 were chosen. Most of the other data came from NETL document 2011/1455, previously cited.

Table 2-8. Capital costs according to PSFM guidelines[14]

Capital cost category	Basis	Factor	Totals for: Portion $ Million	Cumulative $ Million	
BEC - Bare Erected Cost					
Process equipment **	Itemized cost summary		1,315.30		
Support facilities ***	NETL, 2012 update, Case 12		113.1		
Total BEC			1,428.40	1,428.40	
EPC - Engineering Project Costs					
Total EPC portion	0-10% BEC, "process in use"	10%	142.84	**1,571.24**	*
TPC - Total Project Costs					
Process cost	5-20% of process capital	20%	314.248		
Project cost	15-30% of BEC+EPC+process cost	30%	471.372		
Total TPC portion			785.62	2,356.86	
TOC - Total Overnight Cost					
Royalties	Assume zero		0		
Pre-production	Gross estimate		1		
- 6 mos labor	Included in gross estimate				
- 1 mo maintenance materials	Included in gross estimate				
- 1 mo non-fuel consumables	Included in gross estimate				
- 1 mo waste disposable	Included in gross estimate				
Working capital	Accounted for in PSFM model				
Inventory capital:					
- Spare parts	0.5% of cum TPC	0.50%	19.4		
- Initial fuel (60 days)	5,000 ton/d	$36.00	13.34		
- Initial CaCO3 (60 days)	1.45 kg/s = 3.2 lb/s makeup	$0.20	0.1		
Land, for PC-type utility	300 acres	3,000	0.9		
Financing - cost of securing it	Percent of TPC	2.70%	105		
Other owner's costs	Percent of TPC	15%	583.4		
Total Owner's cost			722.14	3,079.00	
TASC - Total As-Spent Capital					
Escalation while expending capital	Accounted for in PSFM model		0		
Interest while expending capital	Accounted for in PSFM model		0		
Total TASC			0	3,079.00	
Analysis:					
TASC by PSFM calculation				2,505.12	**
		w/ TS&M	w/ TS&M		
Benchmark COE	*Case 11, 2012 update*	80.95	N/A		
Benchmark COE w/ 90% CCS	*Case 12, 2012 update*	137.28	147.47		
COE by PSFM	**Includes O&M**	N/A	**121.21**		

* *Cumulative amount goes to Cell B37, "Plant Inputs" page of PFSM workbook*

** *TASC calculation comes from Cell B12 of the "COE Calculation" page of the PSFM workbook*

[14] *Factors adhere to "Cost Estimation for NETL Assessments of Power Plant Performance," April 2011 DOE/NETL-2011/1455*

Table 2-9. Operations and maintenance cost, $ thousand

Operations and maintenance cost, $ thousand

Bold items entered on O&M page of PSFM workbook

Cost items	Measure	Rate	$/h	$1,000/y	PSFM page, Cell ID	Source:
Variable costs:						
Labor:						
		$33.3				
Operating labor base rate	$/hr	6	$33.36	69		BLS, NAICS 221100 job category 51-0000, May 2013
Operating labor burden	% of base	30%	$10.01	**21**	B27	Rate from Exhibit 4-13, Case 12, August 2012
Labor O-H charge rate	% of labor	25%	$10.84	23		Rate from Exhibit 4-13, Case 12, August 2012
Subtotal: Operating labor wages	ex burden, per operator			**92**	B26	*Calculated*
Total: Operating labor cost	per operator			113		*Calculated*
Estimated operating laborers		**65**			B25	*Calculation based on Exhibit 4-13 oper. labor cost*
Administrative and supervisory	Total			1,674		Exhibit 4-13, Case 12, August 2012
Administrative and supervisory	Per operator			**25.56**	B28	*Calculated*
Consumables:						
Water	Total			**3,804**	B31	Exhibit 4-13, Case 12, August 2012
Chemicals	Total			**24,914**	B32	Exhibit 4-13, Case 12, August 2012
Waste disposal	Total			**5,129**	B34	Exhibit 4-13, Case 12, August 2012
Fixed costs:						
Administrative and supervisory	Total			**3,348**	B37	Exhibit 4-13, Case 12, August 2012
Taxes and insurance				**39,025**	B38	Exhibit 4-13, Case 12, August 2012
Maintenance costs	% EPC/yr	3%		**86,527**	B39	Thar assumption
Assumptions and Benchmarks:						
	Base hours in year:	2,080				
	*Operating labor cost:	$7,384,208				per yr
	*Maintenance labor cost:	$12,705,913				per yr (included in overall maintenance percentage)
	*Administrative & support labor cost:	$5,022,530				per yr (assume 1/3 variable, 2/3 fixed)
	*Property taxes and insurance:	$39,024,956				per yr

* *Benchmarks taken from Exhibit 4-13, Case 12, August 2012*

2.4.5.2 *PRESSURIZED OXY-COMBUSTION - DUAL POWER BLOCK*

Process equipment costs rose $137 million because of the increased size of the heat exchangers that are required for transfer of heat to each of the two power blocks, plus the clean-up loop. Because of the significant differences in approach temperatures for the power-block heat exchangers and the cleaning-loop exchangers, the effect of going to a dual loop is to demand relatively less performance from the power-block exchangers, and more from the cleaning exchangers, for a net increase in heat-exchanger size for the dual-loop option. The differences in BEC costs, relative to Table 2-7, are shown in Table 2-10. For both the single- and dual-loop cases, the cost data have been normalized to a 550-MWe basis by multiplying heat exchanger costs of the respective Aspen Plus cases by the ratio of model power output (in megawatts) divided by 550. The dual loop adds approximately $12/MWe to the COE.

Table 2-10. Estimated equipment costs, 550 MW pressurized oxy-combustion power plant, dual power block

Process equipment	Total No spares $ Million	Number of units operating	Cost/ spare $ Million	Spares on hand	With spares $ Million
Core systems, ex power block (See Table 2-7)					1,140.1
HXs, combustion side	$249	8			249.3
-- Spare HX			31.2	2	62.3
1st Subtotal (BEC), Core systems	$249				1,451.8
2nd Subtotal (BEC), Ancilliary systems					113.1
Total BEC, equipment					1,564.9

2.4.5.3 *SUMMARY*

According to the PSFM model, the estimated Cost of Electricity (COE) using the single power-block flowscheme is $121/MWe. This is 49% greater than the benchmark COE of $80.95/MWe for Case 11 of the latest NETL cost assessment for pulverized coal plants without sequestration. This exceeds the stated program objectives of 35% increase in COE, however the supercritical oxy-combustor represents a 21% reduction in COE when compared to current power generation technologies with 90% CO2 capture, while capturing and sequestering 99% of the generated CO2. The revised $121/MWe COE reflects the removal of installation labor costs included in the Total Overnight Cost (TOC) and increasing coal cost per QGESS fuel guidelines based on feedback provided by DOE for the Phase II application, and updates to the fuel consumption rates to match the cycle efficiencies predicted by the cycle models. These revisions reflect a significant decrease from the initial $162/MWe COE estimate provided in the *Technology Engineering Design and Ecconomic Analysis* report submitted with the Phase II proposal.

2.4.6 SUBTASK 2.6 – INITIAL CYCLE ANALYSIS OF SINGLE AND DUAL LOOP CPOC CONFIGURATIONS

Initial evaluation of the CPOC and the supercritical oxy-combustion cycle focused on maximizing thermal efficiency of the power blocks. Cycle models were implemented using Aspen Plus for the respective power blocks, the Cryogenic Pressurized Oxy-Combustion Cycle (CPOC), shown in Figure 2-30, and the supercritical CO2 (sCO2) recompression cycle, shown in Figure 2-31. These models were used to perform an initial comparison of the two cycle configurations to assess thermal efficiency, shown in Figure 2-32 and Figure 2-33, and the

impact of component performance on the overall cycle. This initial analysis showed that the recompression cycle achieved higher thermal efficiencies, near 47% at 650 C and 290 atm, with a similar level of component maturity as the CPOC cycle achieving 38% thermal efficiency for reasonable loop pressures.

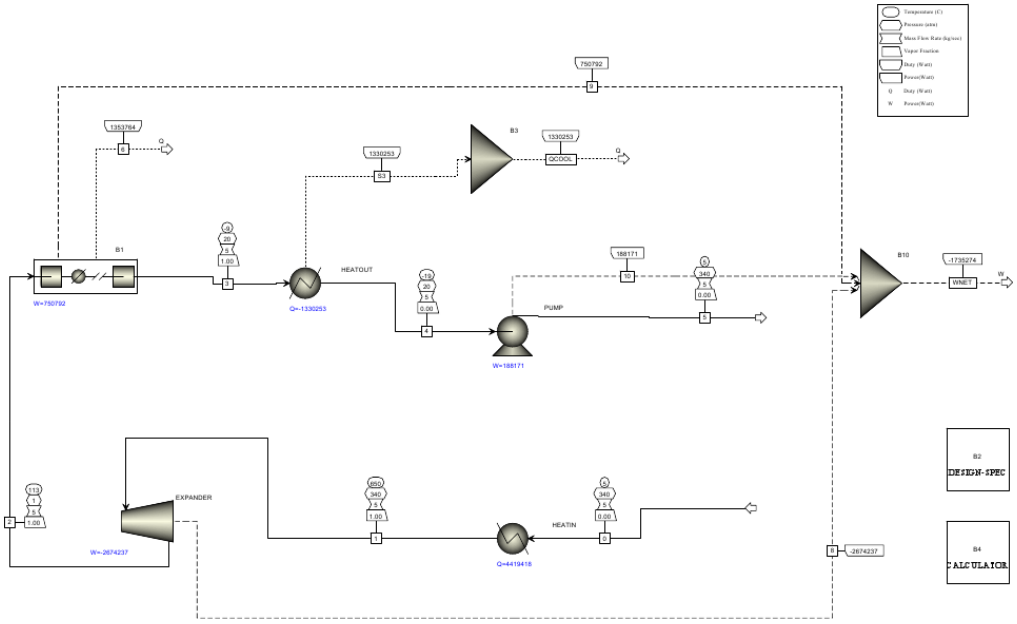

Figure 2-30. Aspen Plus layout of the cryogenic oxy-combustion power block

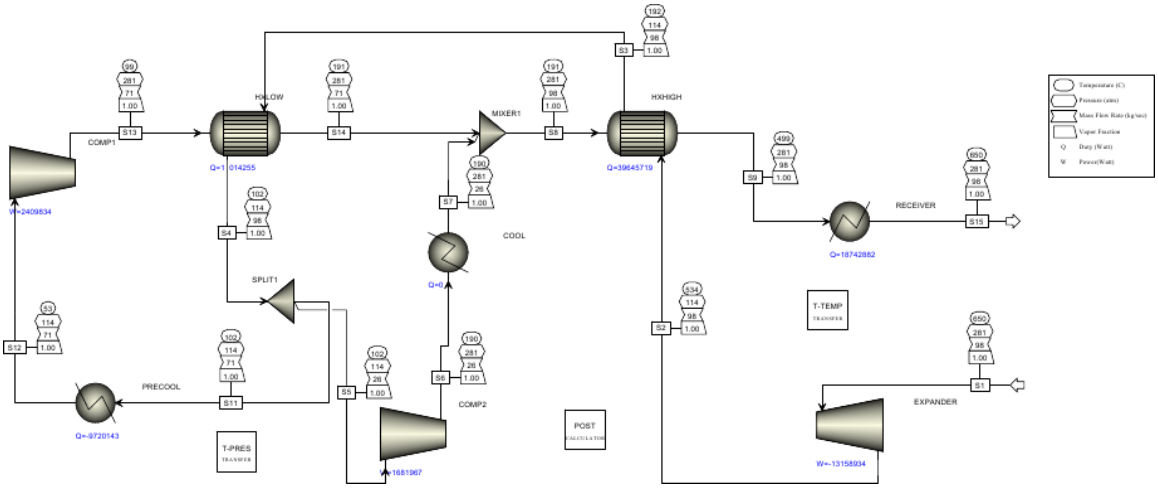

Figure 2-31. Aspen Plus layout of the sCO2 recompression cycle

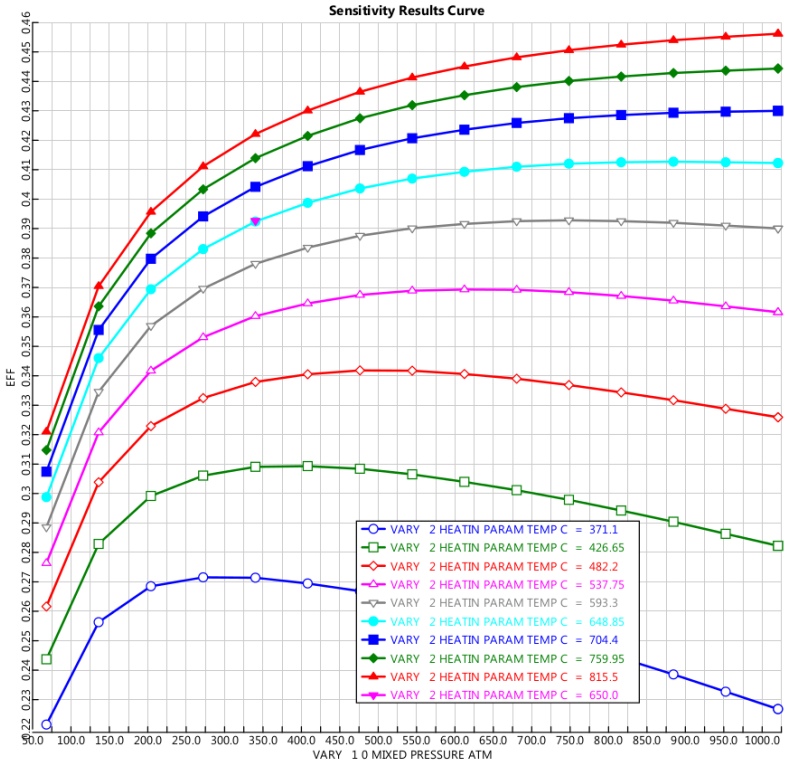

Figure 2-32. CPOC efficiency as a function of temperature and pressure

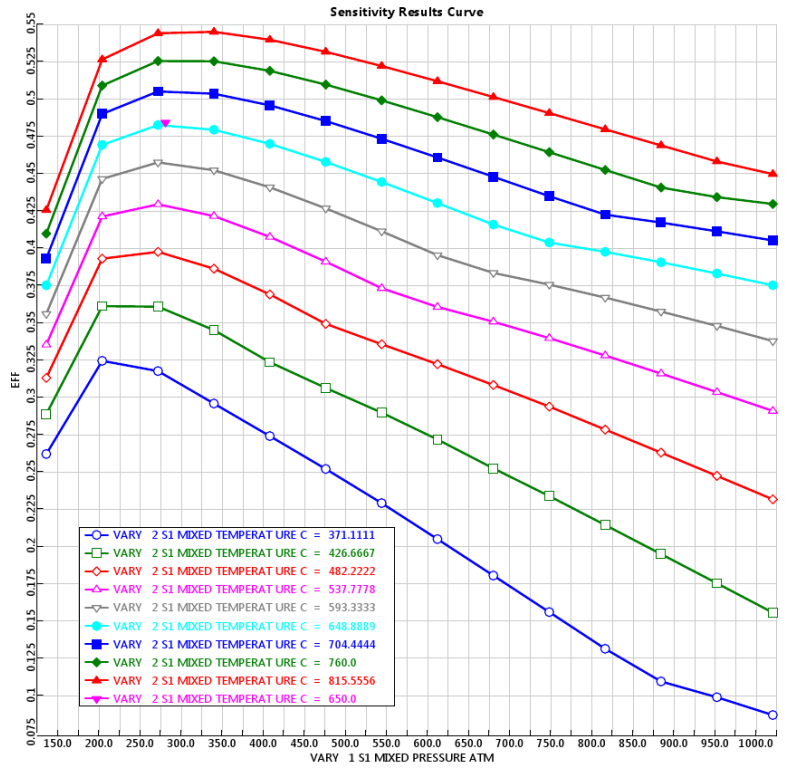

Figure 2-33. sCO_2 recompression efficiency as a function of temperature and pressure

2.4.7 SUBTASK 2.7 – CYCLE OPTIMIZATION FOR HIGH NET EFFICIENCY AND LOW COST

Initial cycle evaluation of the supercritical oxy-combustor and the sCO_2 power block using simplified cycle models indicated that an indirect cycle configuration that allowed the combustion and power loops to operate at differential pressures would be advantageous, as the increase in power block efficiency was greater than the losses associated with the heat exchanger interfacing the two loops. As an added benefit, isolating the post-combustion to the combustion loop minimized wear and fouling of the turbomachinery. This comes at the risk of increased fouling of the less expensive interface heat exchangers. The reduced operating pressure on the combustion side also enables greater re-use of commercially available technologies for flue gas cleanup, decreasing economic and technical risk for developing the supercritical oxy-combustor.

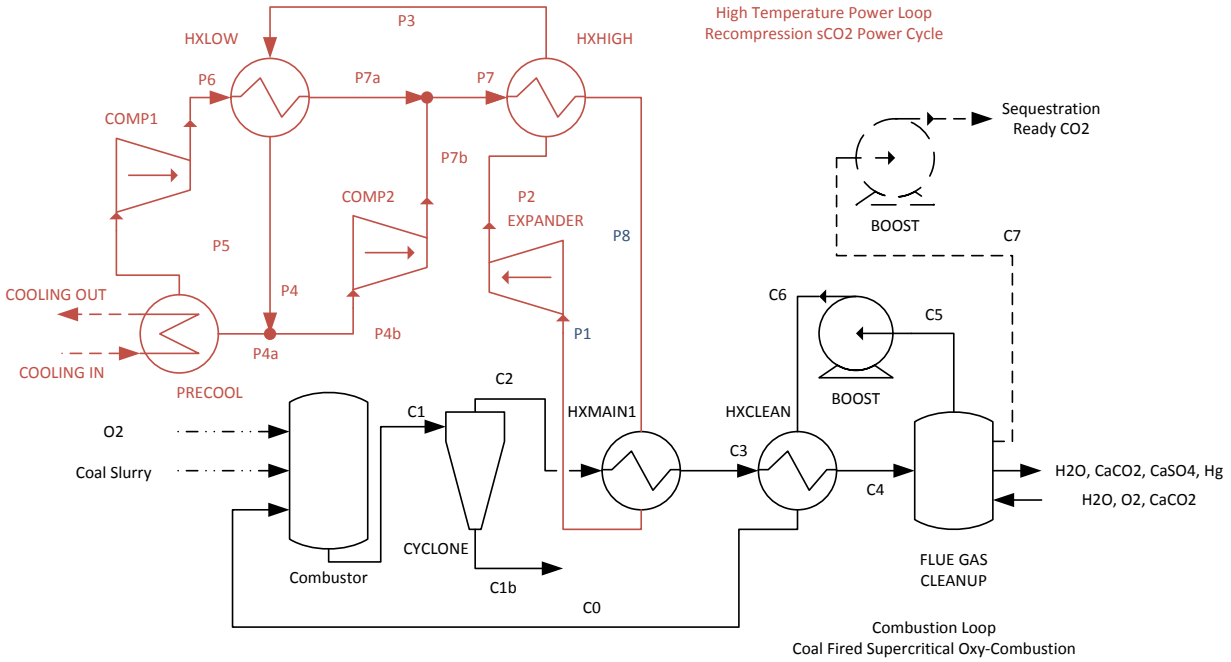

Figure 2-34. Indirect supercritical oxy-combustion cycle layout with a recompression sCO_2 power block

The use of a supercritical CO_2 power block enables high thermal efficiencies, near 48% for 650°C turbine inlet temperature, but also poses a challenge for the cycle design due to the narrow temperature range for the thermal input, as shown in the temperature-enthalpy diagrams in Figure 2-35 for a 700°C sCO_2 power cycle and the supercritical oxy-combustion loop. For the current cycle configuration, shown in Figure 2-34, the temperature difference between the power block outlet to inlet is only 196 C. This has two significant impacts on the cycle design. First, the transfer 1.2 GW of thermal energy from the combustor to the power block across a narrow temperature range requires a significant mass flow of CO2, roughly 4929 kg/s of flue gas. Second, to minimize the amount of fuel and thermal input at the combustor, maximizing cycle efficiencies, the temperature rise in the combustor should be as close as the HX allows, which requires a recycle CO2 temperature near 454°C.

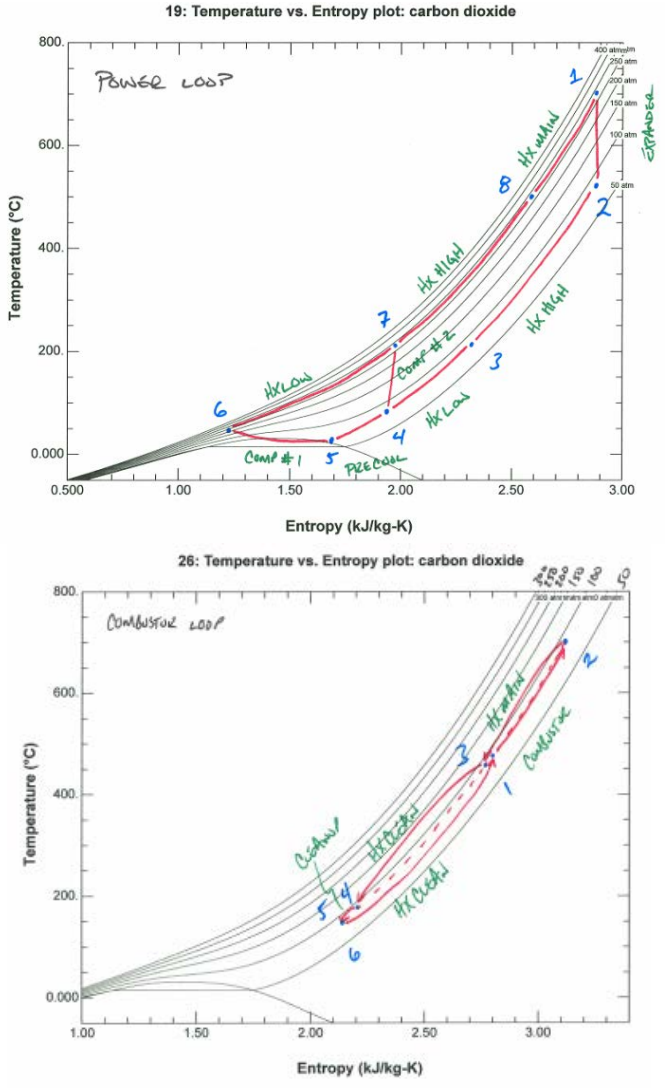

Figure 2-35. Temperature-entropy diagram for a 700 C recompression power and combustion loops

The elevated temperature of the recycle loop poses challenges for flue gas cleanup, which is typically performed at reduced temperatures and pressure as compared to the proposed cycle conditions. In order to use a conventional wet limestone flue gas desulfurization, and minimize temperatures at the boost pump and the CO2 sequestration stream, a recuperater is incorporated into the supercritical oxy-combustion loop, as shown in Figure 2-34, to enable cleanup, dewatering, and re-compression at reduced temperatures.

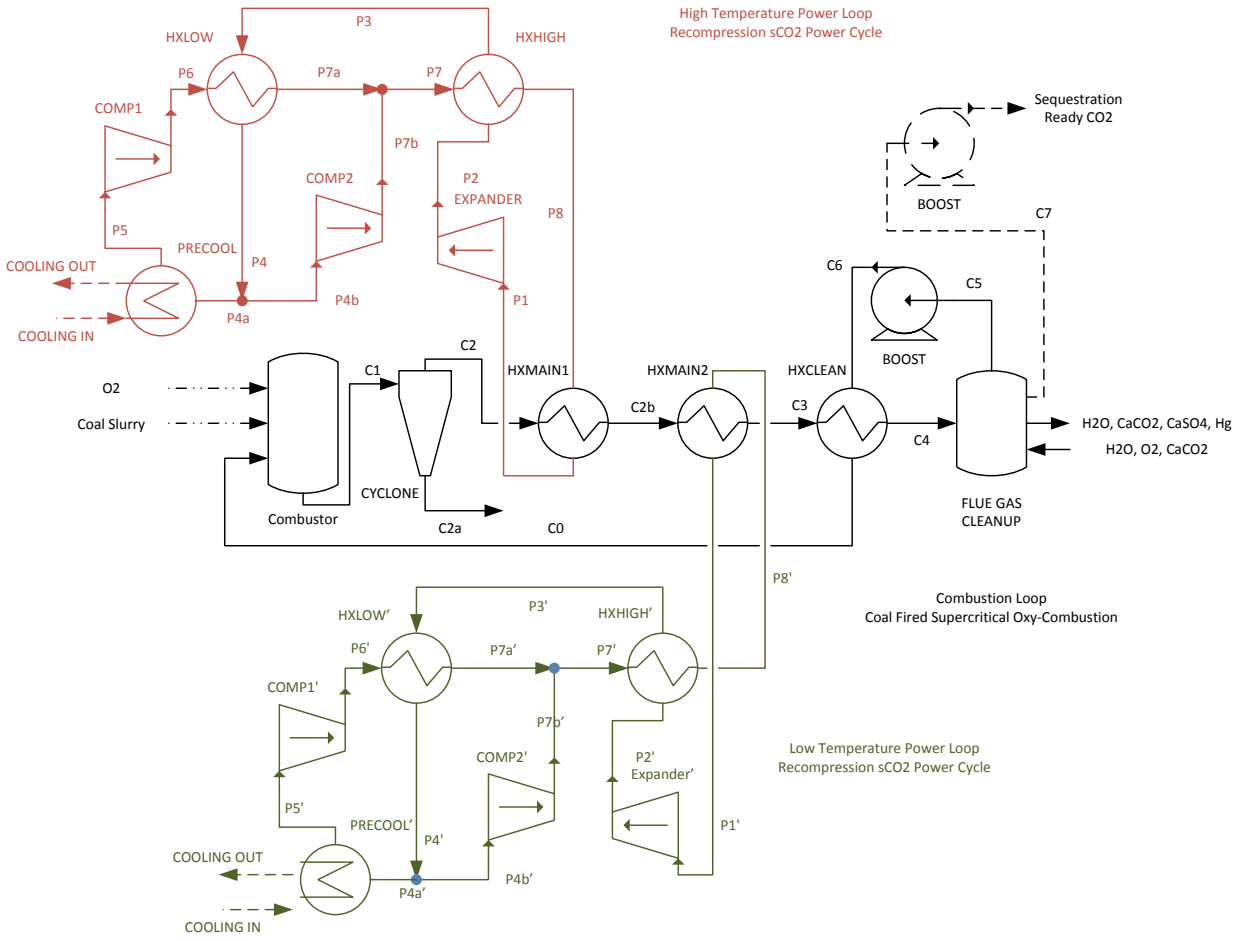

Figure 2-36**. Dual loop oxy-combustion cycle layout with two recompression sCO2 power cycles**

As part of the cycle optimization, an alternative configuration was evaluated which places two smaller sCO2 power blocks in series. This configuration doubles the temperature drop across the combustion loop, leading to lower recycle temperatures and a reduced recycle mass flow. This reduction in mass flow comes at the cost of two smaller power blocks, and two smaller heat exchangers for the same net power output. A schematic for this configuration is shown in

Figure **2-36**. Plant efficiencies for the dual power block configuration were reduced by 1%, impacted by the additional thermal losses associated with the extra heat exchanger, and the loss of power block efficiency for the second power block operating at a lower temperature. Economic analysis of both configurations showed a cost increase of $12/MWe for the dual power block configuration when compared to the single block configuration shown in Figure 2-34.

Based on this analysis, the single block configuration of Figure 2-34 was selected as an optimal configuration for further component and cycle developments. Figure 2-37 is the Aspen Plus flowsheets for the optimized cycle configuration and Figure 2-38 shows the power block. Stream tables for this model are included in Table 2-11 through Table 2-15 for the different component streams.

This cycle configuration is able to achieve 37.9% HHV plant efficiency (39.3% LHV plant efficiency) with 99% carbon capture for a COE of $121/MWe. This exceeds the stated program

objectives of 35% increase in COE, however the supercritical oxy-combustor represents a 21% reduction in COE when compared to current power generation technologies with 90% CO2 capture, while capturing and sequestering 99% of the generated CO2. The selection of 650 as the firing temperature represents a design tradeoff to limit firing temperature in order to use austenitic stainless steels for the high temperature pressure vessels and piping, and to minimize the need for advanced turbomachinery features such as blade cooling.

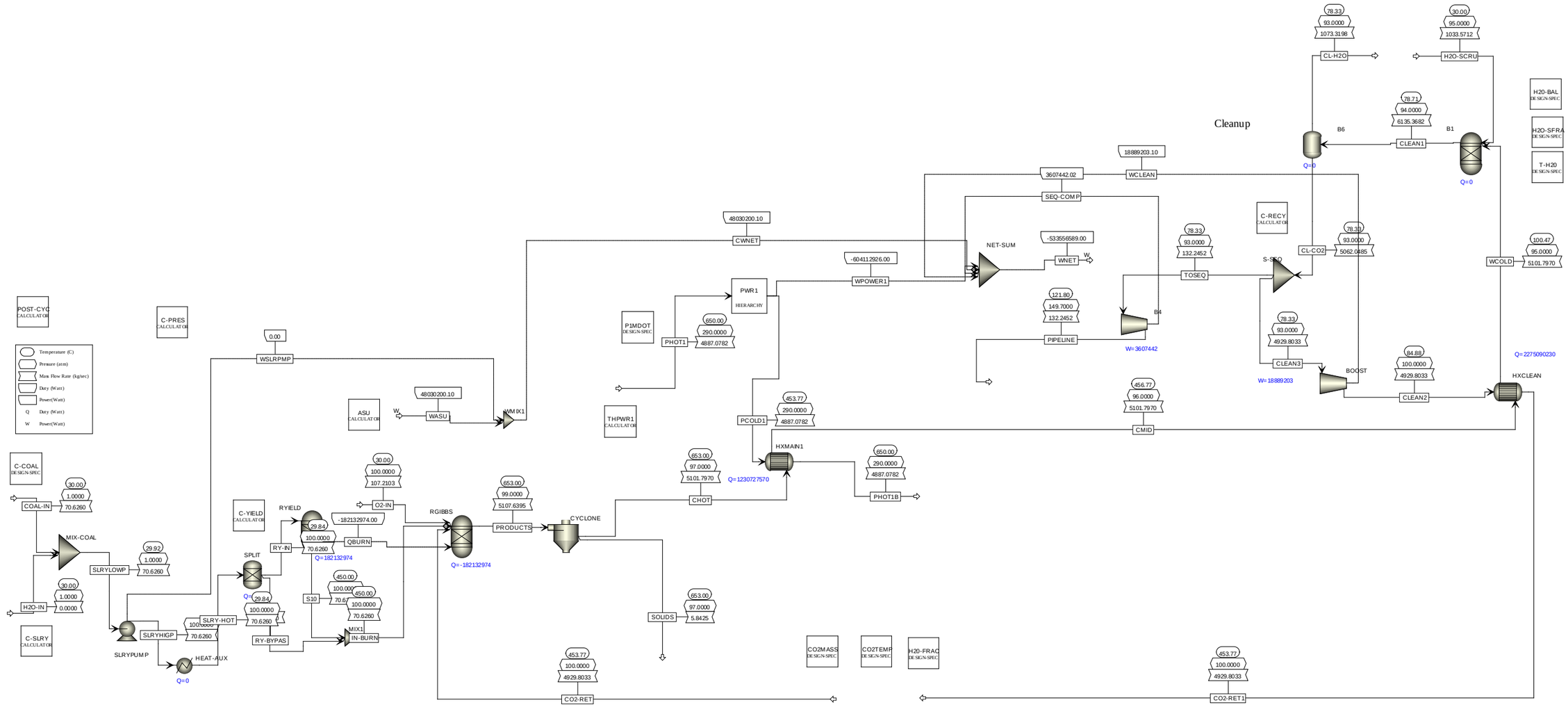

Figure 2-37. Flow sheet for the indirect supercritical oxy-combustion plant

Table 2-11. Stream Table A for the MIXED Process Components

	CHOT	CL-CO2	CL-H2O	CLEAN1	CLEAN2	CLEAN3	CMID	CO2-RET	CO2-RET1	COAL-IN	H2O-IN	H2O-SCRU	IN-BURN	O2-IN
Substream: MIXED														
Mass Flow kg/sec														
H2O	62.81	24.20	988.61	1012.82	23.57	23.57	62.81	23.57	23.57	0.00	0.00	950.00	17.66	0.00
N2	0.51	0.51	0.00	0.51	0.50	0.50	0.51	0.00	0.50	0.00	0.00	0.00	0.51	0.00
O2	0.22	0.03	0.00	0.03	0.03	0.03	0.22	0.00	0.03	0.00	0.00	0.00	7.95	107.21
NO2	0.00	0.00	0.00	0.00	0.00	0.00	0.00	0.00	0.00	0.00	0.00	0.00	0.00	0.00
NO	0.00	0.00	0.00	0.00	0.00	0.00	0.00	0.00	0.00	0.00	0.00	0.00	0.00	0.00
S	0.00	0.00	0.00	0.00	0.00	0.00	0.00	0.00	0.00	0.00	0.00	0.00	0.52	0.00
SO2	0.77	0.00	0.00	0.00	0.00	0.00	0.77	0.00	0.00	0.00	0.00	0.00	0.00	0.00
SO3	0.34	0.00	0.00	0.00	0.00	0.00	0.34	0.00	0.00	0.00	0.00	0.00	0.00	0.00
H2	0.00	0.00	0.00	0.00	0.00	0.00	0.00	0.00	0.00	0.00	0.00	0.00	2.42	0.00
CL2	0.00	0.00	0.00	0.00	0.00	0.00	0.00	0.00	0.00	0.00	0.00	0.00	0.01	0.00
HCL	0.01	0.00	0.00	0.00	0.00	0.00	0.01	0.00	0.00	0.00	0.00	0.00	0.00	0.00
C	0.00	0.00	0.00	0.00	0.00	0.00	0.00	0.00	0.00	0.00	0.00	0.00	0.00	0.00
CO	0.00	0.00	0.00	0.00	0.00	0.00	0.00	0.00	0.00	0.00	0.00	0.00	0.00	0.00
CO2	5037.14	5037.30	14.12	5051.43	4905.70	4905.70	5037.14	4906.23	4905.70	0.00	0.00	13.57	0.00	0.00
CACO3	0.00	0.00	0.00	0.00	0.00	0.00	0.00	0.00	0.00	0.00	0.00	0.00	0.00	0.00
CASO4	0.00	0.00	0.00	0.00	0.00	0.00	0.00	0.00	0.00	0.00	0.00	0.00	0.00	0.00
CACL2	0.00	0.00	0.00	0.00	0.00	0.00	0.00	0.00	0.00	0.00	0.00	0.00	0.00	0.00
Total Flow kmol/sec	117.98	115.82	55.20	171.02	112.80	112.80	117.98	112.79	112.80	0.00	0.00	53.04	2.46	3.35
Total Flow kg/sec	5101.80	5062.05	1002.74	6064.79	4929.80	4929.80	5101.80	4929.80	4929.80	0.00	0.00	963.57	29.06	107.21
Total Flow cum/sec	95.29	25.18	1.37	26.25	23.49	24.52	75.42	69.08	69.08	0.00	0.00	1.28	1.47	0.82
Temperature C	653.00	78.33	78.33	78.71	84.88	78.33	456.77	453.77	453.77		30.00	30.00	450.00	30.00
Pressure atm	97.00	93.00	93.00	94.00	100.00	93.00	96.00	100.00	100.00	1.00	1.00	95.00	100.00	100.00
Vapor Frac	1.00	1.00	0.00	0.68	1.00	1.00	1.00	1.00	1.00		0.00	0.00	1.00	1.00
Liquid Frac	0.00	0.00	1.00	0.32	0.00	0.00	0.00	0.00	0.00		1.00	1.00	0.00	0.00
Solid Frac	0.00	0.00	0.00	0.00	0.00	0.00	0.00	0.00	0.00		0.00	0.00	0.00	0.00
Enthalpy J/kmol	-359760000.00	-393350000.00	-284660000.00	-358270000.00	-393190000.00	-393350000.00	-370190000.00	-373080000.00	-373020000.00		-288420000.00	-288850000.00	-81277000.00	-607880.00
Enthalpy J/kg	-8319600.00	-9000000.00	-15670000.00	-10103000.00	-8996200.00	-9000000.00	-8560900.00	-8535700.00	-8534700.00		-16010000.00	-15900000.00	-6884600.00	-18996.85
Enthalpy Watt	-42450000000.00	-45560000000.00	-15710000000.00	-61270000000.00	-44350000000.00	-44370000000.00	-43680000000.00	-42080000000.00	-42070000000.00		0.00	-15320000000.00	-200040000.00	-2036700.00
Entropy J/kmol-K	15389.07	-36707.17	-155870.00	-75212.65	-36660.38	-36707.17	2829.22	2646.73	2658.11		-169410.00	-168700.00	-19042.78	-40035.63
Entropy J/kg-K	355.88	-839.87	-8580.14	-2120.89	-838.80	-839.87	65.43	60.55	60.82		-9403.46	-9286.17	-1613.03	-1251.16
Density kmol/cum	1.24	4.60	40.17	6.52	4.80	4.60	1.56	1.63	1.63		41.80	41.34	1.67	4.11
Density kg/cum	53.54	201.06	729.80	231.05	209.90	201.06	67.65	71.36	71.36		753.06	751.05	19.75	131.38
Average MW	43.24	43.71	18.17	35.46	43.71	43.71	43.24	43.71	43.71		18.02	18.17	11.81	32.00
Liq Vol 60F cum/sec	6.19	6.16	1.01	7.16	5.99	5.99	6.19	5.99	5.99	0.00	0.00	0.97	0.10	0.18
Substream: $TOTAL														
Total Flow kg/sec	5101.80	5062.05	1073.32	6135.37	4929.80	4929.80	5101.80	4929.80	4929.80	70.63	0.00	1033.57	70.63	107.21
Enthalpy Watt	-42450000000.00	-45560000000.00	-16560000000.00	-62120000000.00	-44350000000.00	-44370000000.00	-43680000000.00	-42080000000.00	-42070000000.00	-365090000.00	0.00	-16160000000.00	-182980000.00	-2036700.00

Table 2-12. Stream Table B for the MIXED Process Components

	PCOLD1	PHOT1	PHOT1B	PIPELINE	PRODUCTS	RY-BYPAS	RY-IN	S5	S6	S10	SLRY-HOT	SLRYHIGP	SLRYLOWP	SOLIDS	TOSEQ	WCOLD
Substream: MIXED																
Mass Flow kg/sec																
H2O	0.00	0.00	0.00	0.63	62.81	0.00	0.00	1.98	1.98	17.66	0.00	0.00	0.00	0.00	0.63	62.81
N2	0.00	0.00	0.00	0.01	0.51	0.00	0.00	0.00	0.00	0.51	0.00	0.00	0.00	0.00	0.01	0.51
O2	0.00	0.00	0.00	0.00	0.22	0.00	0.00	0.00	0.00	7.95	0.00	0.00	0.00	0.00	0.00	0.22
NO2	0.00	0.00	0.00	0.00	0.00	0.00	0.00	0.00	0.00	0.00	0.00	0.00	0.00	0.00	0.00	0.00
NO	0.00	0.00	0.00	0.00	0.00	0.00	0.00	0.00	0.00	0.00	0.00	0.00	0.00	0.00	0.00	0.00
S	0.00	0.00	0.00	0.00	0.00	0.00	0.00	0.00	0.00	0.52	0.00	0.00	0.00	0.00	0.00	0.00
SO2	0.00	0.00	0.00	0.00	0.77	0.00	0.00	0.00	0.00	0.00	0.00	0.00	0.00	0.00	0.00	0.77
SO3	0.00	0.00	0.00	0.00	0.34	0.00	0.00	0.00	0.00	0.00	0.00	0.00	0.00	0.00	0.00	0.34
H2	0.00	0.00	0.00	0.00	0.00	0.00	0.00	0.00	0.00	2.42	0.00	0.00	0.00	0.00	0.00	0.00
CL2	0.00	0.00	0.00	0.00	0.00	0.00	0.00	0.00	0.00	0.01	0.00	0.00	0.00	0.00	0.00	0.00
HCL	0.00	0.00	0.00	0.00	0.01	0.00	0.00	0.00	0.00	0.00	0.00	0.00	0.00	0.00	0.00	0.01
C	0.00	0.00	0.00	0.00	0.00	0.00	0.00	0.00	0.00	0.00	0.00	0.00	0.00	0.00	0.00	0.00
CO	0.00	0.00	0.00	0.00	0.00	0.00	0.00	0.00	0.00	0.00	0.00	0.00	0.00	0.00	0.00	0.00
CO2	4887.08	4887.08	4887.08	131.60	5037.14	0.00	0.00	0.00	0.00	0.00	0.00	0.00	0.00	0.00	131.60	5037.14
CACO3	0.00	0.00	0.00	0.00	0.00	0.00	0.00	0.00	0.00	0.00	0.00	0.00	0.00	0.00	0.00	0.00
CASO4	0.00	0.00	0.00	0.00	0.00	0.00	0.00	0.00	0.00	0.00	0.00	0.00	0.00	0.00	0.00	0.00
CACL2	0.00	0.00	0.00	0.00	0.00	0.00	0.00	0.00	0.00	0.00	0.00	0.00	0.00	0.00	0.00	0.00
Total Flow kmol/sec	111.05	111.05	111.05	3.03	117.98	0.00	0.00	0.11	0.11	2.46	0.00	0.00	0.00	0.00	3.03	117.98
Total Flow kg/sec	4887.08	4887.08	4887.08	132.25	5101.80	0.00	0.00	1.98	1.98	29.06	0.00	0.00	0.00	0.00	132.25	5101.80
Total Flow cum/sec	24.98	31.87	31.87	0.50	93.43	0.00	0.00	0.00	0.00	1.47	0.00	0.00	0.00	0.00	0.66	29.19
Temperature C	453.77	650.00	650.00	121.80	653.00			30.00	31.03	450.00					78.33	100.47
Pressure atm	290.00	290.00	290.00	149.70	99.00		100.00	1.00	95.00	100.00	100.00	100.00	1.00		93.00	95.00
Vapor Frac	1.00	1.00	1.00	1.00	1.00			0.00	0.00	1.00					1.00	0.99
Liquid Frac	0.00	0.00	0.00	0.00	0.00			1.00	1.00	0.00					0.00	0.01
Solid Frac	0.00	0.00	0.00	0.00	0.00			0.00	0.00	0.00					0.00	0.00
Enthalpy J/kmol	-375270000.00	-364190000.00	-364190000.00	-392160000.00	-359760000.00			-288420000.00	-288160000.00	-81277000.00					-393350000.00	-389470000.00
Enthalpy J/kg	-8526900.00	-8275100.00	-8275100.00	-8972800.00	-8319600.00			-16010000.00	-15995000.00	-6884600.00					-9000000.00	-9006800.00
Enthalpy Watt	-41670000000.00	-40440000000.00	-40440000000.00	-1186600000.00	-42450000000.00			-31732000.00	-31702000.00	-200040000.00					-1190200000.00	-45950000000.00
Entropy J/kmol-K	-7231.40	6268.03	6268.01	-36404.72	15214.09			-169410.00	-169270.00	-19042.78					-36707.17	-33849.93
Entropy J/kg-K	-164.31	142.42	142.42	-832.95	351.84			-9403.46	-9396.09	-1613.03					-839.87	-782.81
Density kmol/cum	4.45	3.48	3.48	6.04	1.26			41.80	41.83	1.67					4.60	4.04
Density kg/cum	195.68	153.35	153.35	264.03	54.61			753.06	753.63	19.75					201.06	174.77
Average MW	44.01	44.01	44.01	43.71	43.24			18.02	18.02	11.81					43.71	43.24
Liq Vol 60F cum/sec	5.95	5.95	5.95	0.16	6.19	0.00	0.00	0.00	0.00	0.10	0.00	0.00	0.00	0.00	0.16	6.19
Substream: $TOTAL																
Total Flow kg/sec	4887.08	4887.08	4887.08	132.25	5107.64	0.00	70.63	1.98	1.98	70.63	70.63	70.63	70.63	5.84	132.25	5101.80
Enthalpy Watt	-41670000000.00	-40440000000.00	-40440000000.00	-1186600000.00	-42450000000.00	0.00	-365110000.00	-31732000.00	-31702000.00	-182980000.00	-365110000.00	-365100000.00	-365100000.00	-1201000.00	-1190200000.00	-45950000000.00

Table 2-13. Stream Table for the CIPSD Process Components

	CL-H2O	CLEAN1	H2O-SCRU	IN-BURN	S10
Substream: CIPSD					
Mass Flow kg/sec					
H2O	0.00	0.00	0.00	0.00	0.00
N2	0.00	0.00	0.00	0.00	0.00
O2	0.00	0.00	0.00	0.00	0.00
NO2	0.00	0.00	0.00	0.00	0.00
NO	0.00	0.00	0.00	0.00	0.00
S	0.00	0.00	0.00	0.00	0.00
SO2	0.00	0.00	0.00	0.00	0.00
SO3	0.00	0.00	0.00	0.00	0.00
H2	0.00	0.00	0.00	0.00	0.00
CL2	0.00	0.00	0.00	0.00	0.00
HCL	0.00	0.00	0.00	0.00	0.00
C	0.00	0.00	0.00	35.73	35.73
CO	0.00	0.00	0.00	0.00	0.00
CO2	0.00	0.00	0.00	0.00	0.00
CACO3	68.38	68.38	70.00	0.00	0.00
CASO4	2.20	2.20	0.00	0.00	0.00
CACL2	0.00	0.00	0.00	0.00	0.00
Total Flow kmol/sec	0.70	0.70	0.70	2.97	2.97
Total Flow kg/sec	70.58	70.58	70.00	35.73	35.73
Total Flow cum/sec	0.03	0.03	0.03	0.02	0.02
Temperature	78.33	78.71	30.00	450.00	450.00
Pressure	93.00	94.00	95.00	100.00	100.00
Vapor Frac	0.00	0.00	0.00	0.00	0.00
Liquid Frac	0.00	0.00	0.00	0.00	0.00
Solid Frac	1.00	1.00	1.00	1.00	1.00
Enthalpy	-1208100000.00	-1208000000.00	-1207000000.00	6567360.00	6567360.00
Enthalpy	-11970000.00	-11970000.00	-12059000.00	546779.00	546779.00
Enthalpy	-844910000.00	-844890000.00	-844140000.00	19535300.00	19535300.00
Entropy	-252000.00	-251900.00	-262020.00	12793.47	12793.47
Entropy	-2496.94	-2496.02	-2617.90	1065.15	1065.15
Density	26.93	26.93	27.11	187.33	187.33
Density	2717.76	2717.74	2713.43	2250.02	2250.02
Average MW	100.92	100.92	100.09	12.01	12.01
Liq Vol 60F					

Table 2-14. Stream Table for the NCPSD Process Components

	COAL-IN	IN-BURN	PRODUCTS	RY-IN	S10	SOLIDS
Substream: NCPSD						
Mass Flow kg/sec						
COAL	7.0626E+01	0.0000E+00	0.0000E+00	7.0626E+01	0.0000E+00	0.0000E+00
ASH	0.0000E+00	5.8425E+00	5.8425E+00	0.0000E+00	5.8425E+00	5.8425E+00
Total Flow kg/sec	7.0626E+01	5.8425E+00	5.8425E+00	7.0626E+01	5.8425E+00	5.8425E+00
Temperature	3.0000E+01	4.5000E+02	6.5300E+02	2.9838E+01	4.5000E+02	6.5300E+02
Pressure	1.0000E+00	1.0000E+02	9.9000E+01	1.0000E+02	1.0000E+02	9.7000E+01
Vapor Frac	0.0000E+00	0.0000E+00	0.0000E+00	0.0000E+00	0.0000E+00	0.0000E+00
Liquid Frac	0.0000E+00	0.0000E+00	0.0000E+00	0.0000E+00	0.0000E+00	0.0000E+00
Solid Frac	1.0000E+00	1.0000E+00	1.0000E+00	1.0000E+00	1.0000E+00	1.0000E+00
Enthalpy	-5.1694E+06	-4.2418E+05	-2.0557E+05	-5.1697E+06	-4.2418E+05	-2.0557E+05
Enthalpy	-3.6509E+08	-2.4783E+06	-1.2010E+06	-3.6511E+08	-2.4783E+06	-1.2010E+06
Density	1.4125E+03	3.4869E+03	3.4869E+03	1.4125E+03	3.4869E+03	3.4869E+03
Average MW	1.0000E+00	1.0000E+00	1.0000E+00	1.0000E+00	1.0000E+00	1.0000E+00
COAL PROXANAL						
MOISTURE	2.5000E+01			2.5000E+01		
FC	4.8090E+01			4.8090E+01		
VM	4.0870E+01			4.0870E+01		
ASH	1.1040E+01			1.1040E+01		
COAL ULTANAL						
ASH	1.1030E+01			1.1030E+01		
CARBON	6.7450E+01			6.7450E+01		
HYDROGEN	4.5600E+00			4.5600E+00		
NITROGEN	9.6000E-01			9.6000E-01		
CHLORINE	1.0000E-02			1.0000E-02		
SULFUR	9.8000E-01			9.8000E-01		
OXYGEN	1.5010E+01			1.5010E+01		
COAL SULFANAL						
PYRITIC	6.3000E-01			6.3000E-01		
SULFATE	1.0000E-02			1.0000E-02		
ORGANIC	3.4000E-01			3.4000E-01		
ASH PROXANAL						
MOISTURE		0.0000E+00	0.0000E+00		0.0000E+00	0.0000E+00
FC		0.0000E+00	0.0000E+00		0.0000E+00	0.0000E+00
VM		0.0000E+00	0.0000E+00		0.0000E+00	0.0000E+00
ASH		1.0000E+02	1.0000E+02		1.0000E+02	1.0000E+02
ASH ULTANAL						
ASH		1.0000E+02	1.0000E+02		1.0000E+02	1.0000E+02
CARBON		0.0000E+00	0.0000E+00		0.0000E+00	0.0000E+00
HYDROGEN		0.0000E+00	0.0000E+00		0.0000E+00	0.0000E+00
NITROGEN		0.0000E+00	0.0000E+00		0.0000E+00	0.0000E+00
CHLORINE		0.0000E+00	0.0000E+00		0.0000E+00	0.0000E+00
SULFUR		0.0000E+00	0.0000E+00		0.0000E+00	0.0000E+00
OXYGEN		0.0000E+00	0.0000E+00		0.0000E+00	0.0000E+00
ASH SULFANAL						
PYRITIC		0.0000E+00	0.0000E+00		0.0000E+00	0.0000E+00
SULFATE		0.0000E+00	0.0000E+00		0.0000E+00	0.0000E+00
ORGANIC		0.0000E+00	0.0000E+00		0.0000E+00	0.0000E+00

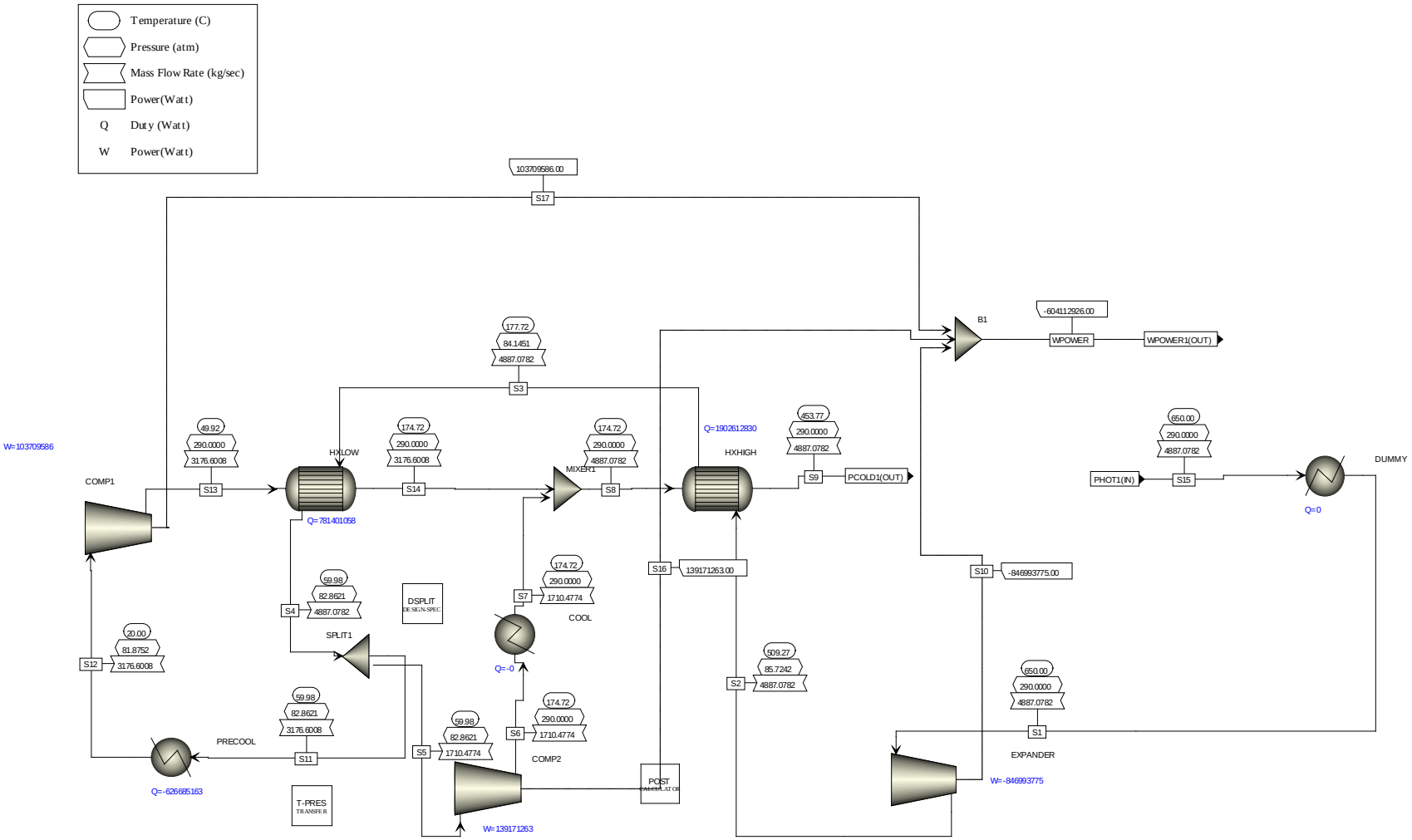

Figure 2-38. Recompression sCO2 power block for the indirect supercritical oxy-combustion plant

Table 2-15. Stream table for the Power Block

	PWR1.S1	PWR1.S2	PWR1.S3	PWR1.S4	PWR1.S5	PWR1.S6	PWR1.S7	PWR1.S8	PWR1.S9	PWR1.S11	PWR1.S12	PWR1.S13	PWR1.S14	PWR1.S15
Substream: MIXED														
Mass Flow kg/sec														
CO2	4887.169	4887.169	4887.169	4887.169	1710.509	1710.509	1710.509	4887.169	4887.169	3176.66	3176.66	3176.66	3176.66	4887.169
Total Flow kmol/sec	111.0473	111.0473	111.0473	111.0473	38.86655	38.86655	38.86655	111.0473	111.0473	72.18074	72.18074	72.18074	72.18074	111.0473
Total Flow kg/sec	4887.169	4887.169	4887.169	4887.169	1710.509	1710.509	1710.509	4887.169	4887.169	3176.66	3176.66	3176.66	3176.66	4887.169
Total Flow cum/sec	31.86987	85.34876	45.52351	24.10655	8.437291	4.42833	4.42833	12.65234	24.97563	15.66926	4.471121	4.016269	8.224005	31.86987
Temperature C	650	509.2691	177.7188	59.98291	59.98291	174.719	174.719	174.7183	453.774	59.98291	20	49.92136	174.7179	650
Pressure atm	290	85.72415	84.14508	82.86208	82.86208	290	290	290	290	82.86208	81.87515	290	290	290
Vapor Frac	1	1	1	1	1	1	1	1	1	1	0	1	1	1
Liquid Frac	0	0	0	0	0	0	0	0	0	0	1	0	0	0
Solid Frac	0	0	0	0	0	0	0	0	0	0	0	0	0	0
Enthalpy J/kmol	-3.6E+08	-3.7E+08	-3.9E+08	-4E+08	-4E+08	-3.9E+08	-3.9E+08	-3.9E+08	-3.8E+08	-4E+08	-4E+08	-4E+08	-3.9E+08	-3.6E+08
Enthalpy J/kg	-8275100	-8448400	-8837700	-8997600	-8997600	-8916300	-8916300	-8916300	-8526900	-8997600	-9194900	-9162300	-8916300	-8275100
Enthalpy Watt	-4E+10	-4.1E+10	-4.3E+10	-4.4E+10	-1.5E+10	-1.5E+10	-1.5E+10	-4.4E+10	-4.2E+10	-2.9E+10	-2.9E+10	-2.9E+10	-2.8E+10	-4E+10
Entropy J/kmol-K	6268.034	8017.065	-20289.9	-38469.8	-38469.8	-37259	-37259	-37259.1	-7231.36	-38469.8	-66424.7	-65755	-37259.2	6268.034
Entropy J/kg-K	142.4236	182.1655	-461.031	-874.12	-874.12	-846.608	-846.608	-846.61	-164.312	-874.12	-1509.32	-1494.1	-846.611	142.4236
Density kmol/cum	3.484398	1.3011	2.439339	4.60652	4.60652	8.776796	8.776796	8.776822	4.446226	4.60652	16.14377	17.97209	8.776835	3.484398
Density kg/cum	153.3476	57.26116	107.3548	202.732	202.732	386.265	386.265	386.2662	195.6775	202.732	710.484	790.948	386.2668	153.3476
Average MW	44.0098	44.0098	44.0098	44.0098	44.0098	44.0098	44.0098	44.0098	44.0098	44.0098	44.0098	44.0098	44.0098	44.0098
Liq Vol 60F cum/sec	5.947448	5.947448	5.947448	5.947448	2.081607	2.081607	2.081607	5.947448	5.947448	3.865841	3.865841	3.865841	3.865841	5.947448
Substream: $TOTAL														
Total Flow kg/sec	4887.169	4887.169	4887.169	4887.169	1710.509	1710.509	1710.509	4887.169	4887.169	3176.66	3176.66	3176.66	3176.66	4887.169
Enthalpy Watt	-4E+10	-4.1E+10	-4.3E+10	-4.4E+10	-1.5E+10	-1.5E+10	-1.5E+10	-4.4E+10	-4.2E+10	-2.9E+10	-2.9E+10	-2.9E+10	-2.8E+10	-4E+10

2.5 TASK 3.0 – TECHNOLOGY GAP ANALYSIS

2.5.1 SUBTASK 3.1 – CRITICAL COMPONENT IDENTIFICATION

The process of identifying components that require further development or adaptation for use with the supercritical oxy-combustion cycle was executed as a parallel task to the Engineering and Economic Analysis. Changes to the cycle layout and results of the thermodynamic analysis were reflected in the components evaluated for the Technical Gap Analysis, and the results of the Technical Gap Analysis were incorporated into the Economic Analysis to determine cost of electricity (COE) and capital costs. The assessment of specific components and technologies progressed as follows:

1. [Month 1]. Identify critical components.
2. [Months 2-4]. For each category of critical components, conduct a thorough review of technological alternatives. For example, in the case of flue gas desulfurization, about two dozen processes were identified, of which five were chosen for detailed review.
3. [Months 4-7]. Following the Step 2 canvassing of the technological universe – and with the benefit of the Aspen Plus model – a down-select of the various candidates was performed to identify those processes and components that could work in the model flow plan. Where no such candidate existed, a technical gap was called out.
4. [Months 4-7]. All categories were judged as to Technology Readiness Level (TRL), a chart of which is provided.
5. [Months 5-8]. For components/processes for which TRL is 9, vendor quotations were sought and sizing calculations were made.
6. For the specific case of the power block, the choice was made to focus on the oxy-combustion specific technologies and leverage power block advancements under an ongoing project, DOE Cooperative Agreement No. DE-EE0005804, "*Development of a high efficiency hot gas turbo-expander and low-cost heat exchangers for optimized CSP supercritical CO2 operation*." Both the participants in this current investigation of oxy-combustion are also participants in the 5804 project.

The various technologies were each analyzed according to: (1) relevancy to oxy-combustion; (2) technology readiness; and (3) cost.

2.5.2 SUBTASK 3.2 – REVIEW OF CRITICAL COMPONENT INTERNAL AND EXTERNAL INVESTIGATIONS

An initial assessment of the key component in the proposed cycle concepts indicated that a majority of the cycle components are commercially available for high pressure applications. Further review of these commercially available components assessed specific challenges, such as material compatibility, specific for a supercritical CO2 environment. Technology levels for key components are outlined in Table 2-16.

Table 2-16. TRL Assessment for Key Components

Process components	Description	Material	Y or N				Operating Conditions				Expected performance characteristics	Assumptions regarding anticipated application issue	TRL
			Basis for Design & performance				Inlet		Outlet				
Coal Pulverizer	Generic		N	Y	N	N					100 micron particulates	No issue is expected	9
Slurry Pumping System	Self-designed batch pressurization of pumped slurry	Carbon steel	Y	Y	N	N	25	1	30	100	1,000 gpm of abrasive slurry, pumped up to 100 bar	6 months lead time for custom pump; pump and pressurization systems are separately TRL=9 but haven't been thoughly demonstrated together.	8
Supercritical oxy-combustor	Slurry-injected jacketed vessel	TBD	Y	N	N	Y	450	94	650	94	Concentrated ignition zone in pressurized atmosphere of CO2 from recycle.	Performance based on extensive CFD modeling.	3
Cyclone separator	Multiple cyclones with replaceable liners ganged in parallel.	Inconel - thick wall	N	Y	N	N	700	94	700	94	~100% removal of particulates $\geq$ 10 micron	Manufacturing: forging of the cyclone sections combined with welding; expected lead time is 6 months	9
Cyclone underflow	Lock chamber with a pair of rotary valves to dissipate pressure of particulate stream.	Combination of Inconel and carbon steels, depending on temperature exposure	Y	N	N	N	600	92	100	1	Letdown of pressure for atmospheric recovery of particulates without loss of pressure in the combustion loop.	Large water consumption, custom designed lock chamber and control valves for high P and high T slurry	5
Recuperator 1 (MAIN)	Microchannel counterflow; design derived from SunShot program	Inconel	Y	N	N	Y	650	94	450	94	Approach temperatures with 5 ^{o}C	Particulate removal is sufficient to avoid clogging 1-mm channels; periodic cleaning offline; Inconel alloy	3
Recuperator 2 (MAIN)	Microchannel counterflow; design derived from SunShot program	Stainless steel	Y	N	N	Y	450	94	330	94	Approach temperatures with 5 ^{o}C	Particulate removal is sufficient to avoid clogging 1-mm channels; periodic cleaning offline; stainless steel	3
Power loop	Modeled after SwRI/GE/Thar SunShot program		Y	N	N	Y					50% efficiency at capital cost of $1,200/kWe	SunShot team meets program objectives	3
Cleaning recuperator	Microchannel counterflow; design derived from SunShot program	Stainless steel	Y	N	N	Y	330	94	90	94	Approach temperatures with 5 ^{o}C	Particulate removal is sufficient to avoid clogging 1-mm channels; periodic cleaning offline; stainless steel	3
Sulfur cleanup	Generic - spray chamber with customized scrubber vessel thickness for large pressure application	Thick stainless steel with linings	Y	Y	N	N	165	94	100	80	Inlet: low sulfur content, but high pressure; 95% SO2 removal, 95% Hg removal	Gas temperature is higher than normal scrubbing condition, but high pressure is assumed to promote the solubility of SO2 and other gases	9
Metals removal	Generic - metals are expected to be oxidized and carried away by wet scrubbers and cyclone separators		N	Y	N	N					90% of oxidized Hg metal is removed	Large L/G ratio is expected to promote high mercury absorption, high level of oxygen helps the oxidation and hence the absorption, negligible chlorine content	9
Re-compressor	Generic		N	Y	N	N	150	80	150	94			9
Air Separation Unit	Generic - Based on cryogenic distillation process		N	Y	N	N	25	1	25	5-10	Large flow rate of 6,220 tpd distributed among 4 units, ~100% purity	Oxygen pumped as liquid directly from cryogenic distillation column before any re-heating ahead of the combustor.	9
Oxygen pump	Liquid oxygen (LOX) pump for high pressure application		Y	N	Y	Y	-183	1	-182	94	1000 gpm at cryogenic state, discharged at 94 bar	LOX pump demonstrated for 150-psi pressure boost can be staged to required combustor pressure.	7
Oxygen compressor	Generic		N	Y	N	N	-115	5-10	40	100	As many as 20 pair of two-stage compressor	Not recommended due to high cost and complexity	NA
Piping and valves	Generic for medium and low temperature applications, customized pipe design and exotic materials for high temperature gas	Inconel in high-temp areas	N	Y	N	N	max 700	max 94	max 700	max 94	Low pressure loss, minimum heat loss	Insulation for heat loss	9

2.5.3 SUBTASK 3.3 – CRITICAL COMPONENT DEVELOPMENT REQUIREMENTS

The Technical Gap Analysis of the supercritical oxy-combustion power cycle identified one critical component with a low Technology Reediness Level (TRL). This component, the supercritical oxy-combustor operating at pressures near 100 atm, is unique to the supercritical oxy-combustion cycle. In addition to the low TRL supercritical oxy-combustor, several secondary systems were identified that are commercially available, but would require adaptation for use with the supercritical oxy-combustion cycle. These secondary systems include the high pressure pulverized coal feed, the high temperature cyclone, the removal of post-combustion particulates from the high pressure cyclone underflow stream, and micro-channel heat exchangers tolerant of particulate loading. Other key findings of the technical gap analysis include:

- Air separation is a major cost item, exaggerated by the need to pressurize the O2 stream to nearly 100 bar. While the technology and manufacturing capability to provide oxygen in the quantity required of a 550 MW oxy-combustion power plant, the state-of-the-art for pumping/compression components is not yet up to commercial readiness.
- Particulate removal technology is available, but with the following caveats: Process engineering is required to develop a system for de-pressurization and recovery of solids. Cyclones should be outfitted with replaceable inner jackets, so as to manage abrasion and wear. The particulates that escape from cyclone separation will likely be in a size range of 1-5 microns; the downstream heat exchangers must be capable of handling these particles.
- Cyclones, heat exchangers, air separation units, and flue gas desulfurization systems should be specified as multiple smaller units in parallel. This is advantages for economy of scale and sparing.
- Compact, low cost heat exchangers are a key technology impacting footprint and cost of the supercritical oxy-combustion cycle. Microchannel heat exchangers are currently at a low TRL, but are actively being developed for multiple applications including supercritical CO2 power cycles. Because it is expected that 1-5 micron may pass through the cyclone separator, heat exchanger sparing and cleaning are important considerations.
- Metals removal, particularly mercury, can occur in the same equipment as used for flue gas desulfurization.
- Desulfurization using limestone slurry with recovery of gypsum byproduct is the preferred flue gas desulfurization method at elevated pressured.
- For slurry handling, conventional progressive-cavity pumps can be used for conveying slurry at low pressure differential into holding tanks. There, the pressurized stream of recycle CO2 can be used to bring the slurry to pressure. Direct feed of dry pulverized coal would be preferred to maximize plant efficiencies, however direct feed systems at high pressures are at a low TRL.

2.6 TASK 4.0 – PHASE II APPLICATION

2.6.1 COMBUSTOR FLOW PATH DESIGN

A literature review on pulverized coal delivery to combustors was first carried out as part of the design process. It is observed that coal water slurry (CWS) is normally employed for injecting at higher operating pressures due to poor transport performance using CO_2 or O_2 as a carrier gas.

Using supercritical CO_2 as a carrier was initially considered for this project, since its density is much higher than CO_2 near standard conditions. However, it was decided that the logistics of mixing coal while maintaining a supercritical state would introduce unnecessary complications to the design. Thus, it has been decided to proceed with a CWS fuel injection system. Various atomizer designs have been utilized with CWS in the past, including pressure nozzles, twin-fluid atomizers, air-assist atomizers, effervescent atomizers, and rotary atomizers[15]. A rotary atomizer design was selected for this project in order to minimize injector clogging issues while providing a good distribution of fuel through the combustor. Breakup and subsequent atomization of the liquid sheet into droplets is primarily a function of the interfacial surface tension between the water and surrounding gas. It has been shown that atomization in a CO_2 diluent environment, as opposed to N_2, results in smaller droplets at elevated pressures (> 5 MPa) due to the smaller interfacial tension of CO_2-water[16]. This implies that pressurized oxy-combustors may produce more efficient combustion, since evaporation time of the coal particles is directly related to surface area.

Computational efforts first focused on sensitivity of wall temperatures to the combustion location/intensity, and sensitivity of reactant mixing to injection properties. The latter is particularly important, since reactant mixing determines the location and extent of the flammable zone. Note that the flammable zone is defined as the region where O_2 and fuel exist in concentrations suitable for sustained combustion. Previous studies have shown ignition behavior of coal in an O_2/CO_2 environment depends heavily on local O_2 concentration[17,18] and the level of CO_2 that is used for thermal control[19].

The software package CFDesign was initially employed to set up cases where a model gas was injected into a domain with an imposed energy source. This provided a rough approximation of thermal effects due to combustion and convective mixing. A simple surface-to-surface radiation model was also incorporated to include the influence of radiation. The size and location of the energy source were varied to study the wall temperature sensitivity.

The initial concept for the Phase II effort includes the construction and proving of a scaled combustion loop to demonstrate the combustor concept and evaluate combustion efficiencies. From the DOE-provided heating value of Montana Rosebud PRB coal, the required feed rate of coal was computed to be 0.052 kg/s for a scaled 500 kW combustor, assuming a 50% thermal efficiency. The required oxygen feed rate based on stoichiometric combustion was then computed from the compositional analysis (ultimate weight percent).

From preliminary CFDesign simulations, it was concluded that a cooled liner would be required to maintain wall temperatures within acceptable limits for the material stresses. For the sake of convenience and efficiency, the coolant chosen was supercritical CO_2 that could be reclaimed from the cycle. As demonstrated by the steady state temperature and velocity contours of Figure 2-39, using CO_2 injection along the sides and partially on the top of the combustor keeps high temperatures in the combustion zone from reaching the walls. Based on this initial work, a rough sizing for the scaled combustor was selected.

---

[15] Chen, L., Yong, S.Z., Ghoniem, A.F., Oxy-fuel Combustion of Pulverized Coal: Characterization, Fundamentals, Stabilization and CFD Modeling, *Progress in Energy and Combustion Science*, 38 (2012) 156-214.

[16] Yan, W., Zhao, G.Y., Chen, G.J., Guo, T.M. Interfacial Tension of (Methane + Nitrogen) + Water and (Carbon Dioxide + Nitrogen) + Water Systems, *Journal of Chemical and Engineering Data*, 46 (2001) 1544-1548.

[17] Xiaohong, H., Zhaohui, L., Jing, L., Ming, Y. Yunye, S., Chuguang, Z., Ignition Behavior of Pulverized Coals in Lower Oxygen Content O_2/CO_2 Atmosphere, *Proceedings of the 2nd Oxyfuel Combustion Conference*, 2011.

[18] Fan, Y., Zou, Z., Cao, Z., Xu, Y., Jiang, X., Ignition Characteristics of Pulverized Coal under High Oxygen Concentrations, *Energy and Fuels*, 22 (2008) 892-897.

[19] Scheffknecht, G., Al-Makhadmeh, L., Schnell, U., Maier, J., Oxy-fuel Coal Combustion – A Review of the Current State-of-the-Art, *International Journal of Greenhouse Gas Control*, 55 (2011) 516-535.

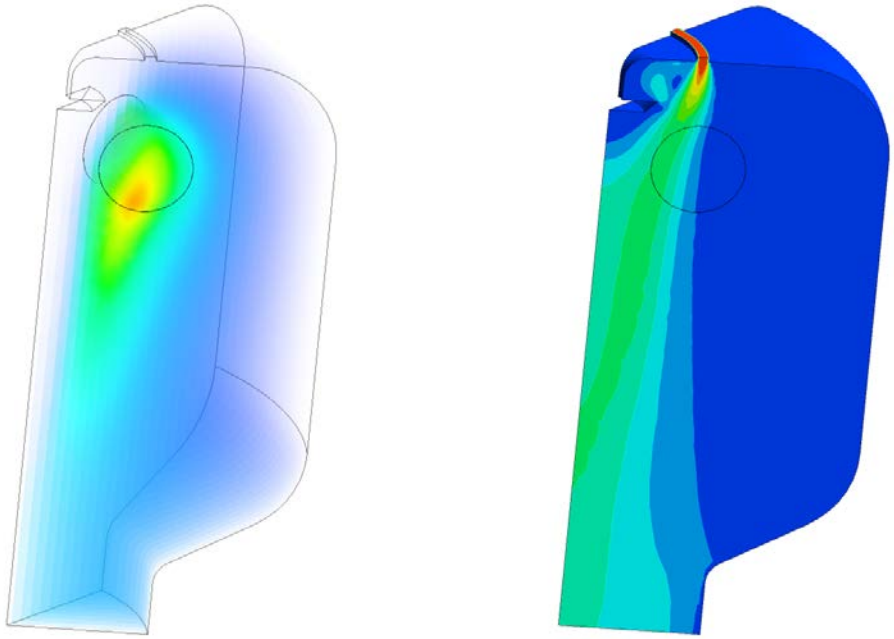

Figure 2-39. Sample results from combustor heat source sensitivity study: (left) temperature and (right) velocity magnitude

Having determined that a supercritical CO_2-cooled liner would be necessary to maintain wall temperatures within acceptable limits, various designs were investigated. To reduce manufacturing costs, a simple straight-hole array has been selected. Sizing and spacing of the holes was based on the uniformity of the velocity profile into the combustor. Sample cases were set up using various sized holes and distributions. In addition, the influence of double-wall versus single-wall liners was explored. Figure 2-40 and Figure 2-41 present velocity distribution contours from several cases. From these, it has been observed that using a double-walled liner design did not reduce the distance from the liner at which the velocity becomes relatively uniform. In addition, it was found that 0.125-inch holes provided a more uniform flow distribution than 0.25-inch holes. Machine tolerance issues and costs associated with requiring holes smaller than 0.125-inch made this a lower design limit bound. In conclusion, the final combustion liner design has been specified as single-wall using 0.125-inch holes and 0.5-inch center-to-center spacing.

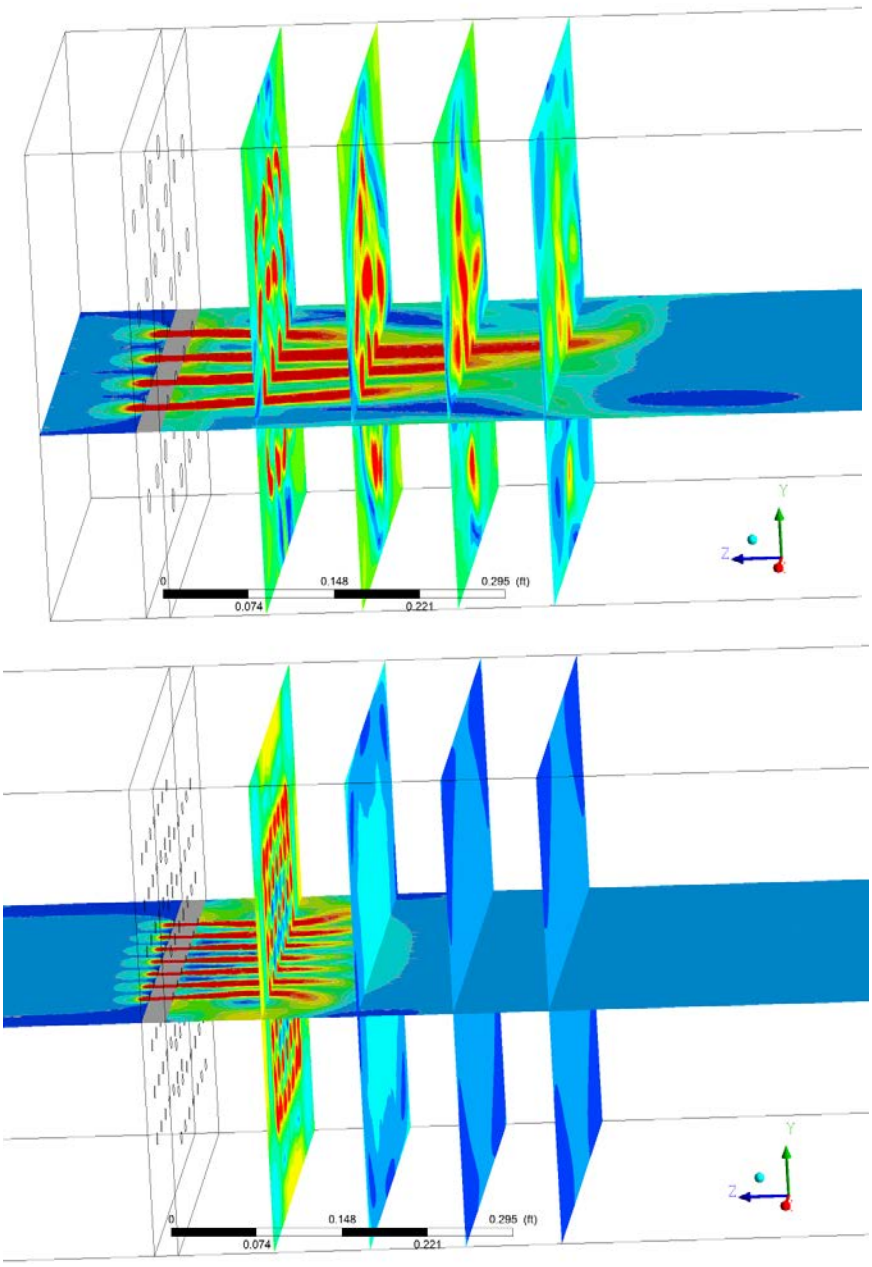

Figure 2-40. Velocity distribution contours from sample of single-wall liner (above) with 0.25-inch holes, and (below) 0.125-inch holes.

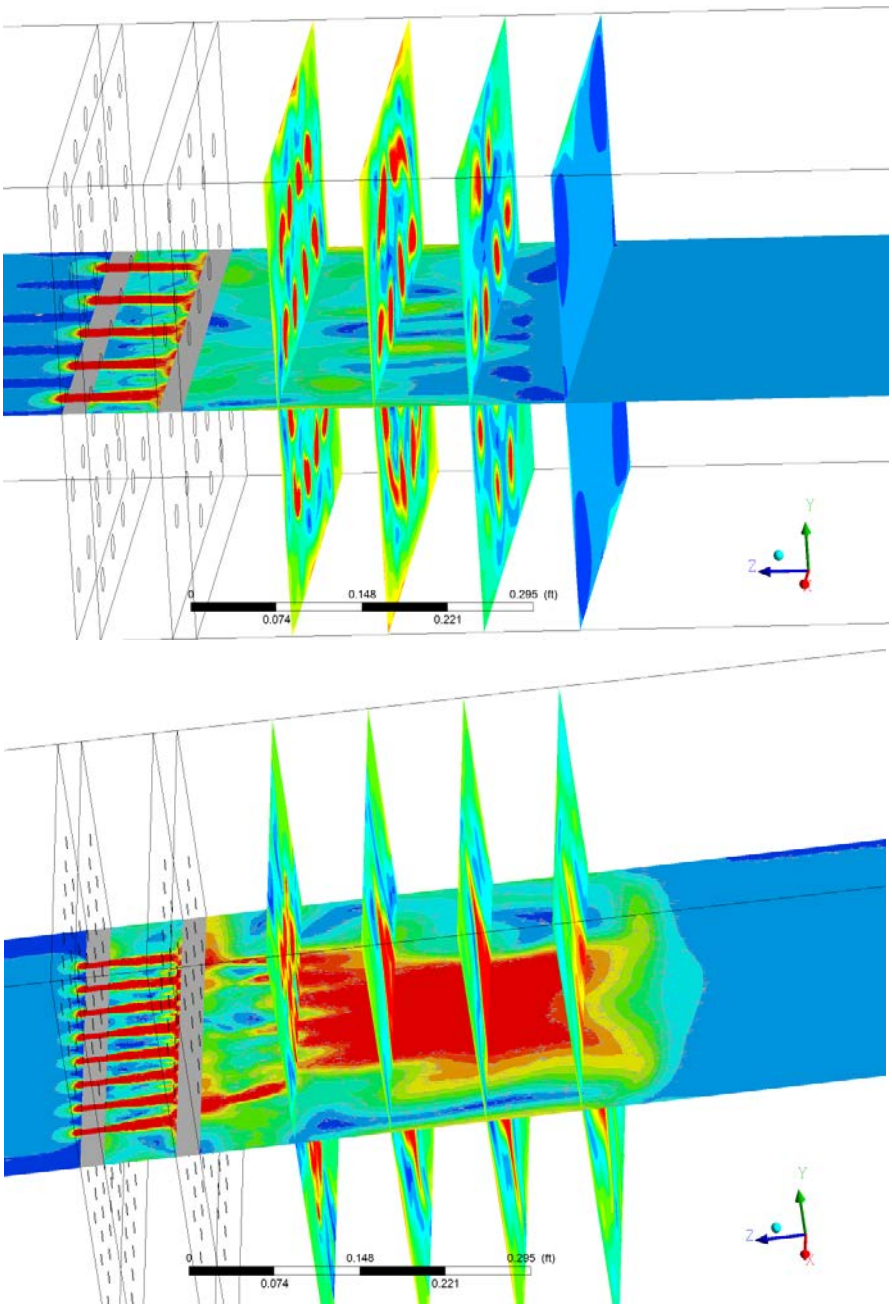

Figure 2-41. Velocity distribution contours from sample of double-wall liner (above) with 0.25-inch holes, and (below) 0.125-inch holes

For the next phase of the combustor design, mixing and combustion of reactants was modeled. Combustion of pulverized coal slurry is a multi-step process. First, particle tracking must be employed to calculate the dispersion of the slurry droplets. Second, vaporization of the water from the slurry droplet must be computed. Third, devolatilization of coal particles is modeled as decomposition into volatiles and char. Fourth, gas phase combustion of volatiles is simulated. ANSYS FLUENT version 14.5 was employed for all these tasks. A brief description of the submodels discussed above is now offered.

Particle tracking for the slurry droplets employed an Eulerian-Lagrangian approach. In this, the gas phase is treated as a continuum, with momentum calculated using the Navier-Stokes

equations. The droplet motion is computed by considering the droplets as dispersed phase particles, and tracking them with a Lagrangian approach through the continuum field. Note that the droplets can exchange momentum, mass, and energy with the fluid phase. For the sake of simplicity, the current case neglects particle-particle interactions and assumes all droplets enter the domain with a uniform diameter. The influence of turbulence on particle dispersion is modeled using a stochastic tracking (random walk) algorithm.

Vaporization of the water from the injected droplets includes several different physical models in FLUENT. Inert heating and cooling laws adjust the energy level in the droplet based on a simple heat balance that relates the particle temperature to convective and radiative heat transfer at the particle surface. This law is applied until the temperature of the particle reaches the vaporization temperature, at which point the droplet evaporation law comes into effect. Once vaporization is initiated, the droplet will continue to experience evaporation until all the liquid is gone or the droplet reaches the boiling point. If the temperature reaches the boiling point, the vaporization model is automatically switched to the boiling model.

Devolatilization of the coal particles begins to take place once the coal particle reaches the temperature at which the volatile components of the coal begin to vaporize. The process continues while any volatile mass remains in the particle. Although various models are available in FLUENT, for the current project a simple constant rate devolatilization model was employed. Heat transfer to the particle included contributions from both convection and radiation during the devolatilization process.

Once fuel is available in gaseous form from the devolatilization process, chemical reactions take place to release energy. Combustion may be modeled with varying level of detail. On one extreme is a single global reaction that converts reactants directly to products. On the other are mechanisms composed of hundreds of reactions that trace the chemical pathways and the formation/consumption of radical species. The current project utilized the following two-equation mechanism:

$$C_{1.18}H_{3.32}O_{0.68}N_{0.0503}S_{0.224} + 1.09O_2 \rightarrow 1.18CO + 1.66H_2O + 0.0251N_2 + 0.0224SO_2$$

$$CO + 0.5O_2 \rightarrow CO_2$$

Note that the stoichiometric coefficients in the reactions are calculated from the ultimate and proximate coal analysis for the Montana Rosebud PBR coal used in bench scale testing.

A variety of simulations have been carried out to investigate the influence of oxidizer injector location and mass flow rate, carbon dioxide flow rate and distribution, water concentration of the coal slurry, and injection particle size. Based upon the results of this work, the scaled combustor design shown in Figure 2-42 was selected. This design includes details on geometry of the rotary injector, motor sizing, pressurized sealing of the vessel, pressure analysis of the casing, and liner design. CFD analysis concentrated primarily on the flow behavior within the liner, the region shown in Figure 2-43. Note that this represents a 45-degree slice of the fluid domain contained within the liner region of the combustor. Rotational periodic boundary conditions were employed at the sliced sides in the simulations. General observations from the FLUENT cases are now discussed.

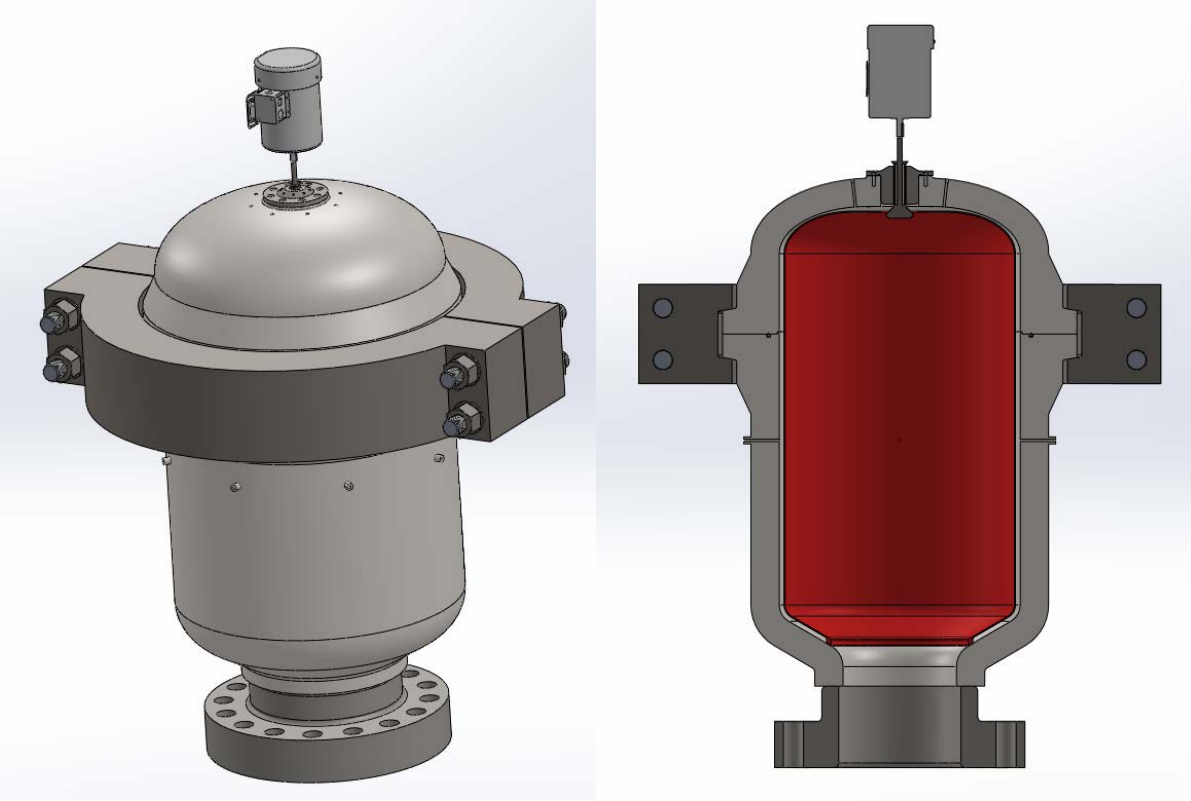

Figure 2-42. Scaled combustor design, including: motor, rotary injector, casing, and liner

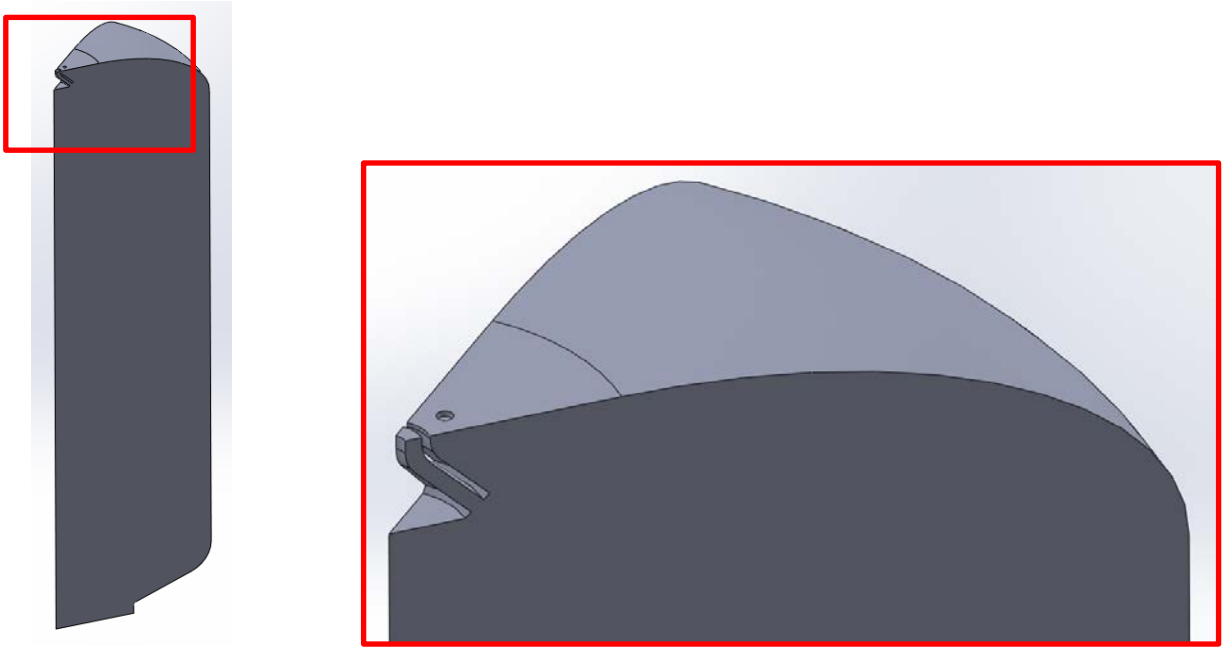

Figure 2-43. Scaled combustor design, showing fluid domain inside liner (1/8th slice)

The first observation from simulation results is that maximum slurry droplet sizes are limited by the evaporation time requirements, combined with the expected residence time of particles in the combustor. Initial simulations used droplet sizes of the order of 2,000 microns. However, it was found that the residence time in the scaled combustor was not sufficient to allow all of the coal to burn before exiting the domain. Using the analytical droplet lifetime relation outlined in

Turns[20], and assuming free stream conditions of 1500˚F and 1400 psi, a 1,000 micron diameter water-only droplet would require almost 10 seconds to evaporate, while a 100 micron droplet would require about 0.1 seconds. In addition to taking much longer to evaporate, the heavier particles also tended to recirculate less in the convective flow. Therefore, it was decided to switch to a 100 micron particle diameter. Using droplets of this size and assuming 20% water by weight in the slurry, particle residence time within the combustor domain increased to an average of about 10 seconds. This allowed sufficient time for evaporation and complete combustion to take place.

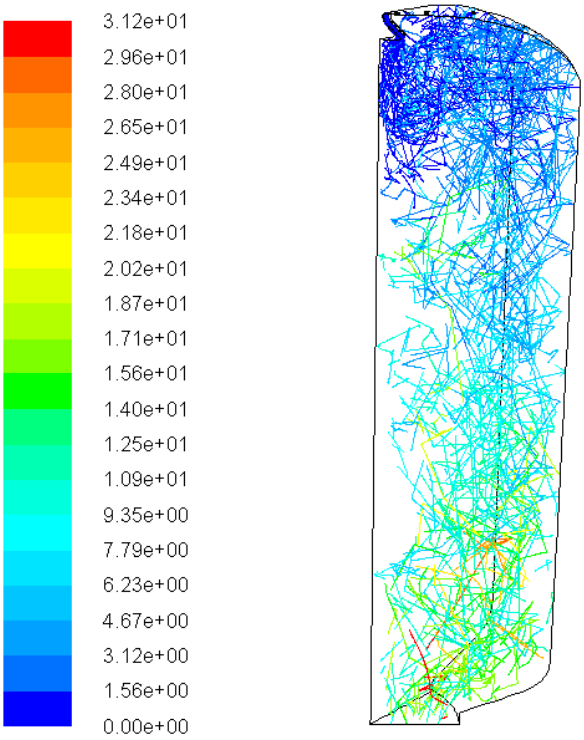

Figure 2-44. Particle traces within domain using 100 μm diameter-sized droplets (color indicates particle residence time [sec]).

A second observation from the CFD studies is the importance of reactant mixing and local concentration on combustion efficiency. Four different locations for oxygen injection were considered, including offset distances from the symmetry axis of 1-inch, 2.75-inch, 6.0-inch, and 9-inch. Combustion was found to be strongest with an offset distance of 1-inch, putting it in closest proximity to the coal slurry injector.

The flow rate of oxygen was also varied as part of the studies. It was decided to inject at a stoichiometric rate based on the known coal flow into the domain. This maximized cycle efficiency by avoiding excessive oxygen use. With the simulated level of fuel/oxidizer mixing in the combustor, both volatiles and char showed closed to 100% conversion rates.

Figure 2-45 and Figure 2-46 show oxidizer, fuel, and water vapor concentrations for the case of stoichiometric oxygen injection rate using a 1-inch centerline offset injector distance. As shown, the water from the slurry droplets evaporates relatively quickly once the slurry exits the injector channel. The coal then devolatilizes to gaseous fuel in close proximity to the oxidizer stream. Figure 2-47 presents a velocity vector map of the centerline plane of the domain. As indicated,

[20] Turns, S.R., *An Introduction to Combustion*, 2nd Edition, McGraw-Hill Companies, New York, NY, 2000.

the injection conditions set up axial swirl in the upper region of the domain. This increases the residence time of the coal, and facilitates reactant mixing for complete combustion.

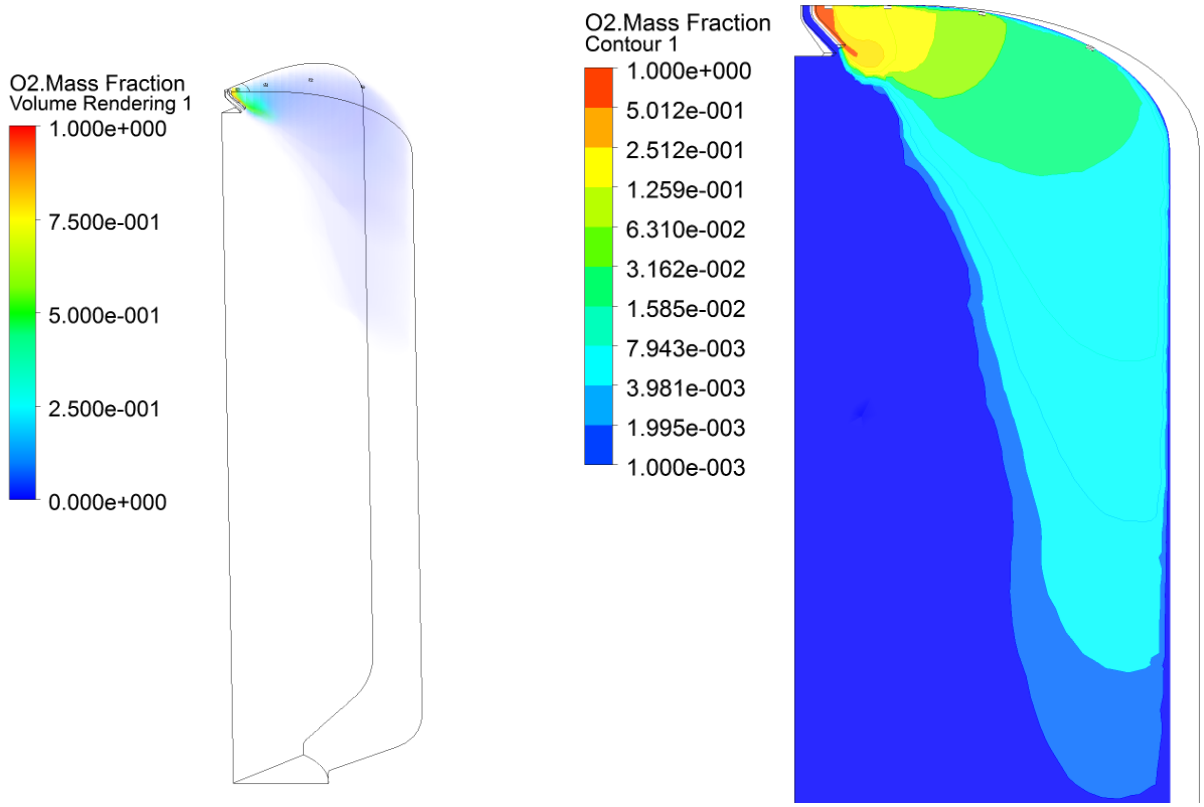

Figure 2-45. Mass fraction of oxygen: (left) volume rendering and (right) centerline plane contours

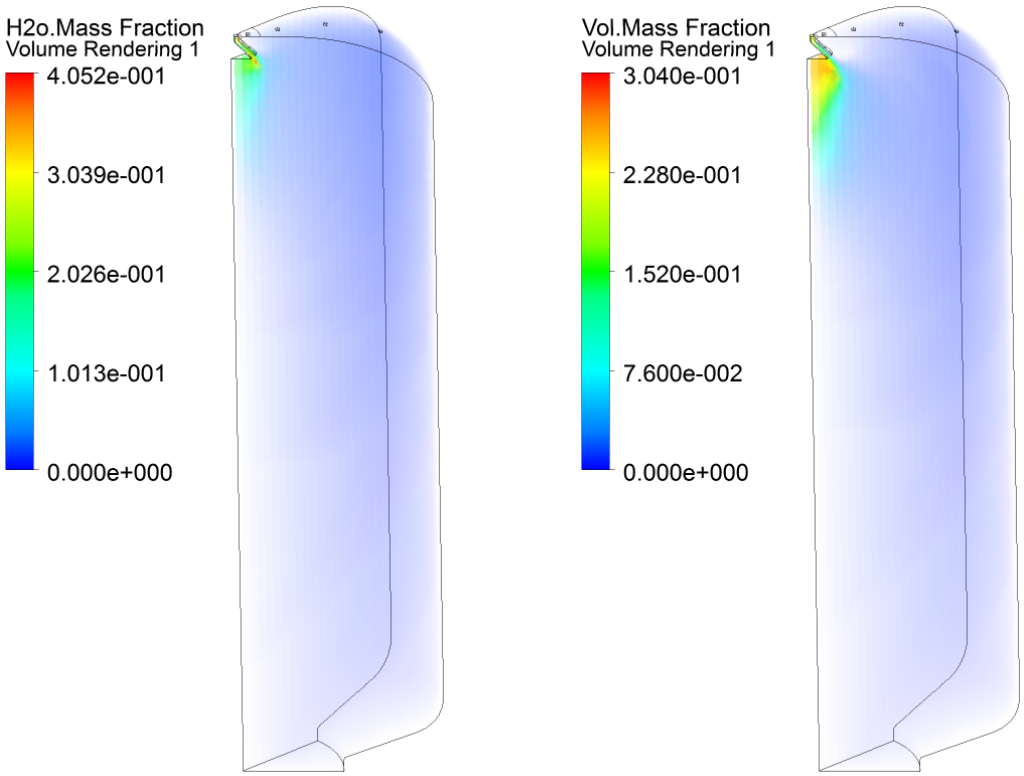

Figure 2-46. Mass fraction volume rendering: (left) water vapor, and (right) gasified volatiles

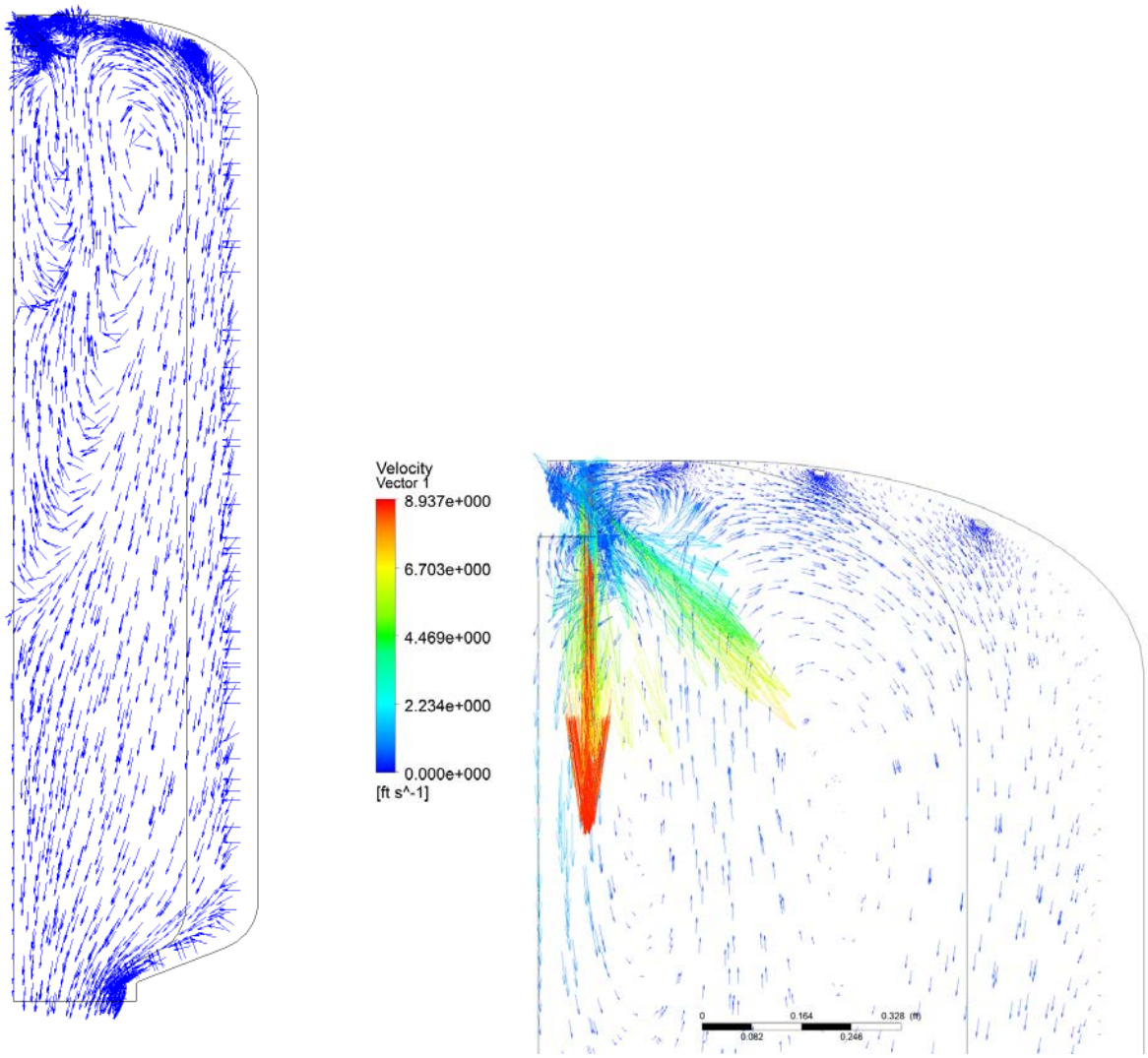

Figure 2-47. Velocity distribution: (left) normalized vectors, and (right) magnitude-scaled vectors

A third observation from the CFD studies is effect of slurry water concentration and diluent gas on both combustion and internal temperatures. Both the water in the slurry and the supercritical carbon dioxide injected to cool the combustor walls act as thermal sinks. Heat is absorbed during the evaporation process of the slurry droplets, and the excess water vapor and CO_2 provide thermal mass to lower the overall temperature of the combustor. Minimizing the water concentration was desirable, as this would lead to shorter evaporation times and higher combustor efficiency. Based on cycle models, a water concentration of 20% (by weight) was the highest desirable level. However, experimental benchtop blending of 30 μm pulverized coal showed that concentrations of coal higher than 50% led to difficulty maintaining a homogeneous flowable mixture. To combat this difficulty, it was decided that a progressive cavity pump would be used to pump the slurry at high pressure into the rotary injector. These types of pumps have historically been used for transport of challenging slurry media. An ideal injection rate of 0.436 kg/s for CO_2 was found based on a balance of cycle efficiency and temperature control of combustor components.

Figure 2-48 and Figure 2-49 present results using a 20% (by weight) coal slurry concentration. Note in Figure 2-48 that while temperature in the peak combustion zone is quite high, lower temperatures are maintained near the combustor liner and injectors. Product temperature from

the exit of the combustor has been calculated as 1,195˚F. Latent heat loss from evaporation is found to represent less than 4% of the total heat generated by combustion. From Figure 2-48, it may be observed that fuel conversion is near 100%. Particle burnout is completed in the upper half of the domain, and the intermediate CO species mass fraction also returns to zero near the lower half of the domain. Based on a comparison of the lower heating value (LHV) of the coal and the heat of reaction (HOR) results, combustion efficiency is computed as $\eta = \frac{HOR}{LHV} = 79.2\%$.

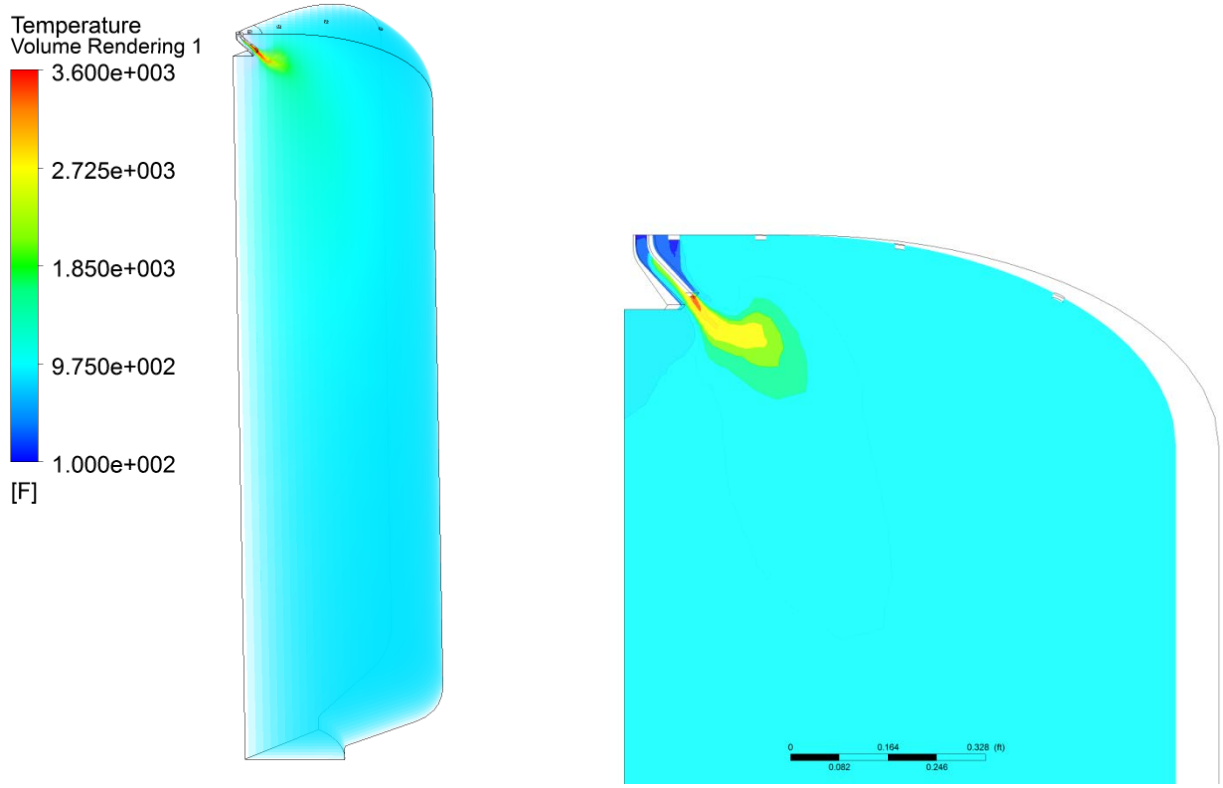

Figure 2-48. Temperature distribution: (left) volume rendering, and (right) centerline plane contours.

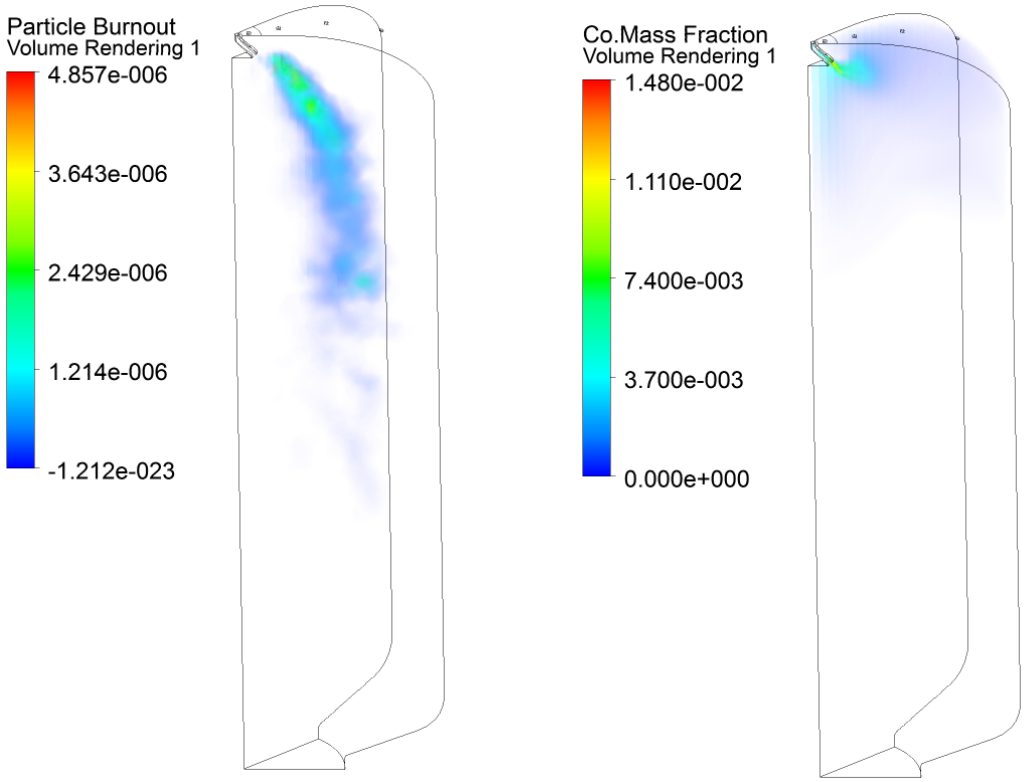

Figure 2-49. Volume rendering: (left) particle burnout [lbm/s], and (right) carbon dioxide mass fraction

It is important to note that the combustion modeling that has been carried out thus far in this project is based upon generalized devolatilization and reaction information for coal. However, the bulk of coal combustion studies in the literature examine coal/air at atmospheric pressure. Some more recent studies investigate coal/O_2 with recycled CO_2. These have found significant differences in chemical and thermal behavior. The partial pressure of triatomic CO_2 is much higher than diatomic N_2, leading to higher radiative emissivity and absorptivity. In addition, CO_2 has a heat capacity about 1.66 times higher than that of N_2. This slows the temperature rise and chemical reaction rates, leading to longer ignition delay. Variation in total pressure can also play a role in combustion. It has been suggested that increased pressure may facilitate coal gasification reactions, increasing char conversion in the products[5]. However, no studies have been found that provide experimental data at pressures as high as considered for this project (between 1,400 and 2,200 psi). For this reason, it is felt that further bench scale testing that provides combustion data at expected operating conditions is an important initial step for more accurate modeling predictions.

2.6.2 COMBUSTOR VESSEL DESIGN

The O_2 Combustor concept is shown in Figure 2-50 and Figure 2-51. The main closure is a clamp style closure with a torispherical head. The head has a 4-inch penetration on the center axis. The inner diameter of the Combustor is 25.5 inches with a plain cylinder length of 28.7 inches. The bottom interface is an ASME flange with a through diameter of 12.9 inches. The transition from the cylinder to the flange is conical with a 30-degree angle. The overall internal length of the combustor is nearly 60 inches.

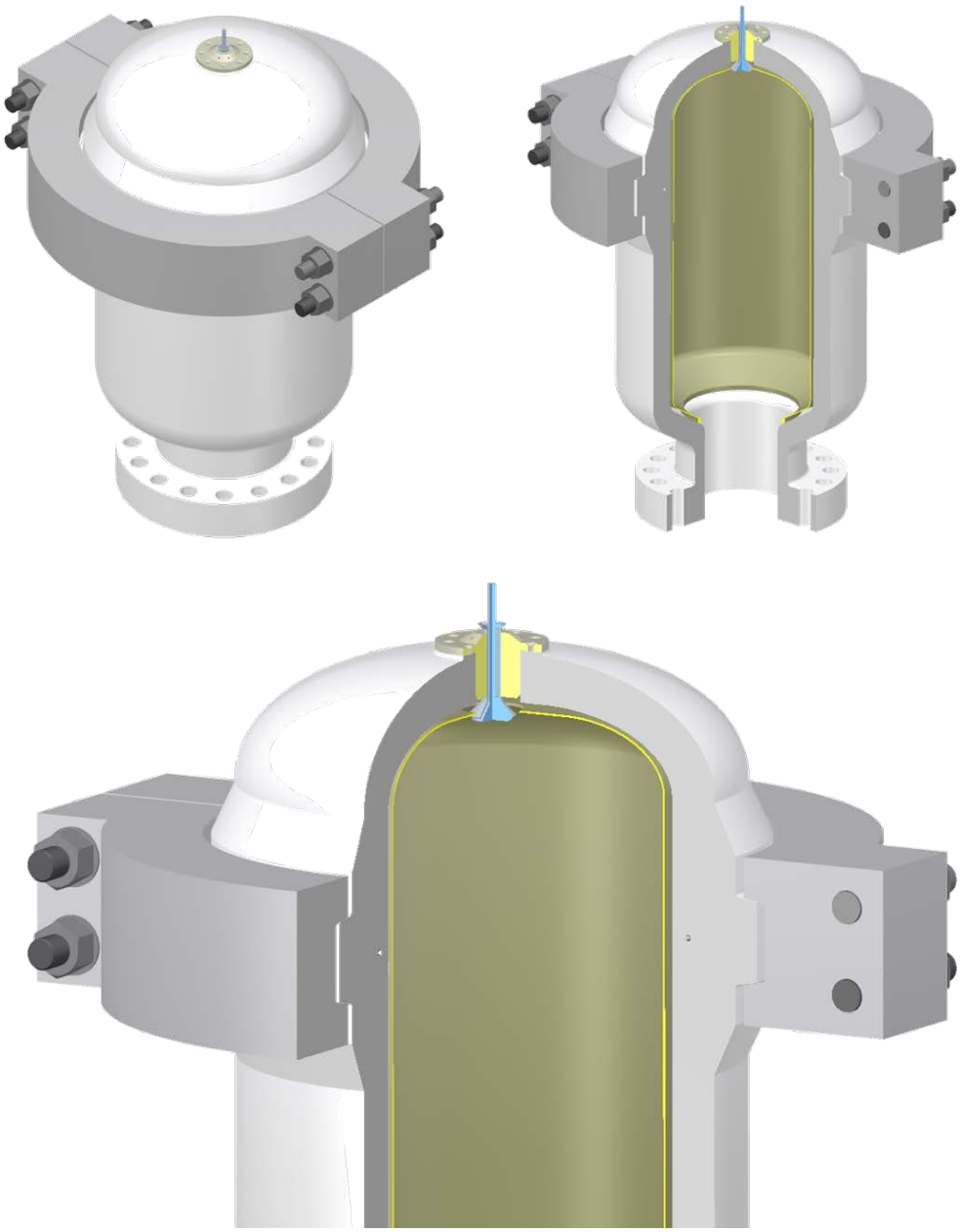

Figure 2-50. O_2 Combustor Concept General Arrangement

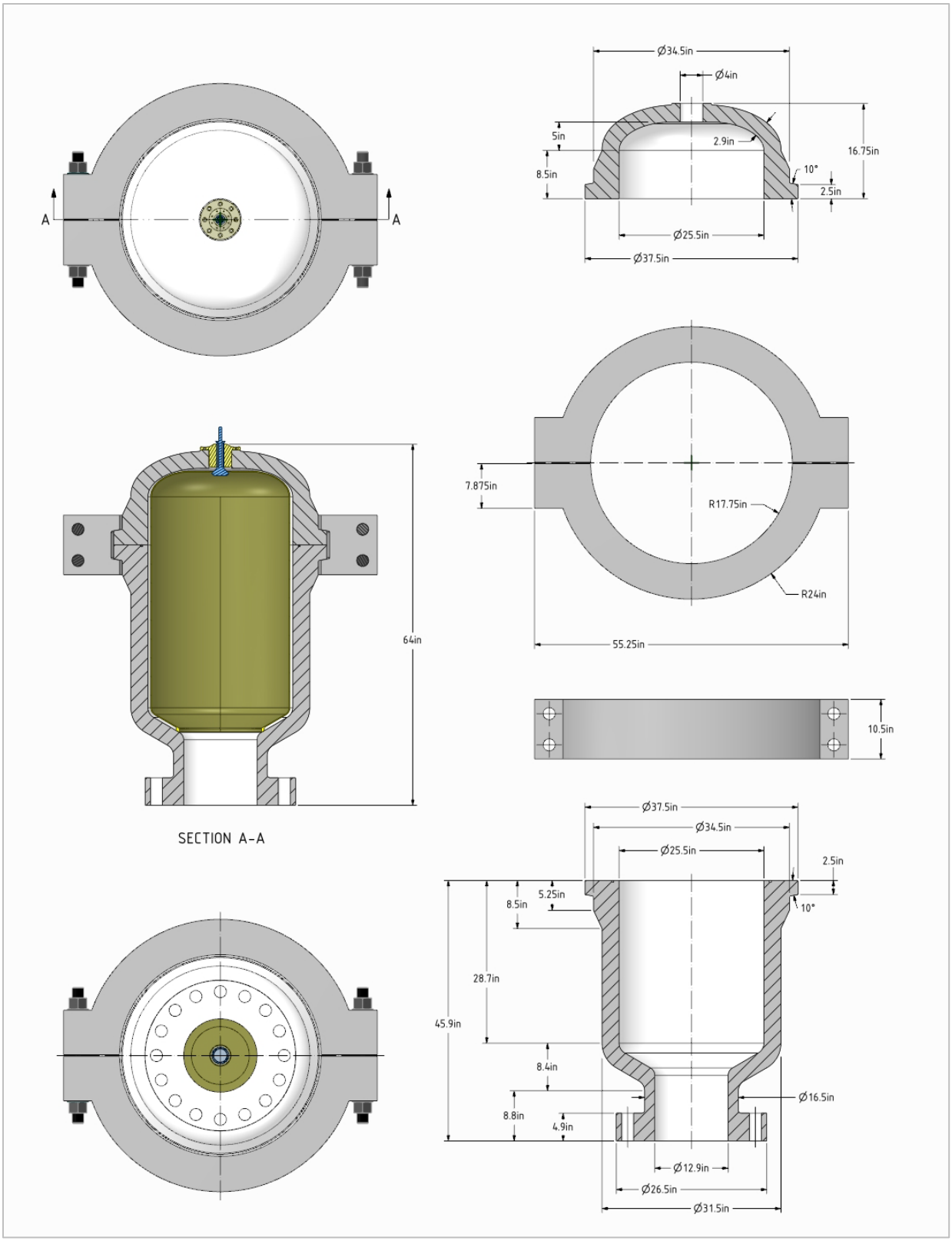

Figure 2-51. O_2 Combustor Concept General Dimensions

A preliminary analysis was run to verify the rough sizing of the O_2 Combustor. The design-by-analysis methodology from Section VIII, Division 2 of the ASME Boiler and Pressure Vessel Code was used.

Material

The material of construction is 316 stainless steel. At the maximum operating temperature of 1,200°F the allowable stress is only 7,400 psi. The allowable stress is derived such that no appreciable creep will occur. Alternatively a creep analysis would have to be performed to determine the permissible life of the chamber at this operating temperature. The elastic modulus at this temperature is 21,200,000 psi.

Analysis Method

The limit load analysis method from Section 5.2.3 of Division 2 was used for this analysis. This method is an alternative to an elastic analysis and stress linearization. The material model is elastic-perfectly plastic with a yield strength of 1.5 times the allowable stress of 7,400 psi (11,100 psi). Small displacement theory is used. For acceptance, the analysis must converge at a load factor of 1.5 (1,500 psi x 1.5 = 2,250 psi). Convergence indicates the component is stable under the applied loads.

Analysis Model

The solid model shown in Figure 2-50 was prepared for analysis and imported into ANSYS Workbench. The meshed model is shown in Figure 2-52. Solid brick elements are used everywhere except for the bolts which are modeled using beam elements. The bolts cut by the symmetry planes use half of the bolt cross section in their section definition. Frictional contact surfaces that allow sliding and separation are used between the clamp and hubs (“B”, “C”, and “D” in Figure 2-53). The penetrator in the torispherical head is included in the model. A no-separation contact definition is used at the interface (“A” in Figure 2-53). The maximum operating pressure of the O_2 Combustor is 1,500 psi. This pressure is applied to the surfaces highlighted in red in Figure 2-54.

The analysis model is a ¼ symmetry model. Symmetry constraints are applied to the surfaces of the solid elements and lines of the beam elements on the XY and YZ planes as shown in Figure 2-55. The beam elements that are perpendicular to the plane of symmetry have a displacement constraint normal to the plane as well as a rotation constraint (Figure 2-56).

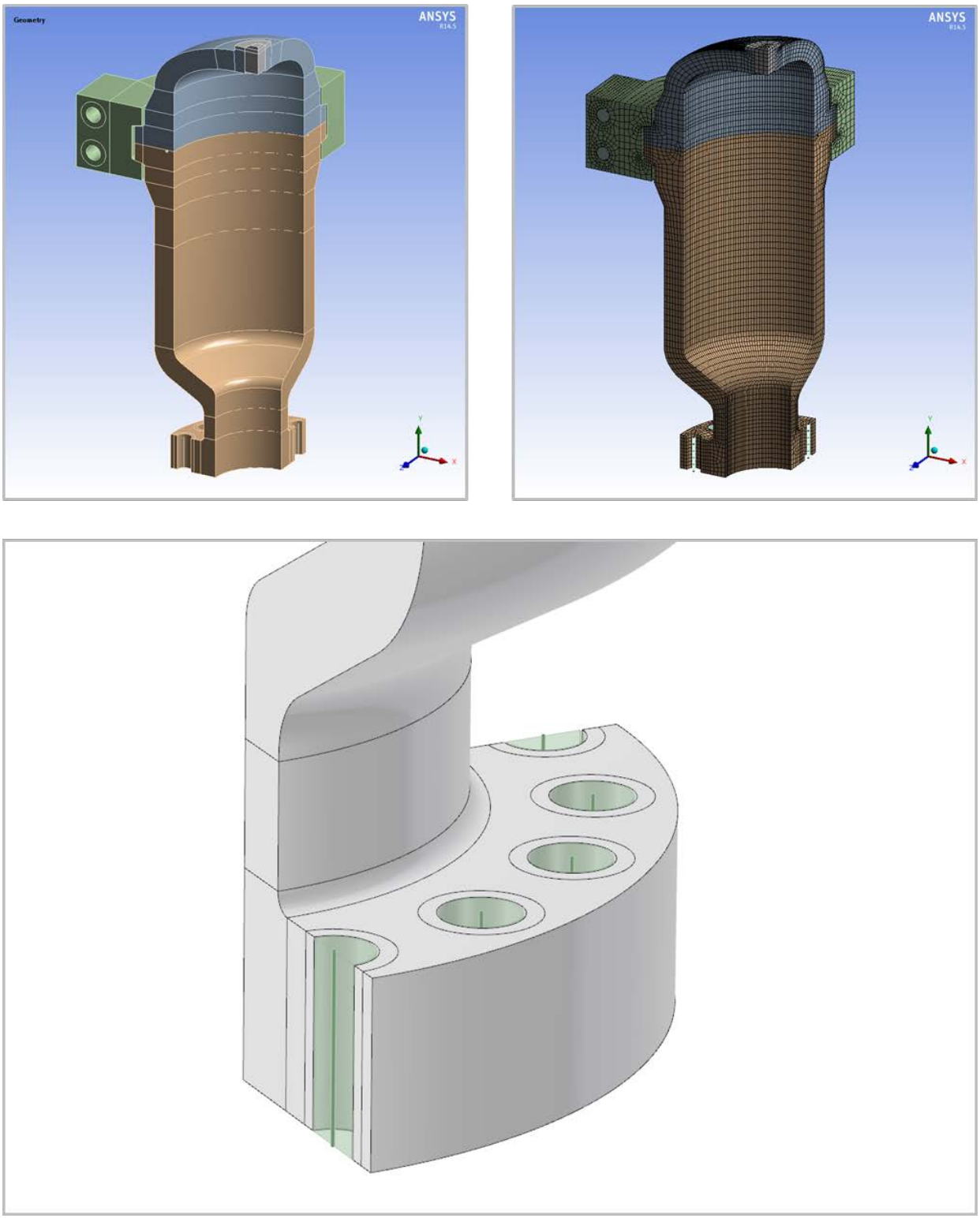

Figure 2-52. Quarter Symmetry Analysis Model

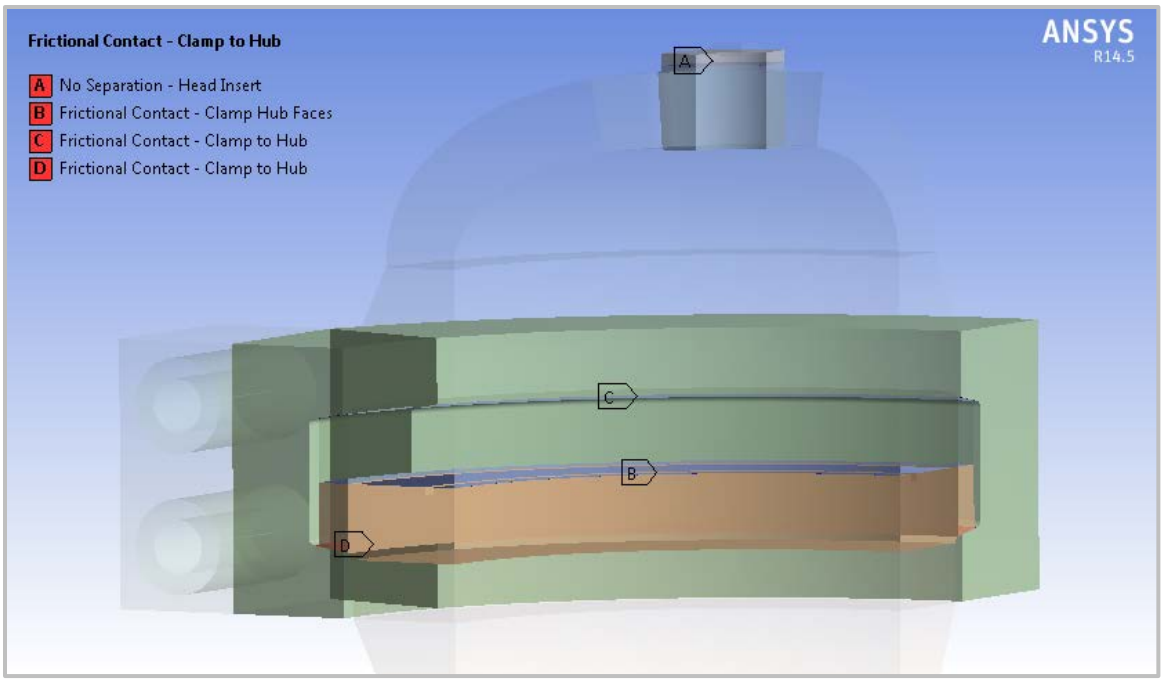

Figure 2-53. Contact Surfaces

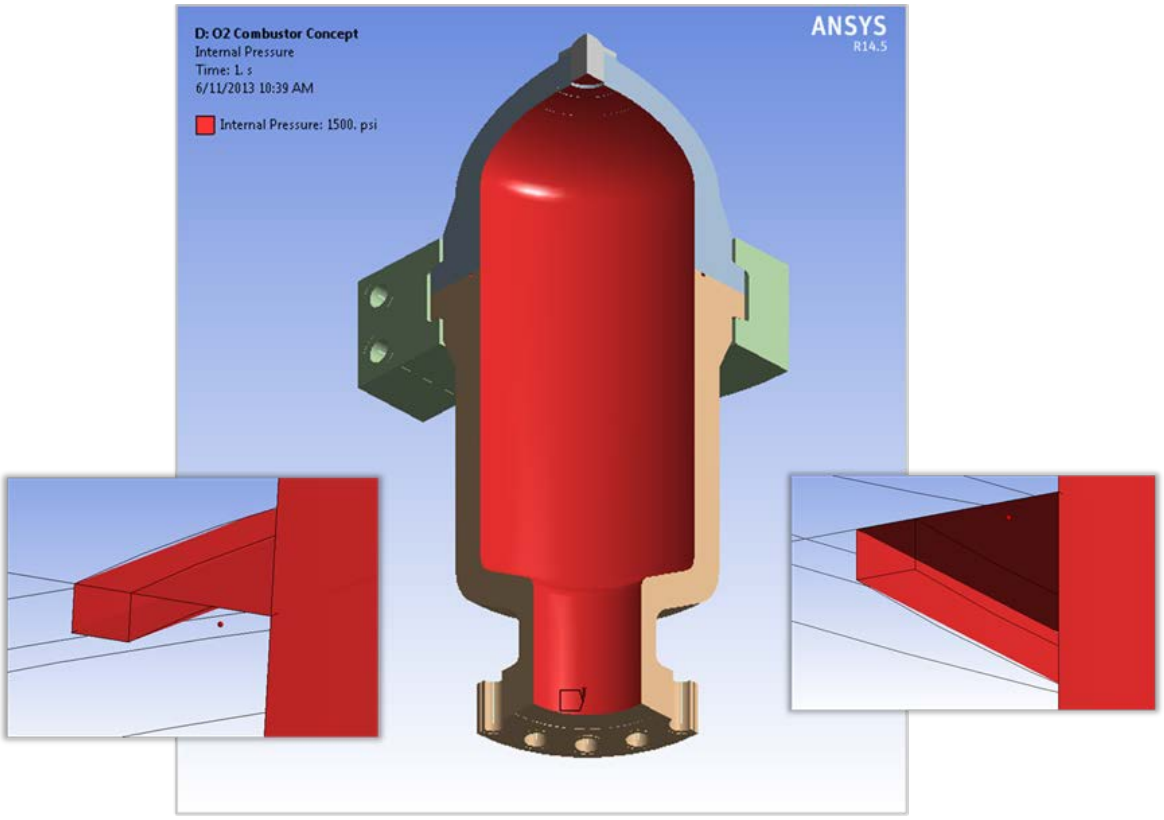

Figure 2-54. Internal Pressure Load of 1,500 psi

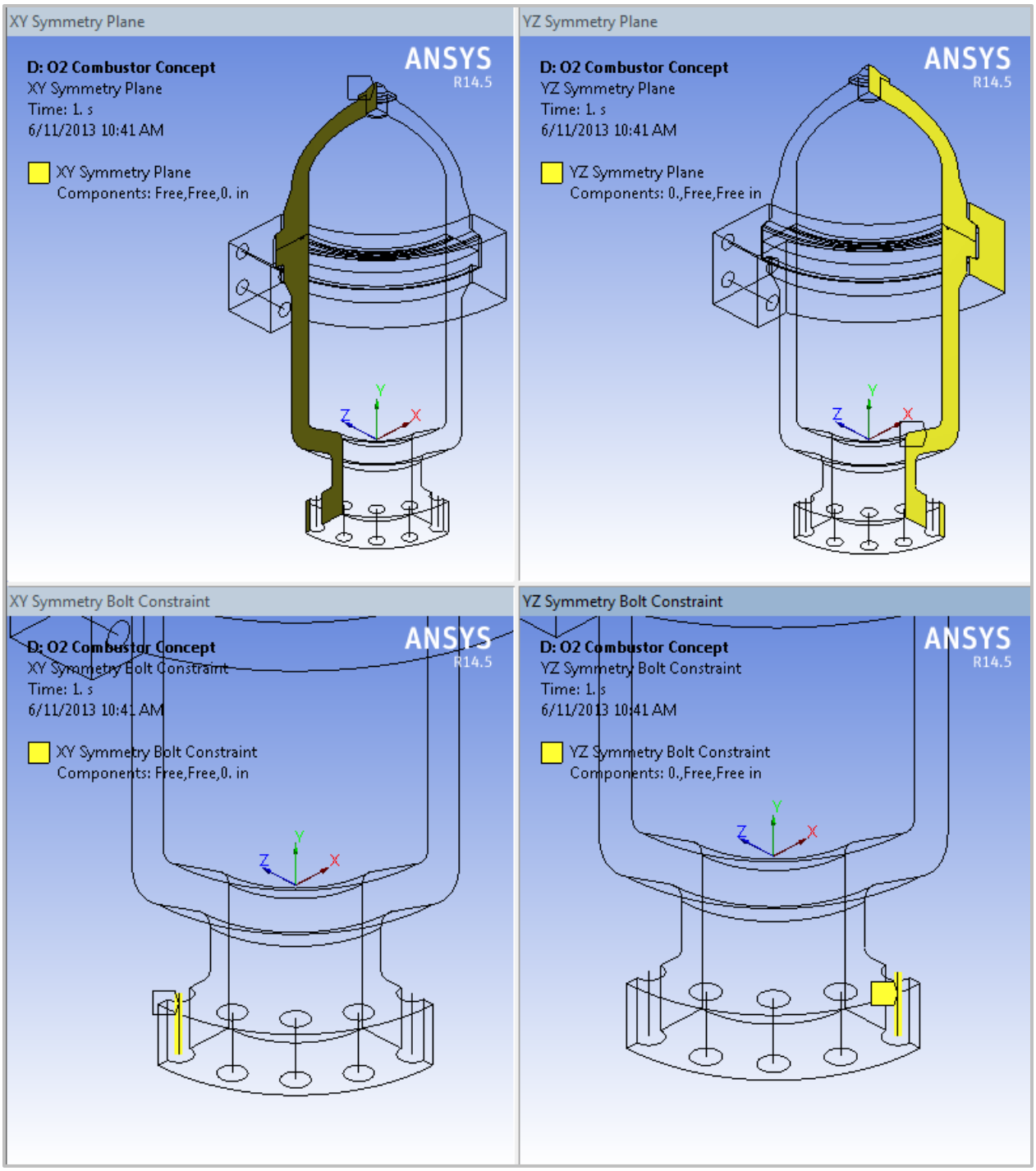

Figure 2-55. Symmetry Constraints

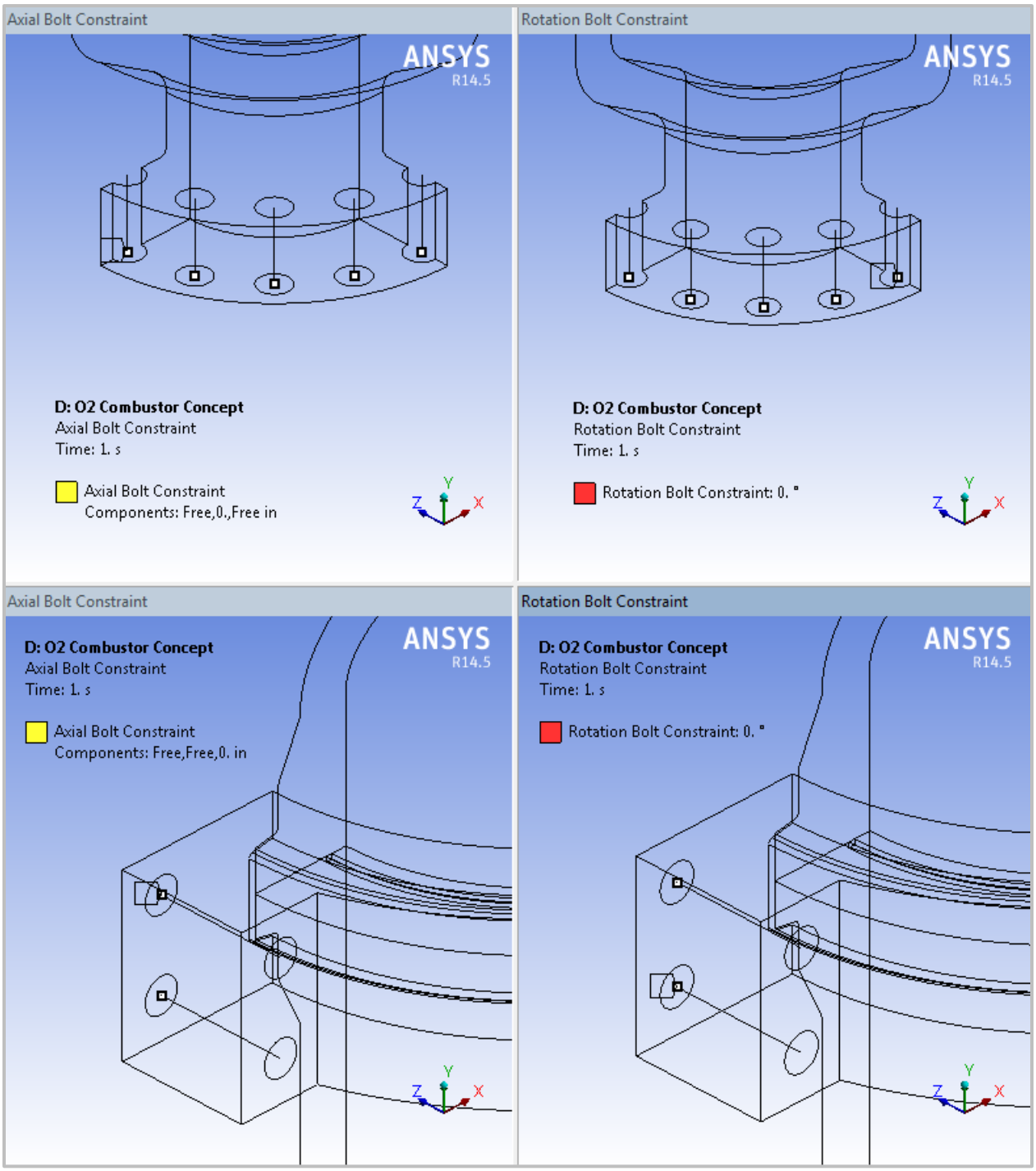

Figure 2-56. Symmetry Constraints

Analysis Results

The analysis was used to determine the stress and deflection with 1,500 psi internal pressure applied. The deflection with an exaggerated scale is shown in Figure 2-57. The pressure load results in bending in the clamp and clamp hubs. The analysis does not include the bolt pretension which should help to reduce the seal gap. Without bolt tension the seal gap is approximately 0.016 inches (Figure 2-58). A Parker high elasticity metal seal will be used for

this design. This is a lower load seal that is used frequently when resiliency or springback is needed to maintain effective sealing during flange separation. This seal should perform well with this seal gap.

The von Mises equivalent stress at 1,500 psi is shown in Figure 2-59. The location's where the general stress (stress through the cross section) is highest is at the intersection of the conical transition and the bottom flange. The general stress is also a little higher in the plain cylinder just below the clamp hub because of the bending created by the clamp closure. The limit load analysis at 2,250 psi confirms that these are the locations that are nearing the stability load limit. The location that is closest to instability is at the intersection of the conical transition and the bottom flange as indicated by the plastic in Figure 2-60. The strain contour from 0.0005948 in/in – 0.0010896 in/in extends through the thickness of the section at this location. The maximum plastic strain of 0.0040584 in/in occurs at the clamped connection. The plastic strain in the clamp is localized and is not causing structural instability.

The analysis has shown that the membrane or average stress through the thickness of a section such as the cylinder body, conical transition, clamp, clamp hubs or flange will not exceed 7,400 psi at 1,500 psi internal pressure. Since this ASME Code requirement is met there should be no appreciable accumulation of creep at 1,200°F for the life of the O_2 Combustor.

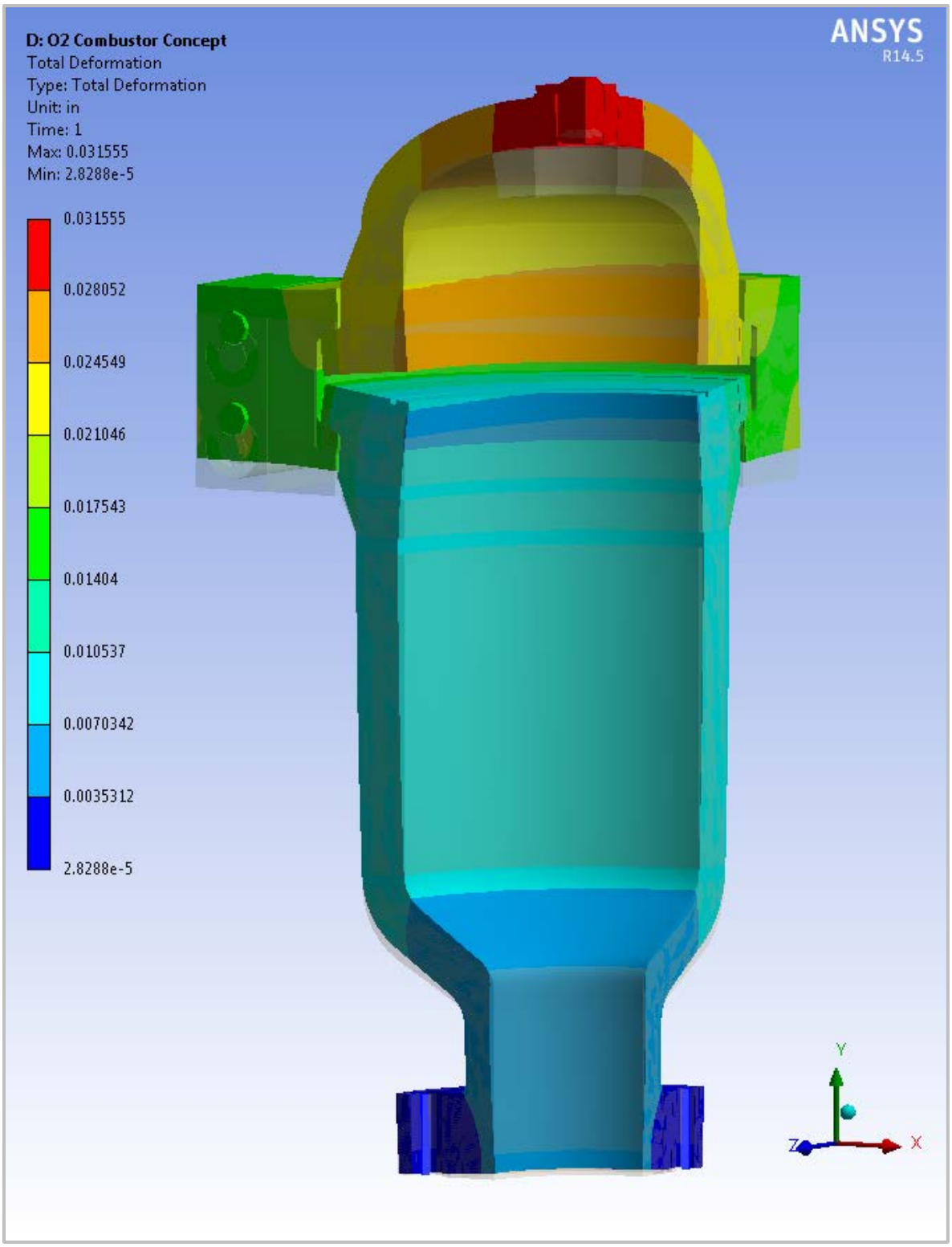

Figure 2-57. Total Deformation with 1,500 psi Internal Pressure (Exaggerated Scale)

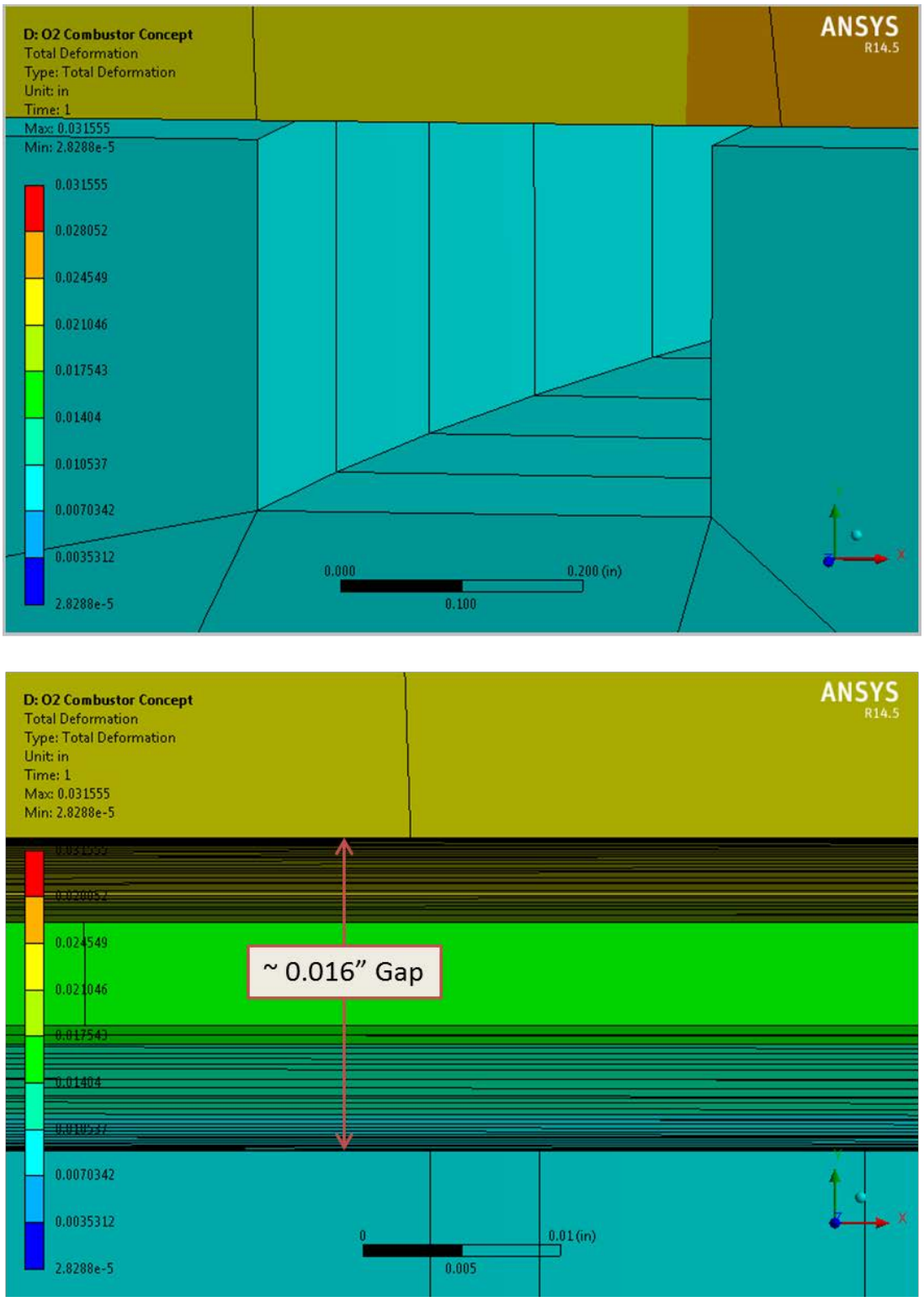

Figure 2-58. Seal Gap (True Scale)

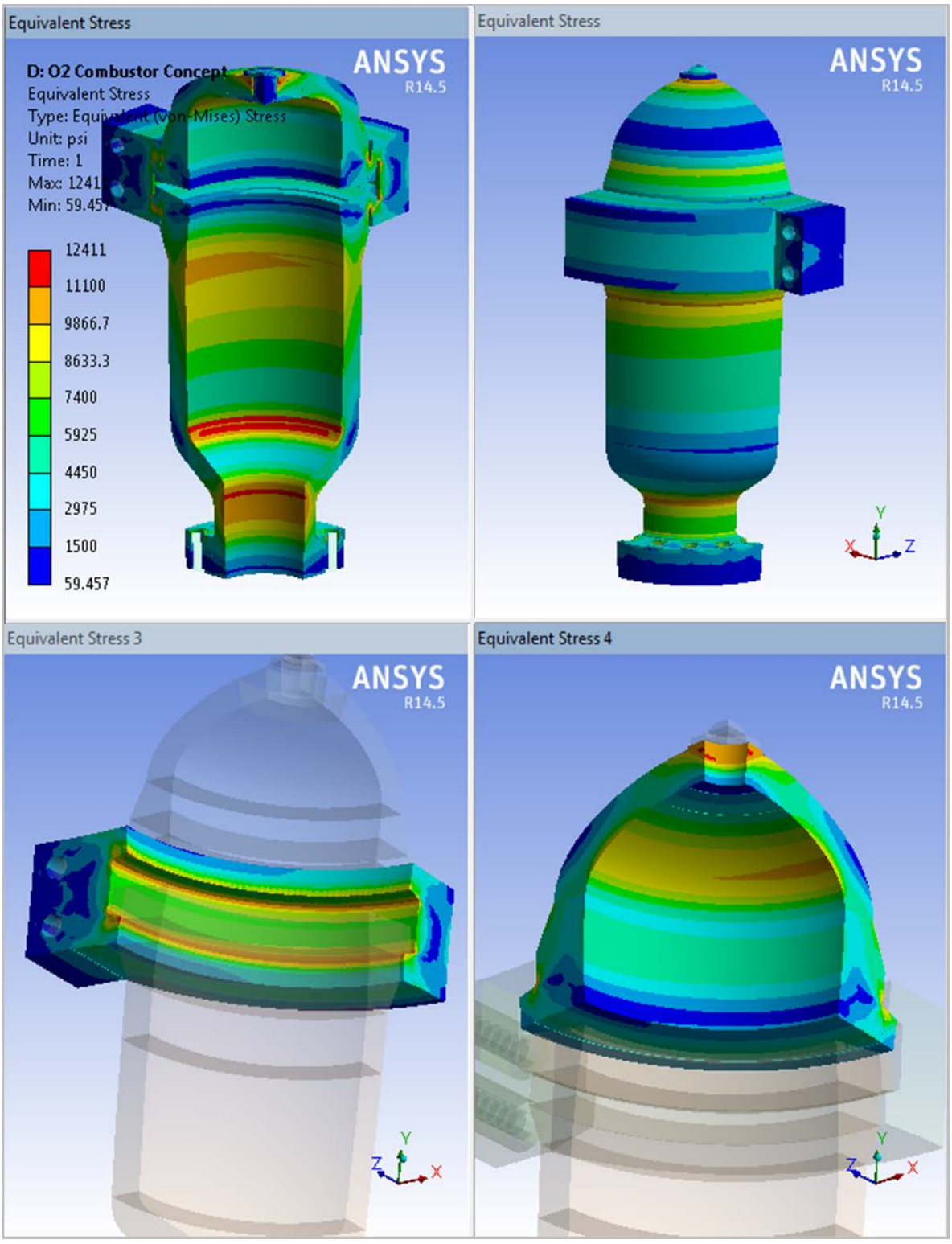

Figure 2-59. von Mises Equivalent Stress at 1,500 psi

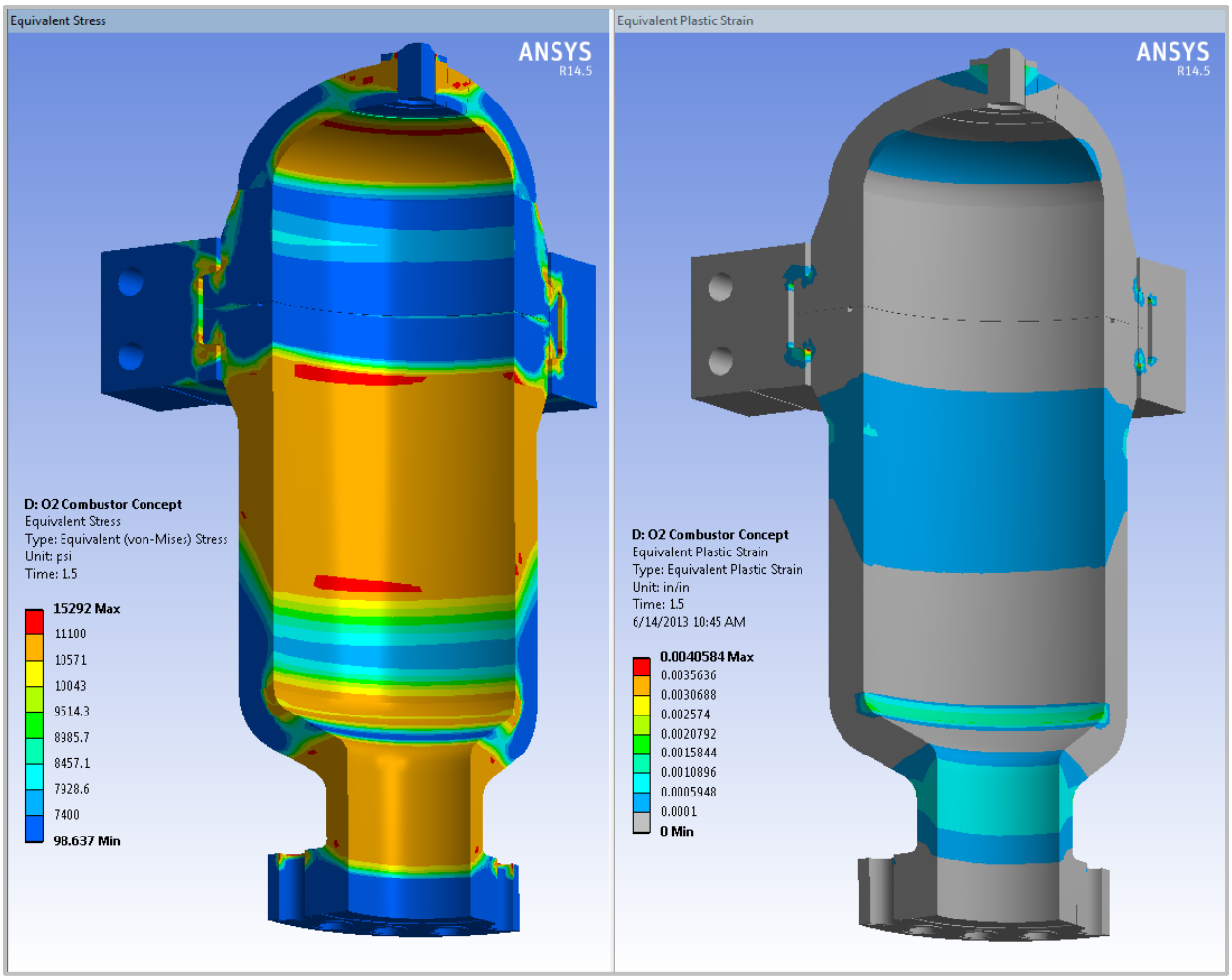

Figure 2-60. Equivalent Stress (Left) and Plastic Strain (right) at the Limit Load of 2,250 psi

2.6.3 PHASE II PILOT SCALE TEST LOOP

Along with the design of the supercritical oxy-combustor, initial design for a 1 MWth pilot scale test loop for the thermal side of the supercritical oxy-combustion cycle has been initiated. This test loop integrates the scaled supercritical oxy-combustor with the cyclone separator for particulate removal, a compact microchannel recuperator, a water scrubber, and boost compressor in a layout representative of the full scale supercritical oxy-combustion cycle, as shown in Figure 2-61. A conceptual rendering of the 1 MWth pilot scale test loop is shown in Figure 2-62. Coal flow rate would be on the order of 0.05 kg/s, with a flue gas recycle rate of 3.4 kg/s.

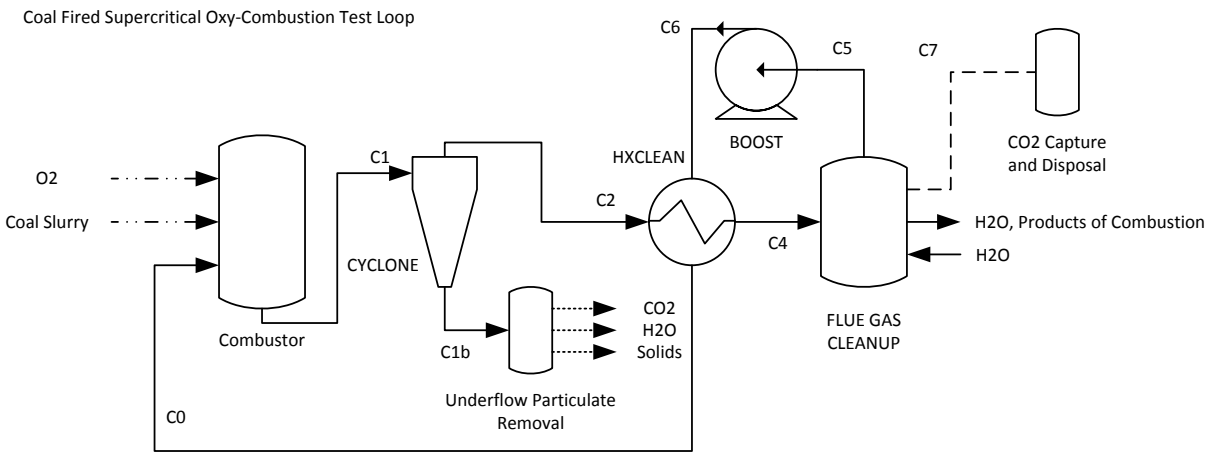

Figure 2-61. Process layout for a pilot scale supercritical oxy-combustion loop

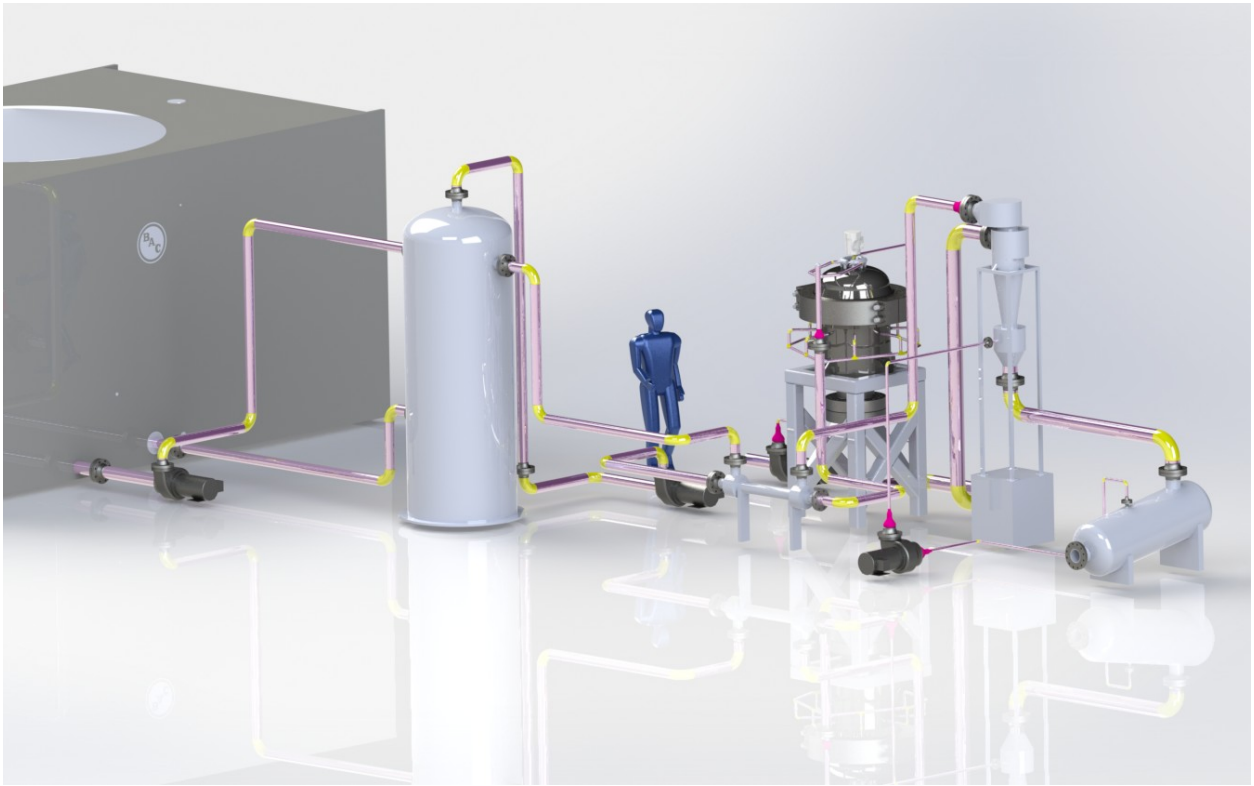

Figure 2-62. Rendering of a 1 MWth supercritical oxy-combustion test loop concept

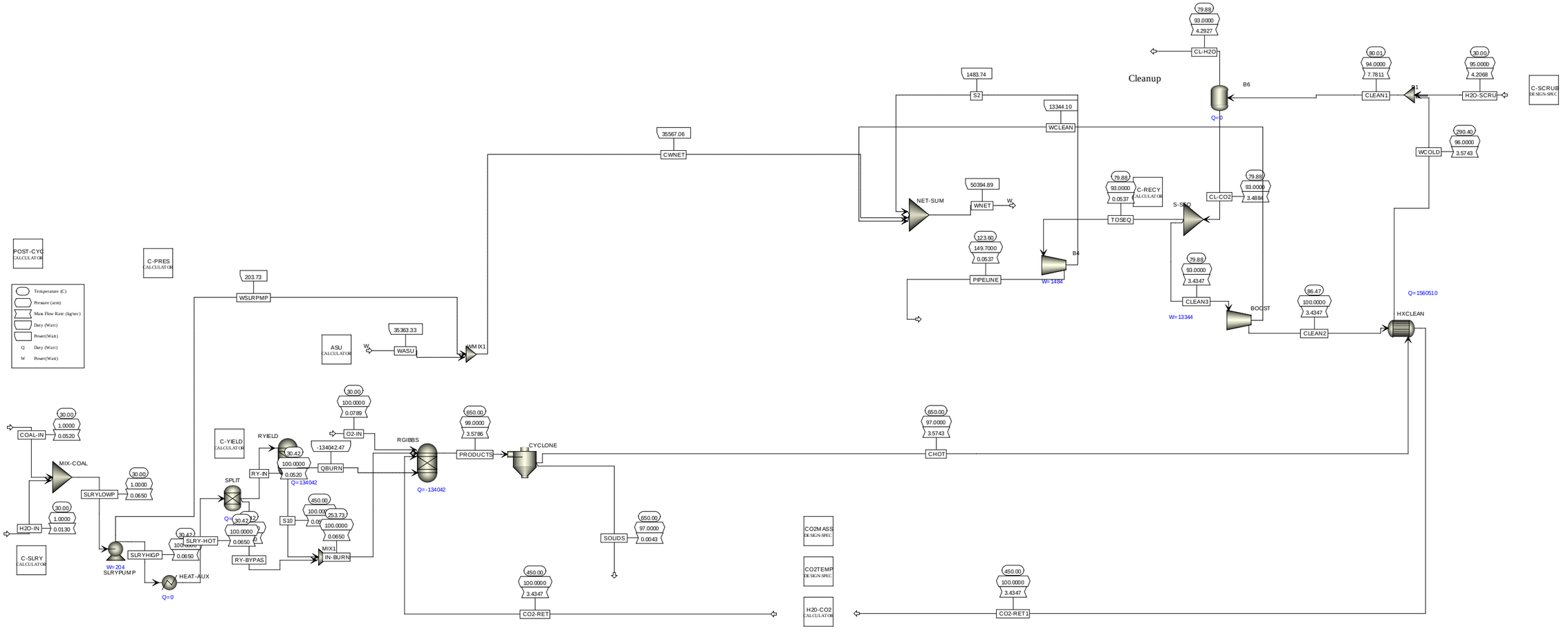

Figure 2-63. Aspen Plus process flowsheet for a 1 MWth pilot scale supercritical oxy-combustion loop

2.7 SUMMARY AND CONCLUSIONS

The team of Southwest Research Institute® (SwRI) and Thar Energy LLC (Thar) applied Technology Engineering and Economic Analysis to evaluate two advanced oxy-combustion power cycles, the Cryogenic Pressurized Oxy-combustion Cycle (CPOC), and the supercritical oxy-combustion cycle, with the goal of achieving at least 90% CO_2 removal at no more than a 35% increase in cost of electricity (COE). The supercritical oxy-combustion power cycle with 99% carbon capture achieves a COE of $121/MWe. This represents a 21% reduction in cost as compared to supercritical steam with 90% carbon capture ($137/MWe), without taking any credits for the additional 9% of carbon capture. However, this represents a 49% increase in the COE over supercritical steam without carbon capture ($80.95/MWe), exceeding the 35% target. The revised $121/MWe COE reflects the removal of installation labor costs included in the Total Overnight Cost (TOC) and increasing coal cost per QGESS fuel guidelines based on feedback provided by DOE for the Phase II application, and updates to the fuel consumption rates to match the cycle efficiencies predicted by the cycle models. These revisions reflect a significant decrease from the initial $162/MWe COE estimate provided in the *Technology Engineering Design and Ecconomic Analysis* report submitted with the Phase II proposal.

The supercritical oxy-combustion cycle with 99% carbon capture achieved a 37.9% HHV plant efficiency (39.3% LHV plant efficiency), when coupling a supercritical oxy-combustion thermal loop to an indirect supercritical CO_2 (sCO_2) power block. In this configuration, the power block achieved 48% thermal efficiency for turbine inlet conditions of 650°C and 290 atm. Power block efficiencies near 60% are feasible with higher turbine inlet temperatures, however a design tradeoff to limit firing temperature to 650°C was made in order to use austenitic stainless steels for the high temperature pressure vessels and piping and to minimize the need for advanced turbomachinery features such as blade cooling.

A Technical Gap Analysis of the supercritical oxy-combustion power cycle identified one critical component with a low Technology Reediness Level (TRL). The supercritical oxy-combustor operating at pressures near 100 atm is a unique component to the supercritical oxy-combustion cycle. In addition to the low TRL supercritical oxy-combustor, several secondary systems were identified that are commercially available, but would require adaptation for use with the supercritical oxy-combustion cycle. These secondary systems include the high pressure pulverized coal feed, the high temperature cyclone, the removal of post-combustion particulates from the high pressure cyclone underflow stream, and micro-channel heat exchangers tolerant of particulate loading.

Key findings of the technical gap analysis include:

- Air separation is a major cost item, exaggerated by the need to pressurize the O2 stream to nearly 100 bar. While the technology and manufacturing capability to provide oxygen in the quantity required of a 550 MW oxy-combustion power plant, the state-of-the-art for pumping/compression components is not yet up to commercial readiness.
- Particulate removal technology is available, but with the following caveats: Process engineering is required to develop a system for de-pressurization and recovery of solids. Cyclones should be outfitted with replaceable inner jackets, so as to manage abrasion and wear. The particulates that escape from cyclone separation will likely be in a size range of 1-5 microns; the downstream heat exchangers must be capable of handling these particles.
- Cyclones, heat exchangers, air separation units, and flue gas desulfurization systems should be specified as multiple smaller units in parallel. This is advantages for economy of scale and sparing.

- Compact, low cost heat exchangers are a key technology impacting footprint and cost of the supercritical oxy-combustion cycle. Microchannel heat exchangers are currently at a low TRL, but are actively being developed for multiple applications including supercritical CO2 power cycles. Because it is expected that 1-5 micron may pass through the cyclone separator, heat exchanger sparing and cleaning are important considerations.
- Metals removal, particularly mercury, can occur in the same equipment as used for flue gas desulfurization.
- Desulfurization using limestone slurry with recovery of gypsum byproduct is the preferred flue gas desulfurization method at elevated pressured.
- For slurry handling, conventional progressive-cavity pumps can be used for conveying slurry at low pressure differential into holding tanks. There, the pressurized stream of recycle CO2 can be used to bring the slurry to pressure. Direct feed of dry pulverized coal would be preferred to maximize plant efficiencies, however direct feed systems at high pressures are at a low TRL.

Bench scale testing was utilized to measure coal combustion properties at elevated pressures in a CO2 environment. This testing included coal slurry preparation, visualization of coal injection into a high pressure fluid, and modification of IQT injectors to facilitate the combustion properties testing. Additional bench scale testing evaluated the effectiveness of a rotary atomizer for injecting coal-water slurry into a fluid with similar densities, as opposed to the typical application where the high density fluid is injected into a low density fluid.

The swirl type supercritical oxy-combustor was developed from initial concept to an advanced design stage through numerical simulation using FLUENT and Chemkin to model the flow through the combustor and provide initial assessment of the coal combustion reactions in the flow path. This effort enabled the initial combustor mechanical layout, initial pressure vessel design, and the conceptual layout of a pilot scale test loop.

A pilot scale demonstration of the supercritical oxy-combustion cycle was proposed as a follow on effort. This demonstration would advance the supercritical oxy-combustion cycle and the supercritical oxy-combustor from a current TRL of 2, Technology Concept, to TRL 6, Pilot Scale System Demonstrated in a Relevant Environment, and enable the evaluation and continued refinement of the supercritical oxy-combustor and critical secondary systems.